NOAA OAR Special Report

PMEL Tsunami Forecast Series: Vol. #

A Tsunami Forecast Model for Kailua-Kona, Hawaii

(Draft)

Liujuan Tang

August 2012

NOAA Center for Tsunami Research (NCTR)
Pacific Marine Environmental Laboratory

Contents

Abstract 3
1 Introduction and Objective 5
2 Forecast Method 7
2.1 Construction of a Propagation Scenario Based on Tsunameter Measurements and Tsunami Source Functions 7
2.2 Coastal Predictions by Running High-Resolution Forecast Models in Real-Time. 10
3 Model Development 12
3.1 Forecast area 12
3.2 Tsunami History 13
3.3 Bathymetry and Topography 16
3.3.1 Hawaiian DEM in 6-arc-sec resolution 16
3.3.2 Kailua-Kona DEM in 1/3-arc-sec resolution 20
3.4 Model Setup 20
4 Results and discussion 22
4.1 Verification and Testing of the Forecast Model 22
4.2 Uncertainty of the Forecast Maximum Amplitudes 25
5 Summary and Conclusions 27
Acknowledgements 29
References 30
Appendix A. 40

List of Tables

Table 1 Tsunami source functions in the Pacific, Atlantic and Indian Oceans. 34
Table 2 Tsunami sources for past events. 35
Table 3 MOST setups of Kona reference and forecast models. 37
Table 4 Computational time vs. number of processors used for the Kona forecast model with MOST version 4. Results are based on an 8-hour event simulation of the 2011 Japan tsunami. 37
Table 5 Maximum wave crest at the Kona warning point computed by the reference and forecast models. 38
Table 6 Sources of the 18 Mw 9.3 synthetic tsunamis and maximum wave crest at the Kona warning point computed by the reference and forecast models. 38
Table 7 Maximum sea surface elevation at the Kona warning point computed by the forecast model with 1 and 20m offshore water depth for past tsunamis. 39
Table 8 Maximum sea surface elevation at the Kona warning point computed by the forecast model with 1 and 20m offshore water depth for simulated M_w 9.3 tsunamis. 39

PMEL Tsunami Forecast Series: Vol.

A Tsunami Forecast Model for Kailua-Kona, Hawaii

Liujuan Tang

Abstract

This report describes the development, verifications, and testing of a tsunami forecast model (2 arc-sec) for Kailua-Kona, Hawaii. A reference inundation model with higher resolution of 2/3 arc-sec was also developed in parallel, to provide modeling references. Both models were tested for 34 scenarios, which includes 16 past tsunamis and a set of 18 simulated magnitude 9.3 tsunamis.

The wave analyses of the amplitude time series show a wide range of resonant periods from 6-126 minutes on the site. 68% of the tested scenarios show peak resonant period (T_P) near 8 (±2) minutes. For some cases, waves of long resonant periods can have similar magnitude as those of short periods.

Tsunamis propagating from the east, particularly from Japan, Kamchatka and Izu subduction zones, have shown the late arrival of the maximum wave η_{max} in high frequency ($T_P \approx 8$ min). The η_{max} could be the 10th - 12th wave, arriving about 1-4 hours after the first wave. Both incident waves from far-fields and local resonances contribute to the late η_{max}. The developed forecast model includes a substantially large A-grid (2 arc-min), covering the entire Hawaiian Ridge, Mid-Pacific Mountains, Mellish Seamount and Southern end of Emperor Seamount Chain including Koko Guyot. This large grid can provide a more accurate simulation of the waves interacting with the major wave-

scattering features that are important to the forecast site, with the cost of longer computational time. It should be noted that the forecast system would adapt MOST version 4 that has parallel computation capability in the near future, which can reduce the computation time to minutes.

The numerical consistency between the two models are good in general, including the amplitude time series at the warning point, and maximum amplitude and current in the forecast area. When T_P >10min, the uncertainty in the forecast η_{max} at the warning point is with 20%. When $T_P \leq$10min and η_{max} > 1m, the uncertainty is within 31%. When η_{max} <1m, the uncertainty in η_{max} is within 25 cm. Scenarios from portion of Central Aleutian subduction zones near Unimak Islands may have additional uncertainty (about 0-41%), depending on whether or not a strong resonance of extremely short period (6 min) is excited on the site.

The simulated magnitude 9.3 tsunamis show an impressive local variability of tsunami amplitudes at Kailua-Kona, indicating the complexity of forecasting tsunami amplitudes at a coastal location. It is essential to use high-resolution models in order to provide accuracy that is useful for coastal tsunami forecast for practical guidance.

The study highlights tsunamis originated from Japan, Kamchatka, Izu, Northern Tonga (Samoa), Aleutian, Southern Chile, East Philippines and Canada, subduction zones, all of which can potentially generate large waves and cause flooding in Kailua-Kona. It also shows the water front near Kona Pier and at end of Kailua bay are under high flooding risk once inundation occurs in the forecast area.

Due to the unique tsunami resonant characteristics of the site, a coastal water level station is highly recommended for Kailua-Kona area, to provide tsunami data for model calibration and to improve forecast accuracy.

1 Introduction and Objective

The National Oceanic and Atmospheric Administration (NOAA) Center for Tsunami Research at NOAA's Pacific Marine Environmental Laboratory (PMEL) has developed a tsunami forecasting system for operational use by NOAA's two Tsunami Warning Centers located in Hawaii and Alaska (Titov et al., 2005; Titov, 2009). The forecast system combines real-time deep-ocean tsunami measurements from tsunameters (Deep-ocean Assessment and Reporting of Tsunami (DART)) stations (González *et al*., 2005; *Meinig*, 2005, *Bernard et al.*, 2006, *Bernard and Titov*, 2007) with the Method of Splitting Tsunami (MOST) model, a suite of finite difference numerical codes based on the nonlinear shallow water wave equations (*Titov and Synolakis*, 1998; *Titov and* González, 1997; *Synolakis*, *et al*., 2008; *Titov et al*., 2011) to produce real-time forecasts of tsunami arrival time, heights, periods and inundation. To achieve accurate and detailed forecast of tsunami impact for specific sites, high-resolution tsunami forecast models are under development for United States coastal communities at risk (Tang *et al.*, 2008[a]; 2009; 2010; Arcas and Uslu, 2010; Wei and Arcas, 2010). The resolution of these models has to be high enough to resolve the dynamics of a tsunami inside a particular harbor, including influences of major harbor structures such as breakwaters. These models have been integrated as crucial components into the forecast system.

Presently, as shown in Figure 1, a system of 55 tsunameter stations, are deployed in the Pacific, Atlantic, Indian Oceans, Caribbean Sea, the Gulf of Mexico and South China Sea (40 U.S.-, 8 Australian-, 1 Chilean-, 1 China-, 2 Indian-, 1 Indonesian-, 1 Thailand- and 1 Russian-owned) [*Spillane et al*., 2008]. The pre-computed propagation models currently have 1,725 scenarios covering the major tsunami-genetic subduction zones in the oceans, and high-resolution forecast inundation models are now set up for 57 U.S. coastal communities. The fully implemented system will use real-time data from the tsunameter network to provide high-resolution tsunami forecasts for at least 75 communities in the U.S. by 2013, with additional models envisioned later for smaller communities. Since its first testing in the 17 November 2003 Rat Island tsunami, the forecast system has produced experimental real-time forecasts for more than 20 tsunamis in the Pacific and Indian oceans (Titov et al., 2005; Wei et al., 2008; Titov, 2009; Titov and Tang, 2011; Tang et al., 2012; http://nctr.pmel.noaa.gov/database_devel.html). The forecast method has also been tested with data from nine additional events that produced deep-ocean tsunameter data and near-field tsunamis (http://nctr.pmel.noaa.gov/database_devel.html; *Wei et al*., 2012).

The recent 2011 Japan tsunami caused severe flooding and damages in the Kailua-Kona area (Figure 2), highlighting the need for a forecast flooding model. The report describes the development, testing and applications of the Kailua-Kona forecast model. The objective is to provide NOAA's Tsunami Warning Centers the ability to assess danger posed to Kailua-Kona following tsunami generation in the Pacific Ocean Basin, and to provide accurate and timely forecasts to enable the community to respond

appropriately. A secondary objective is to explore the potential tsunami impact from earthquakes at major subduction zones in Pacific to the site.

The report is organized as follows. Section 2 briefly introduces NOAA's tsunami forecast method. Section 3 describes the model development. Section 4 presents the results and discussion, which includes sensitivity of the forecast model to model setup, verification, and testing for past and simulated tsunamis. Summary and conclusions are provided in section 5.

2 Forecast Method

NOAA's real-time tsunami forecasting scheme is a process that comprises of two steps: (1) construction of a propagation scenario via inversion of deep ocean tsunameter measurements with pre-computed tsunami source functions; and (2) coastal predictions by running high-resolution forecast models in real time (*Titov et al*. 1999; 2005; Titov 2009; Tang *et al*., 2009, Tang *et al*., 2012). The DART-constrained tsunami source, the corresponding offshore scenario from the tsunami source function database, and high-resolution forecast models cover the entire evolution of earthquake-generated tsunamis, generation, propagation and coastal inundation, providing a complete tsunami forecast capability.

2.1 Construction of a Propagation Scenario Based on Tsunameter Measurements and Tsunami Source Functions

Several real-time data sources, including seismic data, coastal tide gage and deep-ocean data have been used for tsunami warning and forecasting (*Satake et al*., 2008;

Whitmore, 2003; *Titov,* 2009). NOAA's strategy for the real-time forecasting is to use deep-ocean measurements at tsunameter stations as the primary data source due to several key features. (1) tsunameters provide a direct measure of tsunami waves, unlike seismic data, which are an indirect measure of tsunamis. (2) The deep ocean tsunami measurements are in general the earliest tsunami information available, since tsunamis propagate much faster in deep ocean than in shallow coastal area where coastal tide gages are located. (3) Compared to coastal tide gages, tsunameter data with a high signal to noise ratio can be obtained without interference from harbor and local shelf effects. (4) Wave dynamics of tsunami propagation in deep ocean is assumed to be linear (*Kânoğlu and Synolakis*, 2006; *Liu*, 2009). This linear process allows application of efficient inversion schemes.

Time series of tsunami observations in deep-ocean can be decomposed into a linear combination of a set of tsunami source functions in the time domain by a linear Least Squares method (Percival et al., 2011). We call coefficients obtained through this inversion process *tsunami source coefficients*. During real-time tsunami forecasting, seismic waves propagate much faster than tsunami waves so the initial seismic magnitude can be estimated before the tsunameter data are available. Since time is of the essence, the initial tsunami forecast is based on the seismic magnitude only. The tsunameter inverted source will update the forecast when it is available.

Titov et al. (1999; 2001) conducted sensitivity studies on far-field deep-water tsunamis to different parameters of elastic deformation model described in *Gusiakov* (1978) and *Okada* (1985). The results showed source magnitude and location essentially define far-field tsunami signals for a wide range of subduction zone earthquakes. Other

parameters have secondary influence and can be pre-defined during forecast. Based on these results, tsunami source function databases for Pacific, Atlantic, and Indian Oceans have been built using pre-defined source parameters, length = 100 km, width = 50 km, slip = 1 m, rake = 90 and rigidity = 4.5 x 10^{10} N/m^2. Other parameters are location-specific; details of the databases are described in *Gica et al*. (2008). Each tsunami source function is equivalent to a tsunami from a typical M_w = 7.5 earthquake with defined source parameters. Figure 1 shows the locations of tsunami source functions.

The tsunami source functions in the database are computed with a time step of 10 seconds and a spatial resolution of 4-arc-minute (approximately 7.4 km along the N-S direction). The outputs, offshore wave height and depth-average velocities of the entire domain, are then compressed and saved every 1 minute in time and 16-arc-minute in space [*Tolkova*, 2007]. The current propagation scenarios do not include inundation and a vertical wall is placed at 20 m water depth [*Gica et al*., 2008]. The friction term is set to zero. When tsunami waves propagate into shallow water, under the steady-state assumption, where there are not any energy losses or inputs, the decrease in transport speed must be compensated by an increase in energy density in order to maintain a constant energy flux. The low spatial resolution and simplified boundary conditions of the propagation model result in inaccurate near-shore dynamics. As a consequence, the numerical dissipation (due to the low spatial resolution) will cause energy decay in the propagation modeling (Tang et al., 2012). Based on consideration of energy conservation, we have developed high-resolution, site-specific inundation forecast models built on the MOST model to simulate the near shore wave dynamics.

Energy released from an earthquake and then portions of the earthquake energy transferring into water column are complex dynamic processes at the stage of tsunami generation. However, the goal of tsunameter inversion is not to quantify the quantities such as energy at the initial stage of tsunami generation. Instead, we try to quantify the amount of wave energy that propagates outside the source area in the form of surface long gravity waves, which can be well measured by the tsunameter stations. It is also the propagated energy that results in the coastal impacts. Our estimates of the tsunami source (the propagation scenario) focus on the characteristics of tsunami propagation. They are directly constrained by the deep ocean tsunami data. Regardless the details of earthquake processes for tsunami generation at the initial stage, the inversion can ensure the propagation scenario gives the best approximation to the tsunami measurements, and therefore, the best estimation of the total energy transferred by the tsunami waves. The database can provide offshore forecasts of tsunami amplitudes and all other wave parameters immediately once the inversion is complete. The tsunami source, which combines real-time tsunami measurements with tsunami source functions, provides an accurate offshore tsunami scenario without additional time-consuming model runs.

2.2 Coastal Predictions by Running High-Resolution Forecast Models in Real-Time.

High-resolution forecast models are designed for the final stage of the evolution of tsunami waves: coastal runup and inundation. Once the tsunameter-constrained tsunami source is obtained (as a linear combination of tsunami source functions), the pre-computed time series of offshore wave height and depth-averaged velocity from the

model propagation scenario are applied as the dynamic boundary conditions for the forecast models. This saves the simulation time of basin-wide tsunami propagation. Tsunami inundation and nearshore currents are highly nonlinear processes, therefore a linear combination would not provide accurate solutions. A high-resolution model is also required to resolve shorter tsunami wavelengths nearshore with accurate bathymetric/topographic data. The forecast models are constructed with the Method of Splitting Tsunami (MOST) model, a finite difference tsunami inundation model based on nonlinear shallow-water wave equations (*Titov and Gonzalez,* 1997). Each forecast model contains three telescoping computational grids with increasing resolution, covering regional, intermediate and nearshore areas. Runup and inundation are computed at the coastline. For example, Figure 3 shows forecast model setup for several tsunami forecast models in Hawaii, detailing the telescoping grids used:

(a) One regional grid of 2-arc-minute (~3600m) resolution covers the main Hawaiian Islands (Fig. 3.a).

(b) Then the Hawaiian Islands are divided into four intermediate grids of 12- to 18-arc-second (~ 360 –540m) for four natural geographic areas (Figs. 3.b 1-4):

(b1) Ni'ihau, Ka'ula Rock, and Kauai (Kauai complex),

(b2) Oahu,

(b3) Molokai, Maui, Lanai, and Kaho'olawe (the Maui Complex),

(b4) Hawaii.

(c) Each intermediate grid contains 2-arc-second (~60 m) nearshore grids (Figs. 3.c 1-4).

The highest resolution grid includes the population center and coastal water level stations for forecast verification. The grids are derived from the best available bathymetric/topographic data at the time of development, and will be updated as new survey data become available. Forecast models have been developed for 13 coastal communities in Hawaii (Figure 3).

The forecast models are optimized for speed and accuracy. By reducing the computational areas and grid resolutions, each model is optimized to provide 4-hour event forecasting results in 10 minutes of computational time using one single processor, while still providing good accuracy for forecasting. To ensure forecast accuracy at every step of the process, the model outputs are validated with historical tsunami records and compared to numerical results from a reference inundation model with higher resolutions and larger computational domains. In order to provide warning guidance for long duration during a tsunami event, each forecast model has been tested to output up to 24-hour simulation since tsunami generation.

3 Model Development

3.1 Forecast area

The main Hawaiian Islands are the younger and southern portion of the Hawaii Archipelago. From northwest to southeast, the islands form four natural geographic groups by shared channels and inter-island shelf, including (1) Ni'ihau, Ka'ula Rock, and Kauai, (Kauai complex) (2) Oahu, (3) Molokai, Maui, Lanai, and Kaho'olawe, (the Maui Complex), and (4) Hawaii. Kailua-Kona is the chief western city on Hawaii Island. The

Port of Kailua-Kona is located in a popular resort area on the western shores of the Big Island. The whole western coastline of Hawaii island is called Kona, and the largest town in the area is Kailua. The 2010 US Census reported a population of almost 12 thousand residents in the Port of Kailua-Kona. Figure 4 presents an aerial photo of this area and a chart is shown in Figure 5. The population density data is in Figure 6.

The Island of Hawaii (Big Island) is located at the southeast end of the Hawaii Archipelago (Fig. 3). To its northwest, there is the Maui complex, with the deep Alenuihaha Channel in between (water depth > 200m). The coast of Kailua-Kona is characterized by the sudden steep offshore slopes from 100m down to 4000 m depth. From 0 to 100m depth, the slope is quite gentle, only 0.013. From 100m to 1000m water depth, it has the steepest offshore slope of 0.3822, and then 0.15 slope from 1000m to 4000m depth (Fig. 9).

No coastal water level station exists in the forecast area. The Port of Kailua-Kona is about 47km (29 miles) south-southwest of the Kawaihae Harbor and about 97 km (60 miles) west of Hilo Harbor, on the same Hawaii island. At Kawaihae tide station, the mean range of tide is 0.461m, and the mean high water is 0.222 m above mean sea level. Since no coastal water level station is in the area, a point (204.0046 °E, 19.6397° N) at 2.3m water depth near the end of Kailua Bay was chosen as the warning point (Fig. 9d).

3.2 Tsunami History

The Hawaiian Islands have a long history of distant and local destructive tsunamis (Pararas-Carayannis, 1969; Soloviev and Go, 1984; Lander and Lockridge, 1989; Soloviev et al., 1992). The descriptions for Kailua-Kona were extracted from the

references as follows. The height in Pararas-Carayannis (1969) refers to maximum runup height or amplitude. Walker (2004) summarized the runups on the Island of Hawaii for the 1946, 1952, 1957, 1960 and 1964 tsunamis (Figure 7).

On June 15, 1896, a tsunami originated from Sanriku, Japan produced a 2.4 m height at Kailua (Pararas-Carayannis, 1969).

On August 9,1901, a tsunami originated from Rikuchu, Japan, covering wharf to a depth of 1 m. No damage was reported. (Pararas-Carayannis, 1969). The tsunami reached a 1.2 m height.

On August 16, 1906, a tsunami originated from an earthquake near Talcahuano, Chile caused some damage in Kailua (Pararas-Carayannis, 1969).

On March 3, 1933, a series of ten large waves generated by an earthquake near Sanriku, Japan caused considerable damage at Kailui-Kona. The last wave was the highest (Pararas-Carayannis, 1969).

On April 1, 1946, a 3.3 m height was observed at Kailua for the Unimak tsunami (Pararas-Carayannis, 1969).

On March 4, 1952, a tsunami originated from Hokkaido, Japan, producing a 0.6 m height at Kailua (Pararas-Carayannis, 1969). The 4 November 1952 Kamchatka also produced a 0.6 m height.

On March 9, 1957, a 1.5 m height was reported at Kailua for the Andreanof tsunami.

On May 22, 1960, a 2.4 m height was reported at Kailua for the Chile tsunami (Pararas-Carayannis, 1969).

At 17:07:48 UTC (7:07 AM HST in Hawaii) on October 15, 2006, An Mw 6.5 earthquake occurred 29 km NNE of Kailua-Kona, Hawaii (USGS). Numerous people

suffered minor injuries, at least 1,173 buildings damaged, roads damaged and landslides blocked roads on Hawaii. Power outages occurred throughout the Hawaiian Islands. Damage estimated at 73 million dollars. A tsunami with a wave height of 10 cm was recorded at the Kawaihae Harbor. Earthquakes on the volcanic Island of Hawaii are not rare. The largest on record was the magnitude 7.9 1868 earthquake near the south coast which triggered a tsunami that drowned 46 people and which spawned numerous landslides that resulted in 31 deaths (USGS). A magnitude 6.9 tremor on August 21, 1951, damaged scores of homes on the Kona coast and triggered numerous damaging landslides (http://earthquake.usgs.gov/earthquakes/eqinthenews/2006/ustwbh/#summary).

On March 11 2011, the Japan tsunami hit hard (Hawaii County, 2011). The following damage were reported by the Hawaii county reported:

"King Kamehameha's Kona Beach Hotel on Ali'i Drive suffered extensive water damage to its ground floor, and observers reported possible damage to the Ahu'ena Heiau on the hotel grounds. Shops across Ali'i Drive from King Kamehameha's Kona Beach Hotel also suffered extensive damage. Large amounts of debris were also deposited on Kailua Pier, and two vehicles left parked on the pier were damaged when the tsunami pushed them across the pier. A hall at Pu'uhonua Road suffered severe damage, while the Puu O Honaunau National Historic Park (City of Refuge) also reported flooding. Extensive damage was reported to businesses on both sides of Ali'i Drive, including the Bubba Gump Shrimp Company, the ground floor of the Kona Reef Hotel, and the Kona Inn Restaurant. In Kailua-Kona, crews reported one single-family home was destroyed, and one suffered major damage. Six Kailua apartments or condominiums suffered major damage, and 19 had minor damage. The Kona Village Resort had 20 guest units damaged

when they were lifted off their foundations. Two restaurants at the resort were flooded. The Four Seasons Resort Hualalai reported water damage to utility buildings, pools and damage to a restaurant at the resort" (Hawaii County, 2011).

Figure 2 shows four photos taken for the 2011 Japan tsunami. As a city that has repeatedly been damaged and flooded by tsunamis, Kaikua-Kona is in need for a forecast model to aid site-specific evacuation decisions.

3.3 Bathymetry and Topography

Tsunami inundation modeling requires accurate bathymetry in coastal areas as well as high resolution topography and bathymetry in the nearshore area. Two gridded digital elevation models (DEMs), one at medium resolution (6 arc-second) for the Hawaiian Islands and a high resolution (1/3 arc-second) DEM for Kailua-Kona were developed by NCTR and NGDC respectively.

3.3.1 Hawaiian DEM in 6-arc-sec resolution

The 6" Hawaiian DEM was developed at NOAA Center for Tsunami Research in 2007. The same source grid has been used for the forecast model developments for Hilo, Kahului, Honolulu, Pearl Harbor and Lahaina (Tang et al, 2009; 2010). The grid was compiled from several data sources; Figure 8a is an overview of the spatial extents of each data source used. In areas where multiple datasets overlap, higher-resolution and newer datasets were generally preferred, and superseded datasets were used for comparison and verification. An overview of the data sources used is as follows; in

general, the data sources listed first superseded data sources listed later when they overlapped.

Source details for the datasets incorporated into the model grids:

- Joint Airborne Lidar Bathymetry Technical Center of Expertise (JALBTCX), US Army Corps of Engineers, Mobile District. Online reference: http://shoals.sam.usace.army.mil/hawaii/pages/Hawaii_Data.htm.
- Monterey Bay Aquarium Research Institute (MBARI) Hawaii Multibeam Survey, Version 1. Online reference: http://www.mbari.org/data/mapping/hawaii/.
- USGS Pacific Seafloor Mapping Project. Online reference: http://walrus.wr.usgs.gov/pacmaps/data.html.
- Japan Agency for Marine-Earth Science and Technology (JAMSTEC) 1998-1999 multibeam bathymetric surveys. Published in: Takahashi, E., *et al*., eds. (2002): *Hawaiian Volcanoes: Deep Underwater Perspectives*. American Geophysical Union Monograph 128.

  JAMSTEC trackline data was recorded by the R/V *Mirai* during transits near in 1999 and 2002. Online reference: http://www.jamstec.go.jp/mirai/index_eng.html.
- United States Army Corps of Engineers (USACE), Honolulu District. Online reference: http://www.poh.usace.army.mil/.
- NOAA National Geophysical Data Center (NGDC). Online reference: http://www.ngdc.noaa.gov/mgg/gdas/gd_sys.html.

- NOAA National Ocean Service (NOS). Sounding points were digitized from NOS nautical charts 19347, 19358, 19359, 19364, 19366, 19342, 19381, and 19324. Sounding data from electronic chart (ENC) 19357 was used. This data was included in relatively shallow regions where other data sources were sparse or unavailable, or for quality control of other sources.
- Smith, W. H. F., and D. T. Sandwell, Global seafloor topography from satellite altimetry and ship depth soundings, *Science*, v. 277, p. 1957-1962, 26 Sept., 1997. Online reference: http://topex.ucsd.edu/WWW_html/mar_topo.html.
- USGS Geological Long-Range Inclined Asdic (GLORIA) surveys. Online data reference: http://walrus.wr.usgs.gov/infobank/
- NOAA Coastal Services Center. http://www.csc.noaa.gov/. The IfSAR topographic data was collected and processed for CSC by Intermap Technologies Inc. The data is subject to a restrictive license agreement and is not publicly available.
- USGS National Elevation Dataset. Online reference: http://seamless.usgs.gov/

The SHOALS LIDAR project, which provides high-resolution unified topographic and bathymetric data around for nearshore areas of several Hawaiian Islands, including all of Maui, was essential to accurate modeling of reef and intertidal regions where conventional bathymetric survey data is usually coarse or unavailable. Quality data in this region is especially essential because bathymetric inaccuracies have great impact on tsunami wave dynamics in shallow water. The 2005 NOAA CSC IfSAR survey of Maui provided similarly valuable high-resolution topography for the entire island, enabling

greater confidence in predicting inundation extents. The USGS National Elevation Dataset (NED) was used on other islands outside of the primary study area.

High-resolution gridded datasets derived from multibeam surveys are available for many parts of the archipelago, and were used wherever available. In deep water where high-resolution multibeam data were not available, the grid was developed by interpolation of a combination of USGS GLORIA surveys and the Smith and Sandwell two-minute global seafloor dataset.

All selected input datasets were converted to the mean high water (MHW) vertical datum, as necessary. Bathymetry datasets were converted from the survey tidal datum (usually mean lower low water or mean sea level) using offset surfaces interpolated from NOS tide gauges at Kahului, Kawaihae (Hawaii), and Kaunakakai (Molokai). The CSC IfSAR topographic data as obtained was vertically referenced to the GRS80 ellipsoid. It was converted to MHW using an offset surface interpolated from seven National Geodetic Survey (NGS) benchmark stations on Maui that had ellipsoid and tidal heights recorded.

Raw data sources were imported to ESRI ArcGIS-compatible file formats. Horizontal positions were reprojected, where necessary, to the WGS84 horizontal geodetic datum using ArcGIS. In the point datasets, single sounding points that differed substantially from neighboring data were removed. Gridded datasets were checked for extreme values by examination of contour lines, and, where available, by comparison between multiple data sources.

To compile the multiple data sources into a single grid, subsets of the source data were created in the priority order described above. A triangulated irregular network (TIN) was created from the detided vector point data (geodas, usace, csc_lidar). Also added to the TIN were points taken from the edges of the gridded data regions to ensure a smooth interpolated transition between areas with different data sources. This TIN was linearly interpolated using ArcGIS 3D Analyst to produce an intermediate 1 arc-second and 6 arc-second raster grid. The gridded datasets were then bilinearly resampled to these resolutions and overlaid on top of the intermediate grids.

3.3.2 Kailua-Kona DEM in 1/3-arc-sec resolution

A high-resolution DEM in 1/3-arc-sec (~10m) was developed for the Kailua-Kona and Keauhou area by the National Geophysical Data Center (Carignan et al., 2011). The DEM was generated from diverse digital datasets in the region (grid boundary and sources shown in Fig. 8b). The topographical Lidar data from State of Hawaii Civil Defencse /FEMA and HI DBEDT have approximately 1 m spatial resolution. The detail of the data sources and methodology used in developing the DEM can be found in (Carignan et al., 2011).

3.4 Model Setup

By sub-sampling from the DEMs described in section 3.3, two sets of computational grids were derived for Kailua-Kona, a reference inundation model (Fig. 9) and the optimized forecast model (Fig. 10). The reference grids consist of four levels of

telescoped grids with increasing resolution. The A-grid covers the entire Hawaiian Ridge, Mid-Pacfic Mountains, Mellish Seamount, and southern end of the Emperor Seamount Chain including Koko Guyot in 1 arc-min resolution (Fig. 9a). The B-grid covers the Island of Oahu, the Maui Complex and the Island of Hawaii in 6 arc-sec resolution (Fig. 9b). The C-grid covers the southwest coast of Hawaii in 2 arc-sec resolution. D-grid includes Kailua-Kona and Keauhou in 20-m resolution. Run-up and inundation simulations are computed on the coastline in C and D grids (Figs. 9c and 9d). The optimized forecast model has three levels of telescoped grids (Fig. 10). Grid details at each level and input parameters are summarized in Table 3.

It takes approximately 30 minutes for the forecast model for a 4-hr simulation with the current operational MOST version 2 (Table 3). With MOST version 4, the computational time can be reduced to 16 minutes. One reason is, while MOST 2 requires all grids start computation simultaneously, the B- and C-grids of MOST 4 can start computation when the first wave propagates close to the grids. It can save computational time significantly for tsunamis coming from east boundary. MOST 4 has parallel computing capability. Table 4 summarizes the computational time for different numbers of processors used for the Kailua-Kona forecast model for the 2011 Japan tsunami. Since it takes a few hours for the first wave to reach B-grid, the simulation time was set to 8 hours, to ensure there is at least 4-hour tsunami simulation within B- and C-grids. The regular Hawaiian A grid in Fig.3 (210 × 150 nodes usually takes 2-10% of the total computational time. However, the Kailua-Kona A-grid costs 79% of the total computational time, due to its large grid size (1351 x 889 nodes). The efficiency of parallel computing depends on the total node number (grid size), which higher efficiency

can be achieved for grids with large node number. When the total node number is small, such as the 114 by 334 of the forecast C-grid, more processors can actually cost more computational time than a single processor (Table 4).

To achieve timely and effective forecast, and as a transition before MOST version 4 becomes operational, we developed a transitional forecast model for Kailua-Kona, which has the smaller, regular Hawaiian A-grid as many other forecast sites in Hawaii (Figure 3a). We refer is as set 1. It is capable of simulating four hours of tsunami wave dynamics in minutes of computational time. We refer the forecast model with larger A grid here as set 2. Set 2 will replace results from set 1 when it is available during real time. The B- and C-grids are identical for both sets. In the next section, we will show and discuss results from set 2.

4 Results and discussion

4.1 Verification and Testing of the Forecast Model

Since no water level station was available at Kailua-kona, we evaluate the forecast model performance through comparisons of tsunami amplitude time series, peak period, maximum amplitude and current in the area with results from the reference model.

Both the reference and the forecast models were tested with the sixteen past tsunamis summarized in Table 2. Figure 11 shows the modeled amplitude time series at the warning point computed by the both models. The computed maximum water elevation above MHW and maximum current are plotted in Figure 12 for all grids. The 2011 Japan tsunami generated the largest amplitude of 1.38 m at the warning point. It is also the

largest tsunami at Kailui-Kona nearshor among the 16 past events. The 1960 Chile tsunami produced the largest offshore amplitude around Hawaiian Islands. Table 5 summarizes the maximum amplitude (η_{max}) at the warning point for the 16 tsunamis for both the reference and forecast models. The two models produce large discrepancy in η_{max} for the 1946 Unimak and 2011 Japan tsunamis. As will be discussed in section 4.2, it is due to the resonate waves of high frequency exited in the area, which are sensitive to the model setup.

Recorded historical tsunamis provide only a limited number of events, from limited locations. More comprehensive test cases of destructive tsunamis with different directionalities are needed to check the stability and robustness for the forecast model. A similar set of eighteen simulated magnitude 9.3 tsunamis as in Tang *et al*. (2008[a], 2009[b]) was selected here for further testing (Table 6). Results computed by the forecast model are compared with those from the high-resolution reference model in Table 6, Figures 13 and 14. Both models were numerically stable for all of the scenarios and computed similar maximum water elevation and inundation in the study area (Figs. 13 and 14). Waveforms computed by the forecast model agree well with those of the reference model except tsunamis from the Japan and Izu subduction zones (Figs. 13.1 and 13.18).

The amplitude time series at the warning point for 34 scenarios show that tsunami waves with amplitudes that are 2-6 times of the first wave can arrive 1-4 hours later (Figs. 11 and 14). Both incident waves from the far-field and local resonances can attribute to the amplified waves. Therefore, a substantial large A-grid, covering the entire Hawaiian Island Chain, Mid-Pacific Mountains, Mellish Seamount and southern end of the Emperor Seamount Chain including Koko Guyot is necessary to capture the amplified

late waves. The large A-grid provides a more accurate simulation of the waves interacting with the major wave scatterers that are important to the forecast site, with the cost of longer computational time.

The Japan, Izu, Kamchatka, Aleutian, Northern Tonga (Samoa), Canada, Southern Chile and East Philippines subduction zones can potentially generate large amplitude waves and cause inundation in Kailua-Kona. The computed maximum wave amplitude reaches 5 m at the warning point in the Japan M_w 9.3 scenario. The water front near Kona Pier and at end of Kailua Bay are under high flooding risk once inundation occurs in the forecast area.

Tsunami waves in the study area vary significantly for the eighteen magnitude 9.3 scenarios. These results show the complexity and high nonlinearity of tsunami waves and currents nearshore, which again demonstrate the value of the forecast model for providing accurate site-specific forecast details.

Wavelet analyses were performed for the 34 scenarios to explore peak resonant periods for the site. Figs. 16 and 17 show the amplitude spectrograms for the past and simulated tsunamis respectively. The spectrograms show wide range of resonant periods from 6 to 126 minutes. The most common peak period is near 8 (±2) minutes, which was the peak period for 23 scenarios (68% of the testing cases) (Fig. 18). In addition, long resonant periods, such as 67-126 minutes, can have similar amplitude as short period waves (Fig. 16.11 and 16.14). Although the spectrograms of the forecast model show longer peak period of 26 and 38 minutes for the M_w 93 Chile and Central America scenarios respectively, the short 8 minute period , which is the peak period of the

reference model, still exists in both spectrograms as the second peak period. The rest scenarios show excellent agreements in peak period for the reference and forecast models.

4.2 Uncertainty of the Forecast Maximum Amplitudes

Tables 5 and 6 and Figure 18 summarize the difference of the computed η_{max} at the warning point between the forecast and reference models for the 34 scenarios (16 past tsunamis and 18 simulated M_w 9.3 scenarios). For the M_w 9.3 scenarios, the forecast model results show similar η_{max} as those of the reference model except tsunamis coming from the east or northeast direction, particularly from the Japan, Izu, Kamchatka and Central Aleutian subduction zones. Among the 16 past tsunamis, the 1946 Unimak tsunami produces the largest discrepancy, 41% (0.42 m) difference (reference η_{max} = 1.01m). The 2011 Japan tsunami shows second largest discrepancy of 31% (0.43m) to the reference η_{max} =1.38 m.

Next we chose the 1946 Unimak tsunami for further testing. Test results reveal η_{max} is very sensitive to the offshore water depth (d_w) of the reference grids for this tsunami. For the same set of reference grids, 20 m and 1m d_w produce η_{max} of 1.01 m and 0.47 m respectively (Fig. 12). That is to say, difference in d_w may result twice of η_{max}. The forecast model shows η_{max} =0.7 m and 0.59 m for d_w = 20 m and 1m respetively. d_w is a model parameter used for A- and B-grids, at which a vertical wall is placed. Different d_w may represent difference shore line shapes. It may result different numerical dissipation. Without observations, it is difficult to fine-tune this parameter. As in Fig. 16, the 1946 Unimak tsunami is the only tsunami showing a strong resonant period of 6 min, lower than the most commonly seen 8 minutes. This extremely short resonant period may also

attribute to the large discrepancy. The forecast model can underestimate the short period waves due to its low spatial resolution.

Among the 18 M_w = 9.3 scenarios, the No. 1 Japan scenario (T_P = 8min) produces the largest difference of 1.48m or 30% (η_{max} =4.95m for the reference model). The No.2 Kamchatka and No. 18 Izu scenarios (with (T_P = 8 and 9 min) also show relatively large difference of 0.8 m or 25% (η_{max} =3.36 and 3.49 m for the reference model). One common characteristic of the three scenarios is the late arrival of η_{max}, which is the 10th , 12th and 12th wave respectively, arriving about 1-2 hours after the first wave (Figs. 13.1 13.2 and 13.18). For the Japan scenario, even the 24th wave exceeds 3 m elevation (Fig. 14.1). The multiple scattering of the first wave chain with the major wave scatterers in northwest Pacific can amplify these later waves (Tang et al., 2012). Therefore late wave chains are sensitively to model setup, such as the gird resolutions and offshore water depth. The coarse forecast A-grid may have more numerical dissipation in shallow water, especially for large amplitude waves of high frequency.

The forecast model was tested with both d_w=20m and d_w= 1 m for the 34 scenarios. The results are summarized in Tables 7 and 8. Since d_w= 1m produces larger late waves for tsunamis from east, it was chosen for the forecast model.

Figure 18 quantifies the uncertainty in the forecast η_{max}. When T_P >10min, the uncertainty in the forecast η_{max} is with 20%. When T_P ≤10min and η_{max} > 1m, the uncertainty is within 31%. When η_{max} <1m, uncertainty is within 25 cm. Scenarios from portion of Central Aleutian subduction zones near the Unimak Island may have additional uncertainty (about 0-41%), depending on whether or not a strong resonance of extremely short period (6 min) is excited on the site.

5 Summary and Conclusions

A tsunami forecast model was developed for the coastal community of Kailua-Kona, Hawaii. The computational grids for the forecast model were derived from the best available bathymetric and topographic data sources. The forecast model is optimizedly constructed at a resolution of 2-arc-sec (~60 m). A reference inundation model of higher resolution of 2/3 arc-sec (~20 m) was also developed in parallel, to provide modeling references for the forecast model. Both models were tested for 34 scenarios, including 16 past tsunamis and a set of 18 simulated magnitude 9.3 tsunamis. Since not coastal water level station exists in the forecast site, a point at 2.3 m water depth at the end of Kailua bay, east of Kona Pier, was chosen as the warning point.

The wave analyses of the amplitude time series show a wide range of resonant periods in the site, from 6-126 minutes. 68% of the tested scenarios have peak resonant period (T_P) near 8 (±2) minutes. For many cases, waves with very long resonant periods (67-126 minutes) can have similar influence as those of every short periods (6-10 minutes).

Tsunamis propagating from the east, particularly from Japan, Kamchatka and Izu subduction zones, have shown the late arrival of the maximum wave η_{max} of short period (~8 min). The η_{max} could be the 10th - 12th wave, arriving about 1-4 hours after the first wave. Both incident waves from the far-field and local resonances contribute to the late η_{max}. The developed forecast model involves a substantial large A-grid (2 arc-min), covering the entire Hawaiian Island Chain, Mid. Pacific Mountains, Mellish Seamount

and Koko Guyot. It can provide a more accurate simulation of the waves interacting with the major wave scatterers that are important to the forecast site, with the cost of longer computational time. It should be noted that the forecast system would adapt MOST version 4 that has parallel computation capability in the near future. Then the computation time can be reduced to minutes.

To achieve timely and effective forecast, and as a transition before MOST version 4 becomes operational, we developed a transitional forecast model for Kailua-Kona, which has the smaller, regular Hawaiian A-grid as other forecast sites on the Big Island, e.g. Kawaihae and Hilo forecast models. We refer it as set 1. It is capable of simulating four hours of tsunami wave dynamics in minutes of computational time. We refer the forecast model with larger A grid here as set 2. Set 2 will replace results from set 1 when it is available during real time.

The numerical consistency between the model outputs on the amplitude time series at warning point, maximum amplitude and current in the forecast area, are good in general. When T_P >10min, the uncertainty in the forecast $\eta_{\max}$ at the warning point is with 20%. When T_P ≤10min and $\eta_{\max}$ > 1m, the uncertainty is within 30%. When $\eta_{\max}$ <1m, the uncertainty in $\eta_{\max}$ is within 25 cm. Scenarios from portion of Central Aleutian subduction zones near Unimak Islands may have additional uncertainty (about 0-41%), depending on whether or not a strong resonance of extremely low period (6 min) is excited at the site.

The Japan, Kamchatka, Izu, Northern Tonga (Samoa), Aleutian, Southern Chile, East Philippines and Canada, subduction zones can potentially generate large amplitude waves and cause inundation in Kailua-Kona. The computed maximum wave amplitude reaches

1.38m and 5 m at the warning point for the 2011 Japan tsunami and the M_w 9.3 Japan scenario respectively among the past events and simulated scenarios. For the M_w 9.3 Japan scenario, even the 24th wave exceeds 3 m elevation. The water front near Kona Pier and the end of Kailua Bay are under high flooding risk once inundation occurs in the forecast area.

Due to the unique tsunami resonant characteristics of the site, a coastal water level station is highly recommended for Kailua-Kona area, to provide tsunami data for model calibration and to improve forecast accuracy.

Acknowledgements

The author thanks Jean Newman for discussion and assistance; Sandra Bigley for comments and editing; Burak Uslu for providing tables and graphics for the propagation database. Collaborative contributions of the National Weather Service, the National Geophysical Data Center, and the National Data Buoy Center were invaluable.

Funding for this publication and all work leading to development of a tsunami forecast model for Keauhou, Hawaii was provided by the National Oceanic and Atmospheric Administration. This publication was partially funded by the Joint Institute for the Study of the Atmosphere and Ocean (JISAO) under NOAA Cooperative Agreement No. NA17RJ1232, JISAO Contribution No. xxxx. This is PMEL Contribution No. xxxx.

References

Arcas, D., and B. Uslu (2010): A Tsunami Forecast Model for Crescent City, California. NOAA OAR Special Report, PMEL Tsunami Forecast Series: Vol. *2*, 112 pp, Gov. Print. Off., Seattle, Wash.

Bernard, E.N., H.O. Mofjeld, V.V. Titov, C.E. Synolakis, and F.I. González (2006): Tsunami: Scientific frontiers, mitigation, forecasting, and policy implications. Proc. Roy. Soc. Lon. A, 364(1845), doi: 10.1098/rsta.2006.1809, 1989–2007.

Bernard, E., and V.V. Titov (2007): Improving tsunami forecast skill using deep ocean observations, Mar. Technol. Soc. J., 40(3), 23–26.

Carignan, K.S., L.A. Taylor, B.W. Eakins, D.Z. Friday, P.R. Grothe, E. Lim and M. Love (2011): Digital Elevation Models of Keauhou and Kawaihae, Hawaii: Procedures, Data Sources and Analysis. NOAA National Geophysical Data Center (NGDC).

Gica E., Spillane, M.C., Titov, V.V., Chamberlin, C.D. and Newman, J.C. (2008): Development of the forecast propagation database for NOAA's Short-Term Inundation Forecast for Tsunamis (SIFT). NOAA Tech. Memo. OAR PMEL-139, 89pp.

Gusiakov, V.K. (1978): Static displacement on the surface of an elastic space. Ill-posed problems of mathematical physics and interpretation of geophysical data, Novosibirsk, VC SOAN SSSR, 23–51 (in Russian).

Gonzalez, F.I., E.N. Bernard, C. Meinig, M. Eble, H.O. Mofjeld, and S. Stalin (2005): The NTHMP tsunameter network. *Nat. Hazards*, 35(1), Special Issue, U.S. National Tsunami Hazard Mitigation Program, 25-39.

Hawaii County (2011): Hawaii County Surveys Tsunami Damage, Kona hit hard. http://www.bigislandvideonews.com/2011/03/11/hawaii-county-surveys-tsunami-damage-kona-hit-hard/

Lander, J. F. and P.A. Lockridge (1989): *United States Tsunamis 1690-1988*. NOAA National Environmental Satellite, Data and Information Service, National Geophysical Data Center, Boulder, Colorado, August 1989, 265pp.

Liu, P. L.-F. (2009): Tsunami modeling—Propagation, in The Sea, vol. 15, edited by E. Bernard and A. Robinson, chap. 9, pp. 295– 319, Harvard Univ. Press, Cambridge, Mass.

López, A.M. and E.A. Okal (2006); A seismological reassessment of the source of the 1946 Aleutian 'tsunami' earthquake. *Geophysical Journal International*, Volume 165, Issue 3, Page 835-849, Jun 2006, doi: 10.1111/j.1365-246X.2006.02899.x

Meinig, C., S.E. Stalin, A.I. Nakamura, F. González, and H.G. Milburn (2005): Technology Developments in Real-Time Tsunami Measuring, Monitoring and Forecasting. In Oceans 2005 MTS/IEEE, 19–23 September 2005, Washington, D.C.

National Geophysical Data Center, Global Tsunami Database (2000 BC to present):

http://www.ngdc.noaa.gov/seg/hazard/tsu_db.shtml

Okada, Y., 1985; Surface deformation due to shear and tensile faults in a half-space. *Bull. Seismol. Soc. Am*., 75, 1135-1154.

Pararas-Carayannis, G.(1969): *Catalog of Tsunamis in The Hawaii Islands*, World Data Center A Tsunami, ESSA – Coast and Geodetic Survey, 94 pp.

Percival, D.B., D.W. Denbo, M.C. Eble, E. Gica, H.O. Mofjeld, M.C. Spillane, L. Tang, and V.V. Titov (2011): Extraction of tsunami source coefficients via inversion of DART® buoy data. *Nat. Hazards*, 58(1), doi: 10.1007/s11069-010-9688-1, 567–590.

Satake, K., Y. Hasegawa, Y. Nishimae and Y. Igarashi (2008), Recent Tsunamis That Affected the Japanese Coasts and Evaluation of JMA's Tsunami Warnings. OS42B-03, AGU Fall Meeting, San Francisco.

Smith, W. H. F., and D. T. Sandwell (1997), Global seafloor topography from satellite altimetry and ship depth soundings, *Science*, 277, 1957– 1962.

Soloviev, S.L. and Ch.N Go (1984): *Catalog of Tsunamis on the Eastern Shore of Pacific Ocean*. Canadian Translation of Fisheries and Aquatic Sciences, No. 5078, 293 pp.

Soloviev, S.L., Ch.N Go and Kh.S Kim (1992): *Catalog of Tsunamis in The Pacific* 1969-1982. Results of Researches on The International Geophysical Projects, Academy of Sciences of the USSR Soviet Geophysical Committee, Moscow, 1992, 208 pp.

Spillane, M.C., E. Gica, V.V. Titov, and H.O. Mofjeld (2008): Tsunameter network design for the U.S. DART® arrays in the Pacific and Atlantic Oceans, Tech. Memo, OAR PMEL-143, 165pp., Gov. Print. Off., Seattle, Wash.

Synolakis, C.E., E.N. Bernard, V.V. Titov, U. Kânoğlu, and F.I. González (2008): Validation and verification of tsunami numerical models. Pure Appl. Geophys., 165(11–12), 2197–2228.

Tang, L., C. Chamberlin, E. Tolkova, M. Spillane, V.V. Titov, E.N. Bernard, and H.O. Mofjeld (2006): Assessment of potential tsunami impact for Pearl Harbor, Hawaii. NOAA Tech. Memo. OAR PMEL-131.

Tang, L., C. Chamberlin and V.V. Titov, (2008a): Developing tsunami forecast inundation models for Hawaii: procedures and testing, *NOAA Tech. Memo., OAR PMEL -141*, 46 pp.

Tang, L., V.V. Titov, Y. Wei, H.O. Mofjeld, M. Spillane, D. Arcas, E.N. Bernard, C. Chamberlin, E. Gica, and J. Newman (2008b): Tsunami forecast analysis for the May 2006 Tonga tsunami. J. Geophys. Res., 113, C12015, doi: 10.1029/2008JC004922.

Tang, L., V. V. Titov, and C. D. Chamberlin (2009): Development, Testing, and Applications of Site-specific Tsunami Inundation Models for Real-time Forecasting. *J. Geophys. Res*., 114, C12025, doi:10.1029/2009JC005476..

Tang, L., V.V. Titov and C.D. Chamberlin (2010): A Tsunami Forecast Model for Hilo, Hawaii. NOAA OAR Special Report, PMEL Tsunami Forecast Series: Vol. 1, 44 *pp.*

Tang, L., V. V. Titov, E. Bernard, Y. Wei, C. Chamberlin, J. C. Newman, H. Mofjeld, D. Arcas, M. Eble, C. Moore, B. Uslu, C. Pells, M. C. Spillane, L. M. Wright, and E. Gica (2012): Direct energy estimation of the 2011 Japan tsunami using deep-ocean pressure measurements. *J. Geophys. Res., 117*, C08008, doi:10.1029/2011JC007635.

Titov, V. V., C. W. Moore, D. J. M. Greenslade, C. Pattiaratchi, R. Badal, C. E. Synolakis, and U. Kânoğlu (2011): A new tool for inundation modeling: Community Modeling Interface for Tsunamis (ComMIT). Pure Appl. Geophys., 168, 2121–2131, doi:10.1007/s00024-011-0292-4.

Titov, V. V., and L. Tang (2011): Estimating tsunami magnitude in real time usingttsunameter data, paper presented at XXV IUGG General Assembly, Melbourne, Victoria, Australia, 28 Jun to 7 Jul.

Titov, V.V. (2009): Tsunami forecasting. Chapter 12 in The Sea, Volume 15: Tsunamis, Harvard University Press, Cambridge, MA and London, England, 371–400.

Titov, V.V., F.I. González, E.N. Bernard, M.C. Eble, H.O. Mofjeld, J.C. Newman, and A.J. Venturato (2005): Real-time tsunami forecasting: Challenges and solutions. *Natural Hazards*, 35(1), Special Issue, U.S. National Tsunami Hazard Mitigation Program, 41–58.

Titov, V. V., Mofjeld, H. O., Gonza´ lez, F. I., and Newman, J. C.: 2001, Offshore forecasting of Alaskan tsunamis in Hawaii. In: G. T. Hebenstreit (ed.), Tsunami

Research at the End of a Critical Decade. Birmingham, England, Kluwer Acad. Pub., Netherlands, pp. 75–90.

Titov, V.V., H.O. Mofjeld, F.I. Gonzalez and J.C. Newman (1999): Offshore forecasting of Alaska-Aleutian subduction zone tsunamis in Hawaii. NOAA Technical Memorandum. ERL PMEL-114, January 1999, 22 pp.

Titov, V.V. and C.S. Synolakis (1998): Numerical modeling of tidal wave runup. *Journal of Waterway, Port, Coastal and Ocean Engineering*, ASCE, 124(4), 157-171.

Titov, V.V. and F.I. Gonzalez (1997): Implementation and testing of the Method of Splitting Tsunami (MOST) model. NOAA Technical Memorandum. NOAA Pacific Marine Environmental Laboratory, ERL PMEL-112, Nov. 1997, 11 pp.

Tolkova, E. (2007): Compression of MOST Propagation Database. NOAA Tech. Memo. OAR PMEL-134, NTIS: PB2007-108218, 9 pp., Gov. Print. Off., Seattle, Wash.

Pararas-Carayannis, G.(1969): *Catalog of Tsunamis in The Hawaii Islands*, World Data Center A Tsunami, ESSA – Coast and Geodetic Survey, 94 pp.

Walker, D.A. (2004): Regional Tsunami evacuations for the state of Hawaii: a feasibility study on historical runup data. Science of Tsunami Hazards, 22(1), 3-22.

Wei, Y., E. Bernard, L. Tang, R. Weiss, V. Titov, C. Moore, M. Spillane, M. Hopkins, and U. Kânoğlu (2008): Real-time experimental forecast of the Peruvian tsunami of August 2007 for U.S. coastlines. Geophys. Res. Lett., 35, L04609, doi: 10.1029/2007GL032250.

Wei, Y., and D. Arcas (2010): A tsunami forecast model for Kodiak, Alaska. NOAA OAR Spec. Rep./PMEL Tsunami Forecast Ser. 4, 96 pp., Gov. Print. Off., Seattle, Wash.

Wei, Y., C. Chamberlin, V.V. Titov, L. Tang, and E.N. Bernard (2012): Modeling of 2011 Japan Tsunami - lessons for near-field forecast. Pure Appl. Geophys., doi: 10.1007/s00024-012-0519-z.

Whitmore, P.M. (2003): Tsunami amplitude prediction during events: A test based on previous tsunamis. In *Science of Tsunami Hazards*, 21, 135–143.

Table 1 Tsunami source functions in the Pacific, Atlantic and Indian Oceans.

Source Zone			Tsunami source functions	
No.	**Abbr.**	**Name**	**Line/zone**	**Numbers**
1	ACSZ	Aleutian-Alaska-Canada-Cascadia	BAZYXW	184
2	CSSZ	Central-South American	BAZYX	382
3	EPSZ	East Philippines	BA	44
4	KISZ	Kamchatka-Kuril-Japan Trench-Izu Bonin-Marianas-Yap	BAZYXW	229
5	MOSZ	Manus Ocean Convergence Boundary	BA	34
6	NVSZ	New Britain-Solomons-Vanuatu	BA	74
7	NGSZ	North New Guinea	BA	30
8	NTSZ	New Zealand-Kermadec-Tonga	BA	81
9	NZSZ	South New Zealand	BA	14
10	RNSZ	New Ryukus-Kyushu-Nankai	BA	44
11	KISZ	Kamchatskii-Bering Source Zone	BAZ	13
			Subtotal:	**1129**
12	ATSZ	Atlantic	BA	214
13	SSSZ	South Sandwich	BAZ	33
			Subtotal:	**247**
14	IOSZ	Adaman-Nicobar-Sumatra-Java	BAZY	307
15	MKSZ	Makran	BA	20
16	WPSZ	West Philippines	BA	22
			Subtotal:	**349**
			Total:	**1725**

Table 2 Tsunami sources for past events.

Earthquake / Seismic				Model		
Event	**USGS Date Time (UTC) Epicenter**	**CMT Date Time (UTC) Centroid**	**Magnitude Mw (CMT)**	**Tsunami Magnitude[1]**	**Subduction Zone**	**Tsunami Source**
1946 Unimak	01 Apr 12:28:56 52.75ºN 163.50ºW	n/a	[2]8.5	8.5	Aleutian-Alaska-Cascadia (ACSZ)	7.5 × b23 + 19.7 × b24 + 3.7 × b25
1952 Kamchatka	04 Nov 16:58:26.0 [3]52.76ºN 160.06ºE	n/a	[3]9.0	8.7	Kamchatka-Kuril-Japan-Izu-Mariana-Yap (KISZ)	Tang *et al.* (2006)
1957 Andreanov	09 Mar 14:22:31 51.56ºN 175.39ºW	n/a	[3]8.6	8.7	Aleutian-Alaska-Cascadia (ACSZ)	31.4 × a15 + 10.6 × a16 + 12.2 × a17
1960 Chile	22 May 19:11:14 [3]38.29ºS 73.05ºW	n/a	[4]9.5	n/a	Central-South America (CSSZ)	Kanamori & Ciper (1974)
1964 Alaska	28 Mar 03:36:00 [3]61.02ºN 147.65ºW	n/a	[3]9.2	8.9	Aleutian-Alaska-Cascadia (ACSZ)	15.4 × a34+19.4×a35+ 48.3 × z34+18.3×b34+15.1×b35
1994 East Kuril	04 Oct 13:22:58 43.73ºN 147.321ºE	04 Oct 13:23:28.5 43.60ºN 147.63ºE	8.3	8.2	Kamchatka-Kuril-Japan-Izu-Mariana-Yap (KISZ)	1.3 × a20 + 3.2 × z19 +5.9 × b20
1996 Andreanov	10 Jun 04:03:35 51.56ºN 175.39ºW	10 Jun 04:04:03.4 51.10ºN 177.410ºW	7.9	8.0	Aleutian-Alaska-Cascadia (ACSZ)	5.55 × b15
2003 Hokkaido	25 Sep 19:50:06 41.775ºN 143.904ºE	25 Sep 19:50:38.2 42.21ºN 143.84ºE	8.3	8.0	Kamchatka-Kuril-Japan-Izu-Mariana-Yap (KISZ)	3.6m × (100 × 100km) 109#rake, 20#dip, 230#strike, 25 m depth
2003 Rat Island	17 Nov 06:43:07 51.13ºN 178.74ºE	17 Nov 06:43:31.0 51.14ºN 177.86ºE	7.7	7.9	Aleutian-Alaska-Cascadia (ACSZ)	2.7 × b11 + 0.9 × a12
2006 Tonga	03 May 15:26:39 20.13ºS 174.161ºW	03 May 15:27:03.7 20.39ºS 173.47ºW	8.0	8.0	New Zealand-Kermadec-Tonga (NTSZ)	6.6 × b29 (Tang *et al*., 2008)
2006 Kuril	15 Nov 11:14:16 46.607ºN 153.230ºE	15 Nov 11:15:08 46.71ºN 154.33ºE	8.3	8.1	Kamchatka-Kuril-Japan-Izu-Mariana-Yap (KISZ)	3.2×a12+6.0×z12
2007 Kuril	13 Jan 04:23:20 46.272ºN 154.455ºE	13 Jan 04:23:48.1 46.17ºN 154.80ºE	8.1	7.8	Kamchatka-Kuril-Japan-Izu-Mariana-Yap (KISZ)	-3.2 × b13
2007 Solomon	01 Apr 20:39:56 8.481ºS 156.978ºE	01 Apr 20:40:38.9 7.76ºS 156.34ºE	8.1	8.2	New Britain-Solomons-Vanuatu (NVSZ)	12.0 × b10
2007 Peru	15 Aug 23:40:57 13.354ºS 76.509ºW	15 Aug 23:41:57.9 13.73ºS 77.04ºW	8.0	8.3	Central-South America (CSSZ)	3.6×a62+5.7×z63+5.3×b62
2009 Samoa	29 Sep 17:48:10 15.509ºS 172.034ºW	29 Sep 17:48:26.8 15.13ºS 171.97ºW	8.1	8.2	New Zealand-Kermadec-Tonga (NTSZ)	a34×6.4+3.2×c35
2010 Chile	27 Feb 06:34:14 35.909ºS 72.733ºW	27 Feb 06:35:15.4 35.95ºS 73.15ºW	8.8	8.8	Central-South America (CSSZ)	a87× 9.68+z88 ×24.5+a88×15.35+a91× 13.19+z92×24.82

[1] Preliminary source – derived from tsunami source functions and deep-ocean observations
[2] López and Okal (2006)
[3] United States Geological Survey (USGS)
[4] Kanamori and Ciper (1974)
[5] Tsunami source was obtained in real time and applied to the forecast

2011 Japan	11 March 05:46:23 38.322ºN 142.369 E	11 March 05:47:32.8 37.52ºS 143.05 E	9.1	8.8	Kamchatka-Kuril-Japan-Izu-Mariana-Yap (KISZ)	[5]4.66× b24 + 12.23 ×b25+26.31× a26+21.27×b26+22.75 ×a27+4.98× b27

Table 3 MOST setups of Kona reference and forecast models.

Grid	Region	Reference Model				Forecast model		
		Coverage Lon. (^oE) Lat. (^oN)	**Cell Size (")**	**Time Step (sec)**		**Coverage Lon. (^oE) Lat. (^oN)**	**Cell Size (")**	**Time Step (sec)**
A	Hawaii	165 - 210 10.4 - 40	60 (2701x 1777)	4	A	199 - 205.9667 18.0317 - 22.9983	120 (1351 x 889)	8.4
B	Big Island	201-206 17.5-22	6 (3001 x 2701)	0.7	B	202.84833 - 205.395 18.695 - 21.4283	24 (383 x 411)	2.8
C	Southeast Big Island	2203.87 – 204.1392 19.015 – 19.8483	2 (482 x 1501)	0.3	C	203.9248 - 204.0594 19.47065 - 19.8161	2-6 (144 x 334)	0.4
D	Kona	203.9388-204.0879	2/3 (806 x 1313)	0.12				

Minimum offshore depth (m)		20	1
Water depth for dry land (m)		0.1	0.1
Manning coefficient		0.025	0.04
Computational time for a 4-hr simulation	MOST V2		**30 minutes**
	MOST V4, 1 processor		**16 minutes**
	MOST V4, 2 processors		**10 minutes**

Table 4 Computational time vs. number of processors used for the Kona forecast model with MOST version 4. Results are based on an 8-hour event simulation of the 2011 Japan tsunami.

Number of Processors	1	2	4	8	16
A-grid (min)	26.0	18.1	11.4	6.9	4.9
B-grid (min)	3.2	2.2	1.6	1.3	1.3
C-grid (min)	4.0	3.2	2.9	4.0	4.5
Total time (min)	33.1	23.5	15.8	12.2	10.6

Table 5 Maximum wave crest at the Kona warning point computed by the reference and forecast models.

No.	Event ID	Ref. model η_{max} (m)	Ref. model tmax (hour)	Forecast Model η_{max} (m)	Forecast Model tmax (hour)	Error (m)	Error (%)
1	19460401	0.47	5.717	0.59	5.489	0.12	25
2	19521104	0.35	7.973	0.24	9.945	-0.11	-31
3	19570309	0.78	8.273	0.55	8.571	-0.24	-30
4	19600522	0.63	14.857	0.63	14.876	-0.01	0
5	19640328	0.21	6.612	0.15	5.558	-0.06	-27
6	19941004	0.34	9.918	0.28	9.933	-0.06	-17
7	19960610	0.25	8.217	0.17	10.493	-0.08	-32
8	20030925	0.04	9.218	0.03	9.222	-0.01	0
9	20031117	0.10	7.791	0.07	7.931	-0.04	-35
10	20060503	0.13	7.553	0.12	7.558	-0.01	0
11	20061115	0.10	8.184	0.10	8.210	-0.00	0
12	20070113	0.15	8.446	0.12	10.102	-0.03	-22
13	20070815	0.02	13.053	0.02	13.067	-0.00	0
14	20090929	0.17	6.217	0.16	6.213	-0.00	0
15	20100227	0.22	15.851	0.22	15.851	-0.00	0
16	20110311	1.38	8.718	0.95	8.748	-0.43	-31

Table 6 Sources of the 18 Mw 9.3 synthetic tsunamis and maximum wave crest at the Kona warning point computed by the reference and forecast models.

No.	Subd. Zone	Source	alpha	Ref. model η_{max} (m)	Ref. model tmax (hour)	Forecast Model η_{max} (m)	Forecast Model tmax (hour)	Error (m)	Error (%)	Location
1	KISZ AB	22-31	29	4.95	8.866	3.47	8.884	-1.48	-30	Japan
2	KISZ AB	1-10	29	3.36	7.977	2.53	8.008	-0.83	-25	Kamchatka
3	ACSZ AB	16-25	29	2.49	7.519	1.91	5.512	-0.58	-23	Central Aleutian
4	ACSZ AB	22-31	29	1.54	7.212	1.58	6.038	0.03	2	Unimak
5	ACSZ AB	50-59	29	1.33	7.970	1.52	6.215	-1.21	14	Canada
6	ACSZ AB	56-65	29	0.80	6.767	0.61	7.040	-0.20	-25	Cascadia
7	CSSZ AB	1-10	29	0.26	7.170	0.26	7.164	-0.00	0	Central American
8	CSSZ AB	41-50	29	0.27	12.300	0.27	12.302	0.00	0	Columbia-Ecuador
9	CSSZ AB	86-95	29	0.97	16.433	0.80	16.429	-0.16	-17	Chile
10	CSSZ AB	100-109	29	2.39	16.534	2.31	16.384	-0.07	-3	Southern Chile
11	NTSZ AB	20-29	29	0.63	8.463	0.58	8.465	-0.05	-8	Tonga
12	NTSZ AB	30-39	29	2.81	6.166	2.68	6.171	-0.13	-5	Northern Tonga
13	NVSZ AB	28-37	29	1.02	8.034	1.18	8.029	0.16	16	Vanuatu
14	MOSZ AB	1-10	29	1.13	8.300	1.19	8.275	0.05	5	Manus
15	NGSZ AB	3-12	29	0.34	11.700	0.31	11.715	-0.03	-9	New Guinea
16	EPSZ AB	6-15	29	1.89	11.752	1.74	11.732	-0.15	-8	East Philippines
17	RNSZ AB	12-21	29	0.81	10.551	0.71	10.529	-0.10	-12	Nankai
18	KISZ AB	32-41	29	3.49	8.984	2.65	8.998	-0.84	-24	Izu

Table 7 Maximum sea surface elevation at the Kona warning point computed by the forecast model with 1 and 20m offshore water depth for past tsunamis.

No.	Event ID	d_w =1m η_{max} (m)	tmax (hour)	d_w =20m η_{max} (m)	tmax (hour)	Error (m)	(%)
1	19460401	0.59	5.489	0.70	5.734	0.12	20
2	19521104	0.24	9.945	0.32	8.342	0.08	33
3	19570309	0.55	8.571	0.52	8.571	-0.02	-4
4	19600522	0.63	14.876	0.63	14.876	0.00	0
5	19640328	0.15	5.558	0.16	6.622	0.01	0
6	19941004	0.28	9.933	0.28	9.926	0.00	0
7	19960610	0.17	10.493	0.17	11.305	-0.01	0
8	20030925	0.03	9.222	0.03	9.222	0.00	0
9	20031117	0.07	7.931	0.07	7.931	-0.00	0
10	20060503	0.12	7.558	0.11	7.558	-0.00	0
11	20061115	0.10	8.210	0.10	8.210	-0.00	0
12	20070113	0.12	10.102	0.13	8.485	0.00	0
13	20070815	0.02	13.067	0.02	13.067	-0.00	0
14	20090929	0.16	6.213	0.16	6.213	-0.00	0
15	20100227	0.22	15.851	0.22	15.851	-0.00	0
16	20110311	0.95	8.748	0.87	8.867	-0.08	-8

Table 8 Maximum sea surface elevation at the Kona warning point computed by the forecast model with 1 and 20m offshore water depth for simulated M_w 9.3 tsunamis.

No.	Subd. Zone	Source	alpha	d_w =1 m η_{max} (m)	tmax (hour)	d_w =20 m η_{max} (m)	tmax (hour)	Error (m)	(%)	Location
1	KISZ	AB 22-31	29	3.47	8.884	3.16	8.891	-0.31	-9	Japan
2	KISZ	AB 1-10	29	2.53	8.008	2.50	8.344	-0.03	-1	Kamchatka
3	ACSZ	AB 16-25	29	1.91	5.512	2.05	5.512	0.14	7	Central Aleutian
4	ACSZ	AB 22-31	29	1.58	6.038	1.48	5.541	-0.09	-6	Unimak
5	ACSZ	AB 50-59	29	1.52	6.215	1.82	6.215	0.30	20	Canada
6	ACSZ	AB 56-65	29	0.61	7.040	0.53	6.081	-0.08	-13	Cascadia
7	CSSZ	AB 1-10	29	0.26	7.164	0.28	9.866	0.03	12	Central American
8	CSSZ	AB 41-50	29	0.27	12.302	0.27	12.295	-0.00	0	Columbia-Ecuador
9	CSSZ	AB 86-95	29	0.80	16.429	0.76	16.429	-0.05	-6	Chile
10	CSSZ	AB100-109	29	2.31	16.384	2.26	16.384	-0.05	-2	Southern Chile
11	NTSZ	AB 20-29	29	0.58	8.465	0.59	8.465	0.01	0	Tonga
12	NTSZ	AB 30-39	29	2.68	6.171	2.71	6.171	0.03	1	Northern Tonga
13	NVSZ	AB 28-37	29	1.18	8.029	1.18	8.029	0.00	0	Vanuatu
14	MOSZ	AB 1-10	29	1.19	8.275	1.18	8.275	-0.01	0	Manus
15	NGSZ	AB 3-12	29	0.31	11.715	0.29	11.715	-0.03	-8	New Guinea
16	EPSZ	AB 6-15	29	1.74	11.732	1.83	11.725	0.09	5	East Philippines
17	RNSZ	AB 12-21	29	0.71	10.529	0.70	10.529	-0.01	0	Nankai
18	KISZ	AB 32-41	29	2.65	8.998	2.30	8.998	-0.35	-13	Izu

Appendix A.

The following appendix lists the input files for Kona developed in 2012.

A1. Reference model *.in file for Kona , Hawaii for MOST version 4.0

```
# -----------   MOST Run 1  -------------
# 0. Preparations
echo '#-------------------------------------------------#'
echo '#                Preprocess MOST input         #'
echo '#-------------------------------------------------#'
set main_dir="/home/tg23/data/tang/sims/kona/"
set path_w="$main_dir/konav4_H12_20070113_rb3_12h/"
set path_e="/grid/tg23/data/tolkova/public_html/v4/v4code/RttdMost_mp"

if ( -d $path_w )  then
echo $path_w 'exist'
echo ' Removing files '
  cd $path_w
#   rm -r *
else
  echo Creating directory $path_w
  mkdir $path_w
  cd  $path_w
endif

ln -sf /home/tg23/data/tang/bathy/kona/kona_rb3r1/*.nc .

# ---------------------------------------------------------
# 1. Generate INPUT for MOST
# ~~~~~~~~~~~~~~~~~~~~~~~~
# ~~~~~~~~~~~A~~~~~~~~~~~~
cat > most3_facts_nc.inA<< EOF
0.001     Minimum amplitude of input offshore wave (m):
20        Input minimum depth for offshore (m)
0.1       Input "dry land" depth for inundation (m)
0.0009    Input friction coefficient (n**2)
2         Number of grids
2         Interpolation domain for outer boundary
2         inner boundary
RA_HI_1min_20120417.nc
RB_keauhou_6s_20111107.nc
1           Runup flag
4      Input time step (sec)
10800     Input amount of steps
0              COntunue after input stops
15     Input number of steps between snapshots
1      saving inner boundaries every n-th timestep
1        ...Saving grid every n-th node, n=
0        1=initial deformation
EOF
cp most3_facts_nc.inA most3_facts_nc.in
setenv OMP_NUM_THREADS 6
#$path_e A  $path_src most3_facts_nc.in
# ~~~~~~~~~~~~~~~~~~~~~~~~
```

```
# ~~~~~~~~~~~B~~~~~~~~~~~~
cat > most3_facts_nc.inB<<EOF
0.001    Minimum amplitude of input offshore wave (m):
20       Input minimum depth for offshore (m)
0.1      Input "dry land" depth for inundation (m)
0.0009   Input friction coefficient (n**2)
2        Number of grids
2        Interpolation domain for outer boundary
2        inner boundary
RB_keauhou_6s_20111107.nc
RC_BIgIs_SW2s_20120417.nc
1        Runup flag
0.7      Input time step (sec)
61714    Input amount of steps
0        COntunue after input stops
86    Input number of steps between snapshots
1      saving inner boundaries every n-th timestep
1       ...Saving grid every n-th node, n=
0       1=initial deformation
EOF
cp most3_facts_nc.inB most3_facts_nc.in
setenv OMP_NUM_THREADS 4
# $path_e B A most3_facts_nc.in

# ~~~~~~~~~~~C~~~~~~~~~~~~
cat > most3_facts_nc.inC<< EOF
0.001      Minimum amplitude of input offshore wave (m):
-300       Input minimum depth for offshore (m)
0.1        Input "dry land" depth for inundation (m)
0.0016     Input friction coefficient (n**2)
2          Number of grids
2
2
RC_BIgIs_SW2s_20120417.nc
RD_Keauhou_Kona_20m_20120424.nc
2          runup
0.3        Input time step (sec)
320000     Input amount of steps
0          countinue after input stop
100        Input number of steps between snapshots
1          ...Saving inner boundary
1          ...Saving grid every n-th node, n=
0
EOF
cp most3_facts_nc.inC most3_facts_nc.in
setenv OMP_NUM_THREADS 2
$path_e C B  most3_facts_nc.in
# ~~~~~~~~~~~~~~~~~~~~~~~~
# ~~~~~~~~~~~D~~~~~~~~~~~~
cat > most3_facts_nc.inD<< EOF
0.001      Minimum amplitude of input offshore wave (m):
-300       Input minimum depth for offshore (m)
0.1        Input "dry land" depth for inundation (m)
0.0009     Input friction coefficient (n**2)
1          Number of grids
2
2
RD_Keauhou_Kona_20m_20120424.nc
2          runup
0.12       Input time step (sec)
```

```
1440000     Input amount of steps
0         countinue after input stop
120        Input number of steps between snapshots
1         ...Saving inner boundary
1         ...Saving grid every n-th node, n=
0
EOF
cp most3_facts_nc.inD most3_facts_nc.in
setenv OMP_NUM_THREADS 2
$path_e D C  most3_facts_nc.in &
```

A2. Forecast model *.in file for Kona, Hawaii for MOST version 2.0

```
0.0001                  Minimum amplitude of input offshore wave (m):
1                        Input minimum depth for offshore (m)
0.1                     Input "dry land" depth for inundation (m)
0.0016    Input friction coefficient (n**2)
1                       runup flag for grids A and B (1=yes,0=no)
300.0                   blowup limit
0.4                     Input time step (sec)
180000                  Input amount of steps
21                      Compute "A" arrays every n-th time step, n=
7                       Compute "B" arrays every n-th time step, n=
63                      Input number of steps between snapshots
1                       ...Starting from
1                        ...Saving grid every n-th node, n=
FA_HI_CP_2min_20120418.ssl
FB_keauhou_24s_20111107.ssl
Kona_2x2_6x6_20120420_subsR1.ssl
/home/tg23/data/tang/src_nc/src_sim_test/kona//
./
 1 1 1 1
1
1 66  112               Kona warning point 204.0046 °E, 19.6397 °N, water depth of 2.3 m
```

Figures

Figure 1 (a) Overview of the tsunami Forecast System. System components include tsunameter (DART) network (triangles), pre-computed tsunami source function (unfilled black rectangles) and high-resolution forecast models (red squares). Filled color shows the offshore forecast of the computed maximum sea surface elevation in m for the March 11, 2011 tsunami. Contours indicate the travel time in hours. (b) Sixteen past tsunamis and (c) eighteen simulated magnitude 9.3 tsunamis tested in this study. 3

Figure 2 Photos show (a-c) water levels and (d) aftermath at Kailua-Kona, Hawaii from the 2011 Japan tsunami. (a and b) Kailua Bay low and high water during the tsunami. (d) Damage at Alii Drive Kailua-Kona. (Photos a, b and d taken by Joel Noa; photo c from http://logisticsmonster.com/2011/03/10/8-9-magnitute-earthquake-hits-japan-major-tsunami-warnings/) 5

Figure 3 Forecast model setups for 13 forecast sites in Hawaii: (a) 2-arc-min (~3600m) regional, (b) 12-18-arc-sec (~360-540m) intermediate and (c) 2-arc-sec (~60m) nearshore grids for Nawiliwili, Honolulu, Kahului and Hilo. Red dots, coastal tide stations. 6

Figure 4 An aerial photo of Kona-Kailua (Image courtesy Pacific Disaster Center 2000). 7

Figure 5 A chart of the Big Island, Hawaii (NOAA Chart 19010). Soundings in fathoms at Mean Lower Low Water. Contour and summit elevation values ate in feet above Mean Sea Level. 8

Figure 6 Population density, Hawaii. (Source: 2000Census) 9

Figure 7 Run-ups in feet for Kailua-Kona coast for the 1946, 1952,1957, 1960 and 1964 tsunamis (Image from Walker, 2004). 10

Figure 8 Bathymetric and topographic data source overview. (a) 6" sec (~180m) Hawaii DEM 11

Figure 9 The Kailua-Kona reference model includes four layers of grids with increasing resolutions of (a) 60" (1800m), (b) 6" (180m),(c) 2" (60m) and (d) 2/3" (20m). □, nested grid boundary; ● warning points 13

Figure 10 The Kailua-Kona forecast model include three layer of grids with increasing resolutions of (a) 120" (3600m), (b) 24" (720m) and (c) 2- 6 "(60-180m). (d) Each line represents every 4th node in C-grid. □, nested grid boundary; ●, Kailua-Kona warning point at 204.0046 °E, 19.6397 °N, water depth of 2.3 m. 15

Figure 11 Modeled time series of sea surface elevation η at Kailua-Kona warning point for the past 16 tsunamis. o and + η_{max} , computed by the reference and forecast models respectively. 19

Figure 12 Computed η with different model setups for the 1946 Unimak tsunami.. 20

Figure 13 Computed maximum sea surface elevation and current by the Kailua-Kona reference and forecast models for the sixteen past tsunami..... 36

Figure 14 Modeled time series of sea surface elevation η at Kailua-Kona warning point for the eighteen simulated magnitude 9.3 tsunamis. o and + η_{max} , computed by the reference and forecast models respectively..... 39

Figure 15 Computed maximum sea surface elevation and current by the Kailua-Kona reference and forecast models for the eighteen simulated magnitude 9.3 tsunami... 58

Figure 16 (a) Modeled η time series at Kailua-Kona warning point for the past 16 tsunamis. (b) Wavelet–derived amplitude spectra for the reference model. (c and d) Real part of the spectrograms computed by the reference and forecast models. 64

Figure 17 (a) Modeled η time series at Kailua-Kona warning point for the 18 simulated M_w=9.3 tsunamis. (b) Wavelet–derived amplitude spectrogram for the reference model. (c and d) Real part of the spectrograms computed by the reference and forecast models. 71

Figure 18 (a) Uncertainty in the η_{max} at Kailua-Kona warning point computed by the reference and forecast models for the 34 scenarios. (b) Large Uncertainty is associated with short peak wave period near 8 min. Filled markers, 16 past tsunamis; open markers, 18 simulated M_w = 9.3 tsunamis..... 72

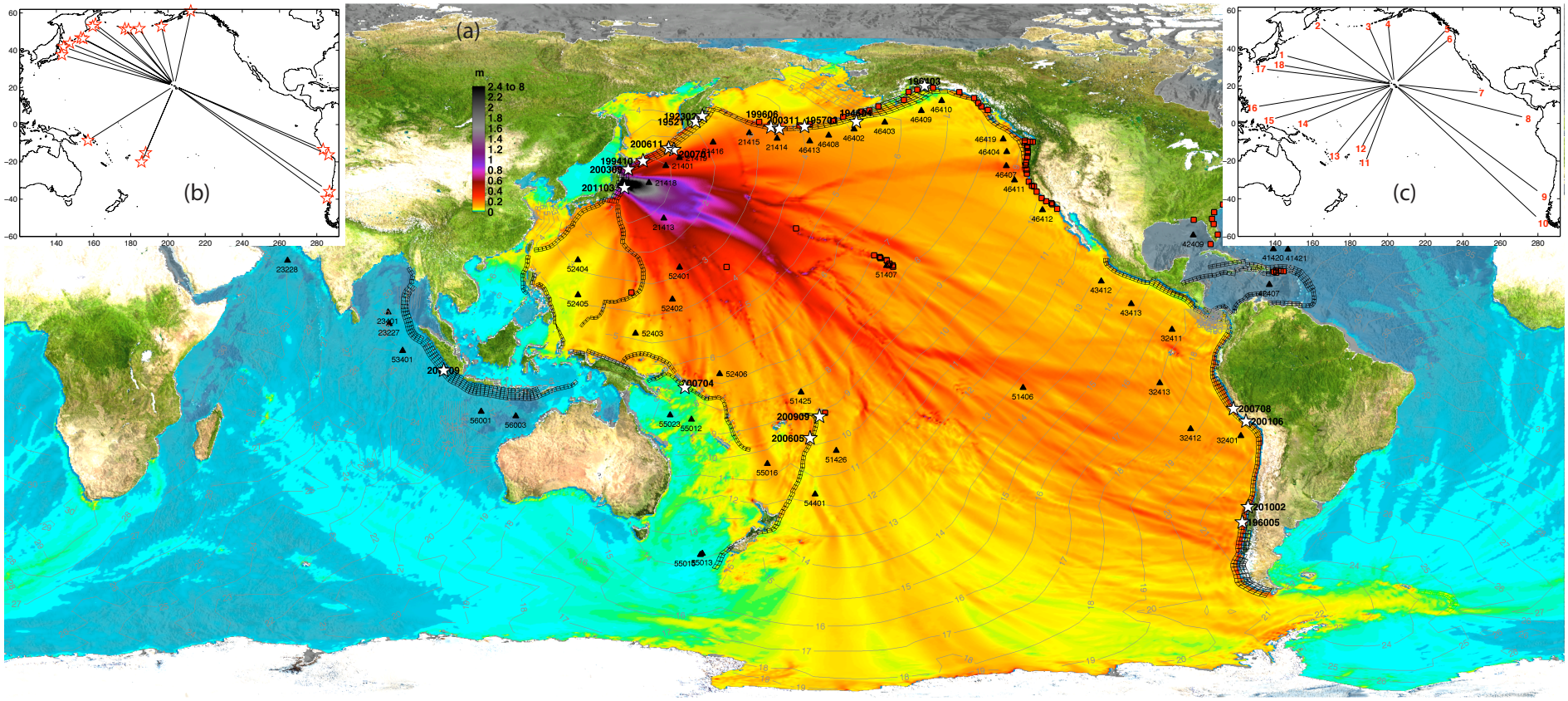

Figure 1 (a) Overview of the tsunami Forecast System. System components include tsunameter (DART) network (triangles), pre-computed tsunami source function (unfilled black rectangles) and high-resolution forecast models (red squares). Filled color shows the offshore forecast of the computed maximum sea surface elevation in m for the March 11, 2011 tsunami. Contours indicate the travel time in hours. (b) Sixteen past tsunamis and (c) eighteen simulated magnitude 9.3 tsunamis tested in this study.

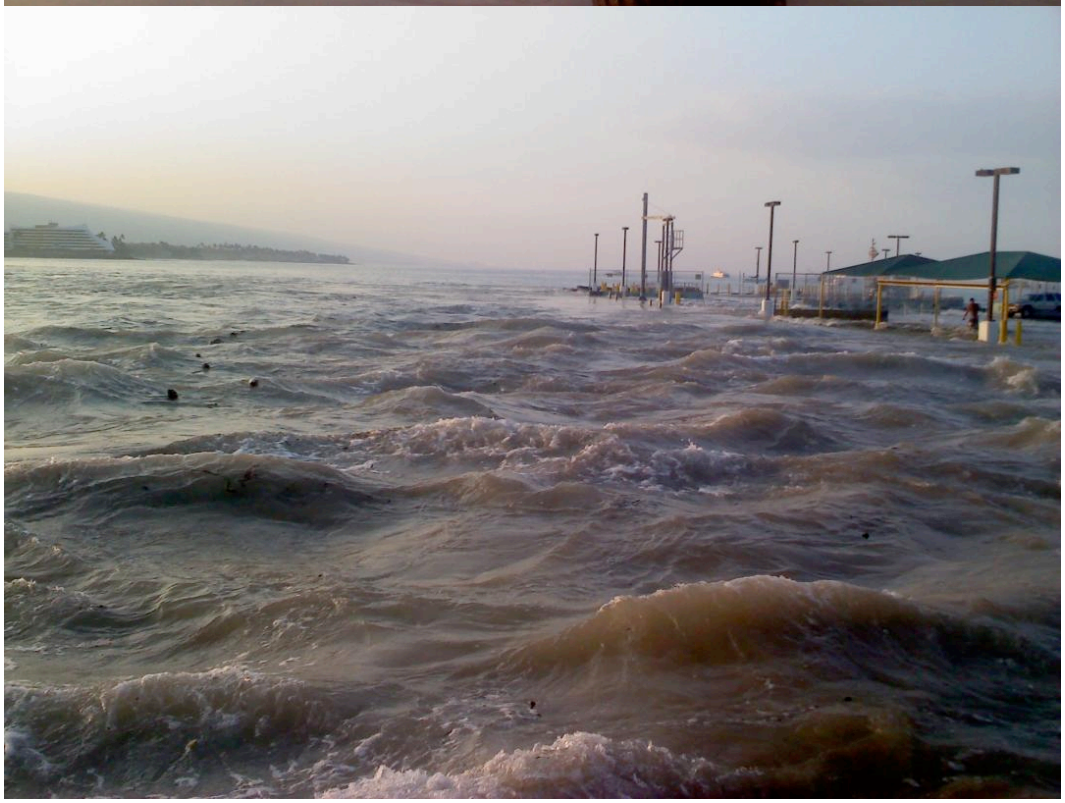

Figure 2 Photos show (a-c) water levels and (d) aftermath at Kailua-Kona, Hawaii from the 2011 Japan tsunami. (a and b) Kailua Bay low and high water during the tsunami. (d) Damage at Alii Drive Kailua-Kona. (Photos a, b and d taken by Joel Noa; photo c from http://logisticsmonster.com/2011/03/10/8-9-magnitute-earthquake-hits-japan-major-tsunami-warnings/)

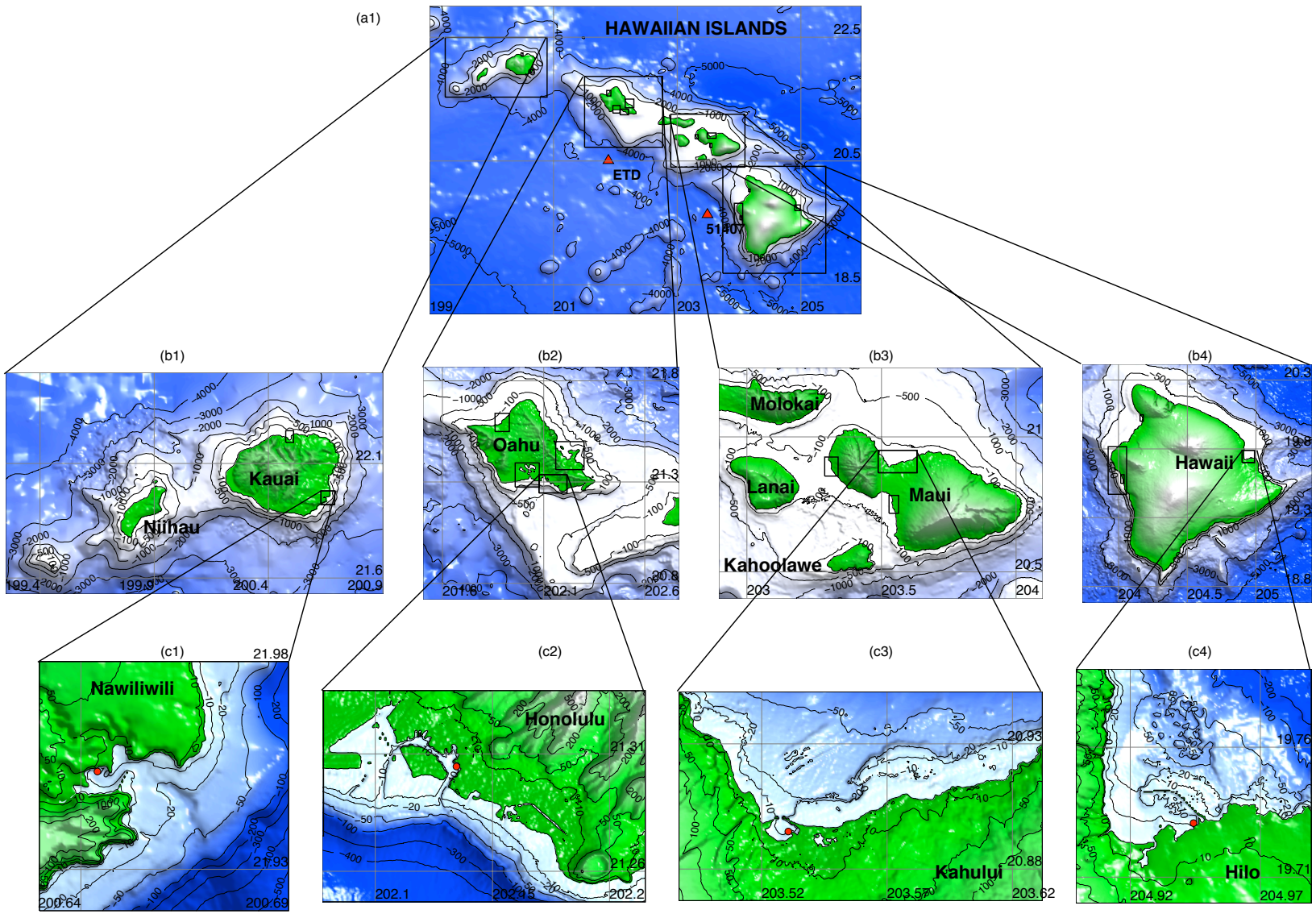

Figure 3 Forecast model setups for 13 forecast sites in Hawaii: (a) 2-arc-min (~3600m) regional, (b) 12-18-arc-sec (~360-540m) intermediate and (c) 2-arc-sec (~60m) nearshore grids for Nawiliwili, Honolulu, Kahului and Hilo. Red dots, coastal tide stations.

Figure 4 An aerial photo of Kona-Kailua (Image courtesy Pacific Disaster Center 2000).

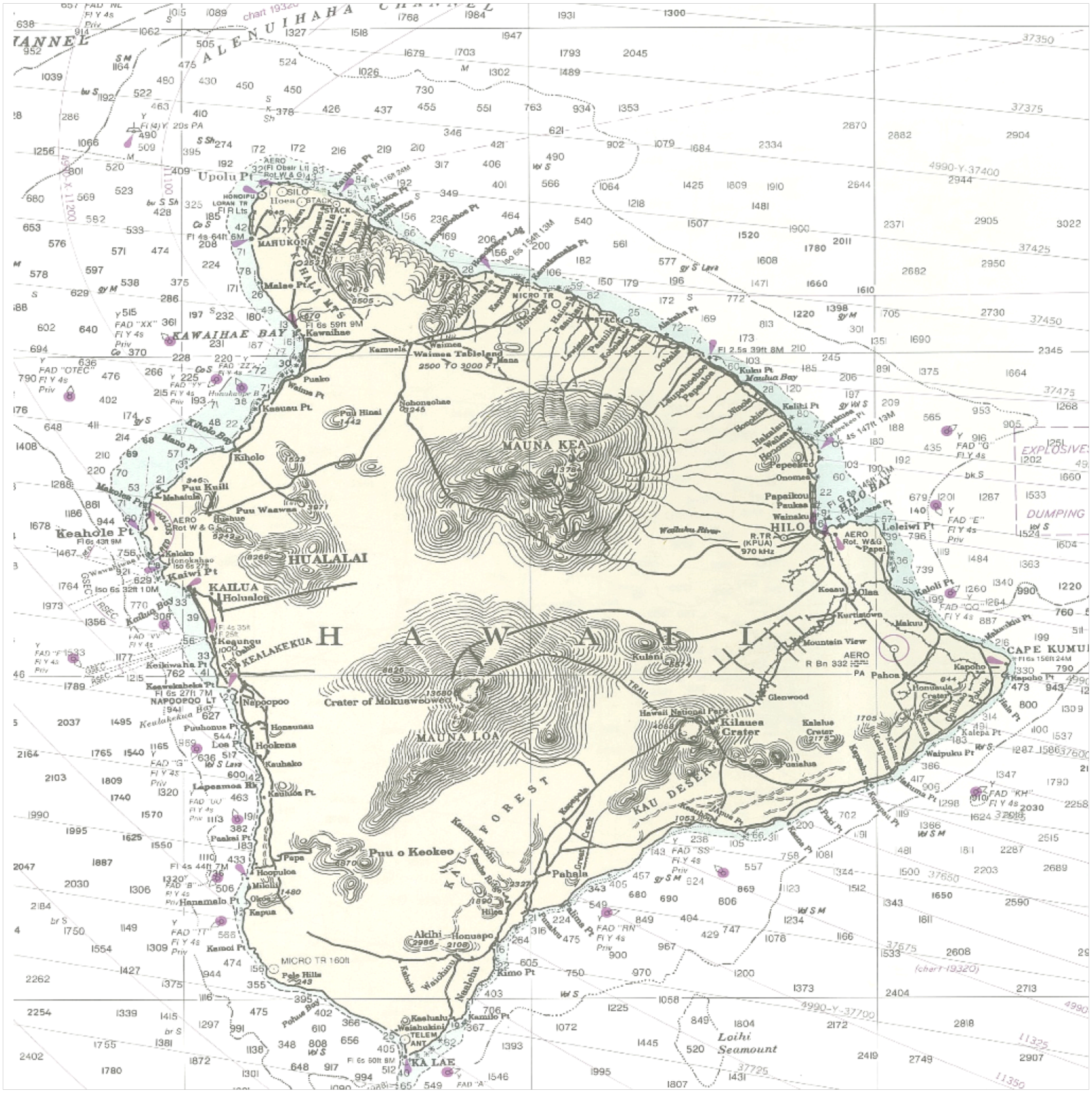

Figure 5 A chart of the Big Island, Hawaii (NOAA Chart 19010). Soundings in fathoms at Mean Lower Low Water. Contour and summit elevation values ate in feet above Mean Sea Level.

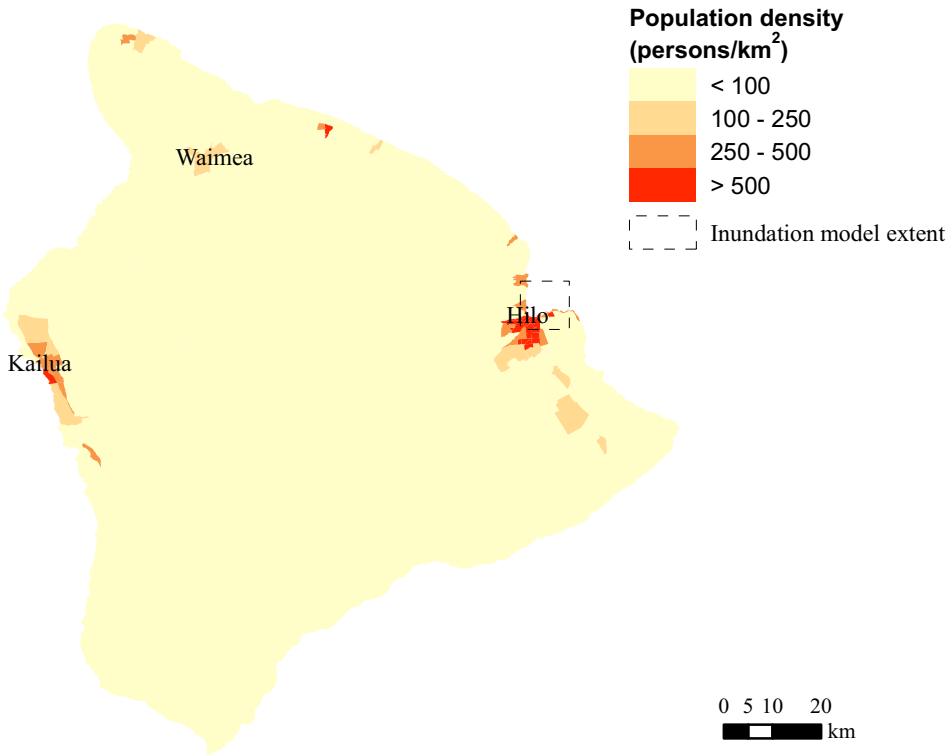

Figure 6 Population density, Hawaii. (Source: 2000Census)

Figure 7 Run-ups in feet for Kailua-Kona coast for the 1946, 1952,1957, 1960 and 1964 tsunamis (Image from Walker, 2004).

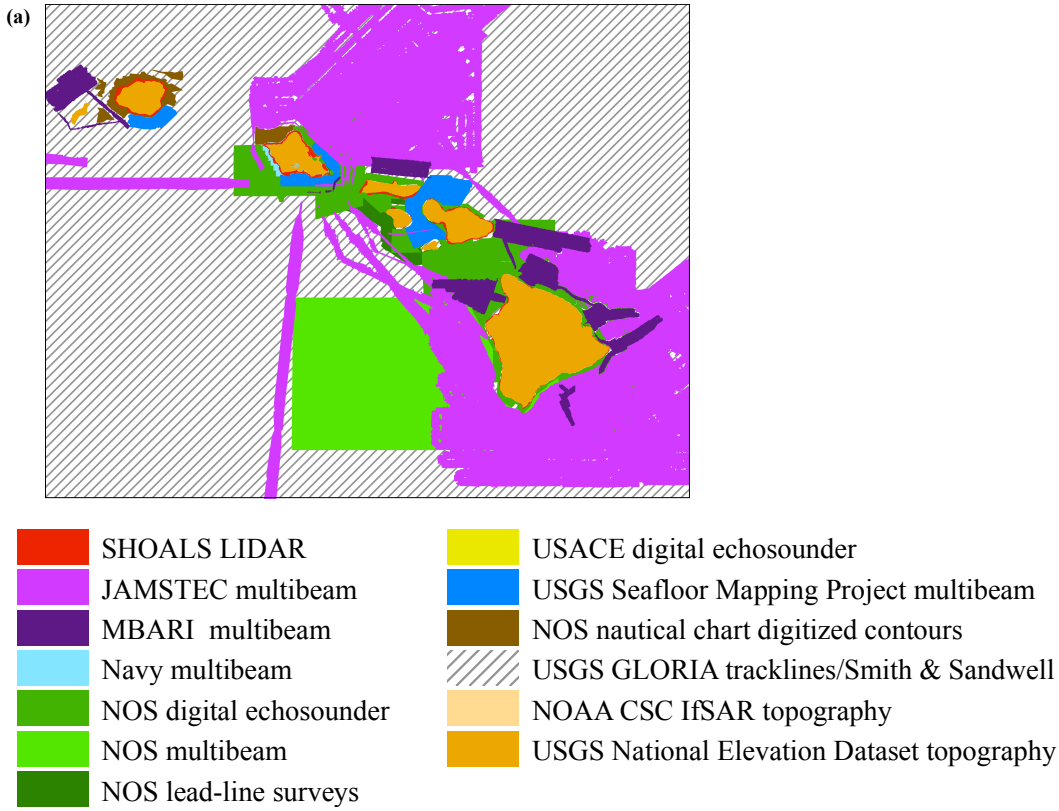

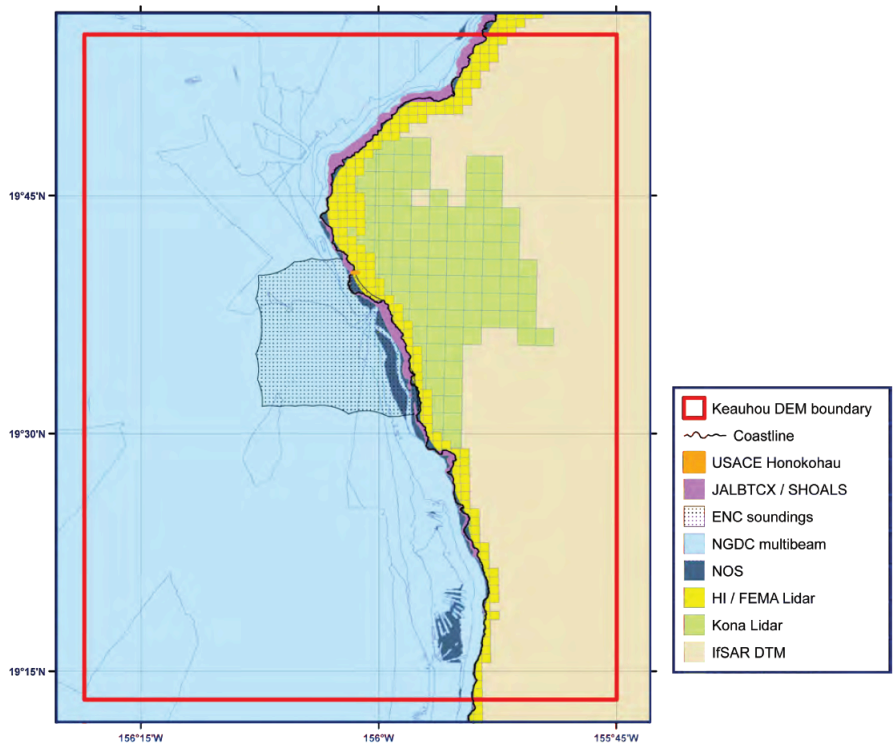

(b)

Figure 8 Bathymetric and topographic data source overview. (a) 6" sec (~180m) Hawaii DEM developed at NCTR; (b) 1/3" (~10m) Keauhou DEM developed by NGDC (Image from Carignan et al., 2011).

(a)

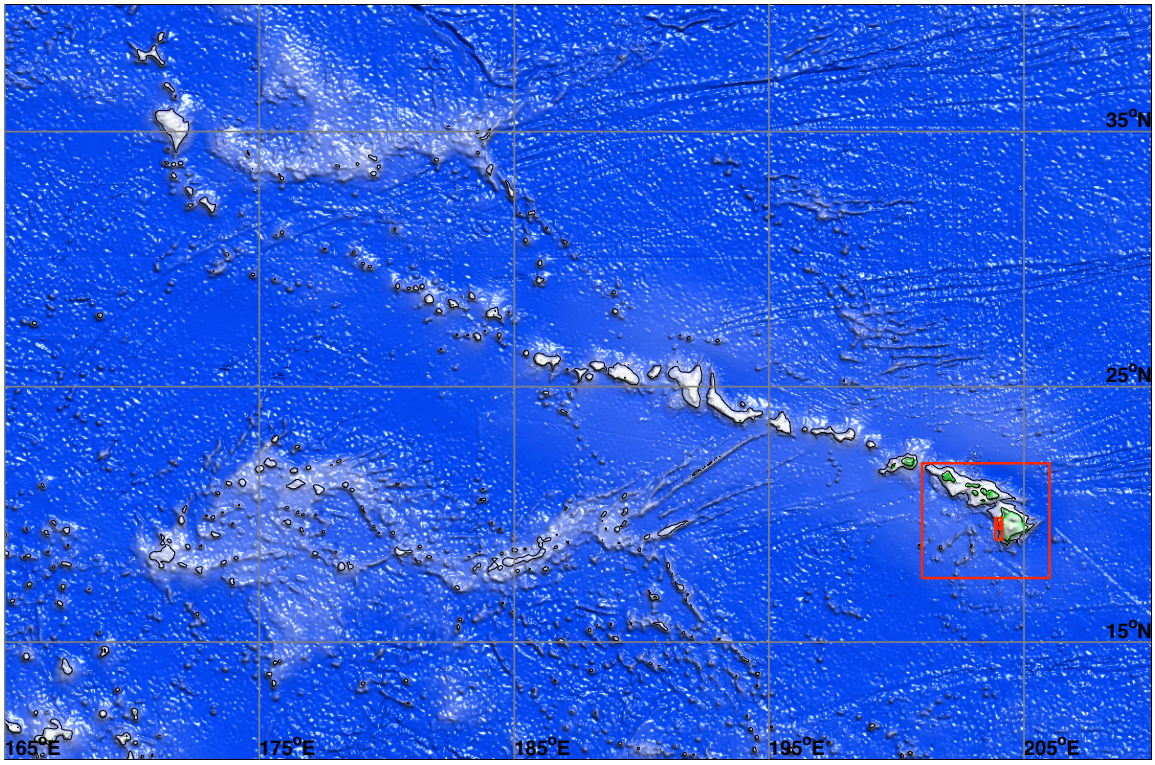
35°N
25°N
15°N
165°E
175°E
185°E
195°E
205°E

(b)

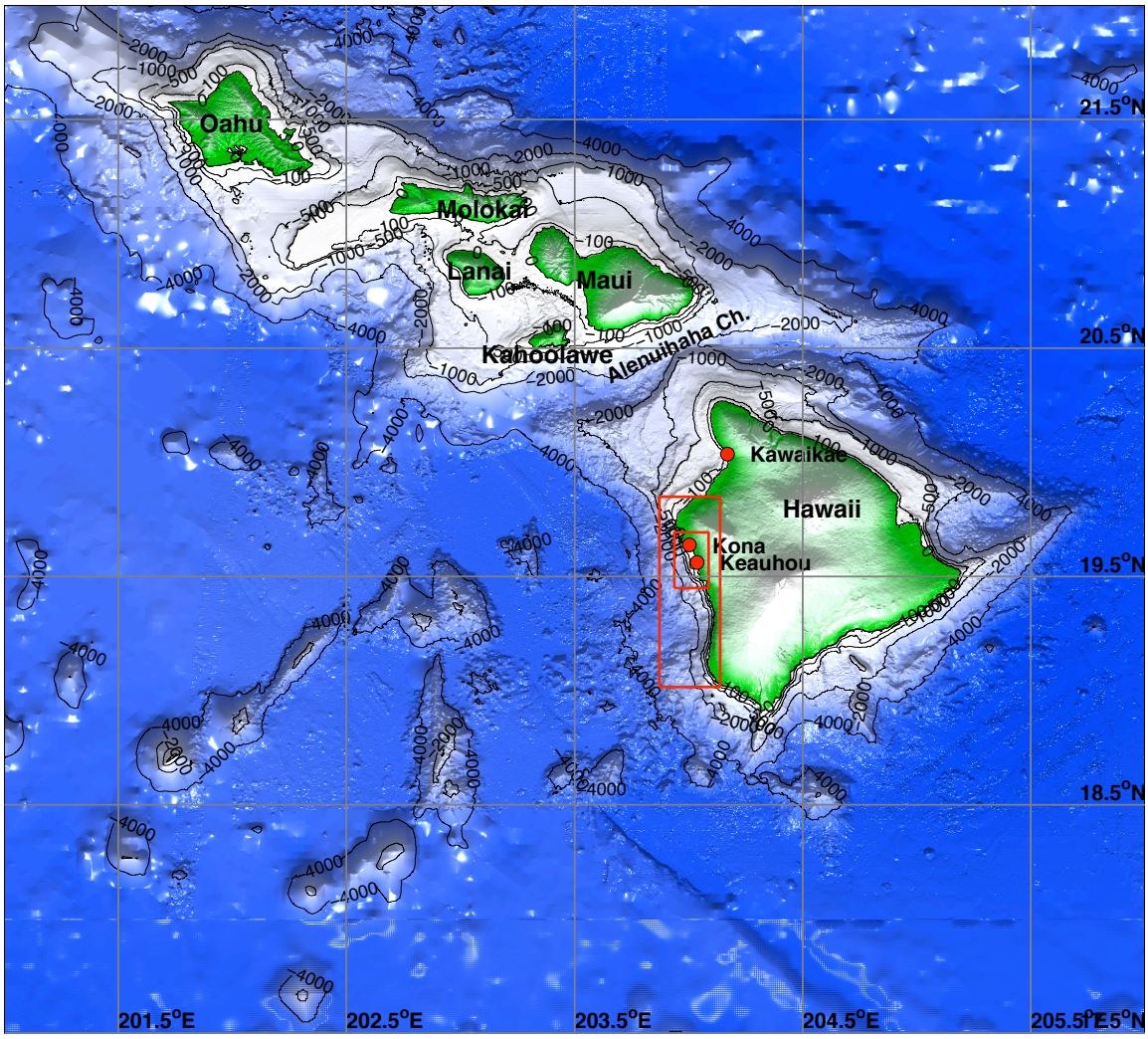
Oahu
Molokai
Lanai
Maui
Kahoolawe
Alenuihaha Ch.
Kawaikae
Hawaii
Kona
Keauhou
21.5°N
20.5°N
19.5°N
18.5°N
201.5°E
202.5°E
203.5°E
204.5°E
205.5°E

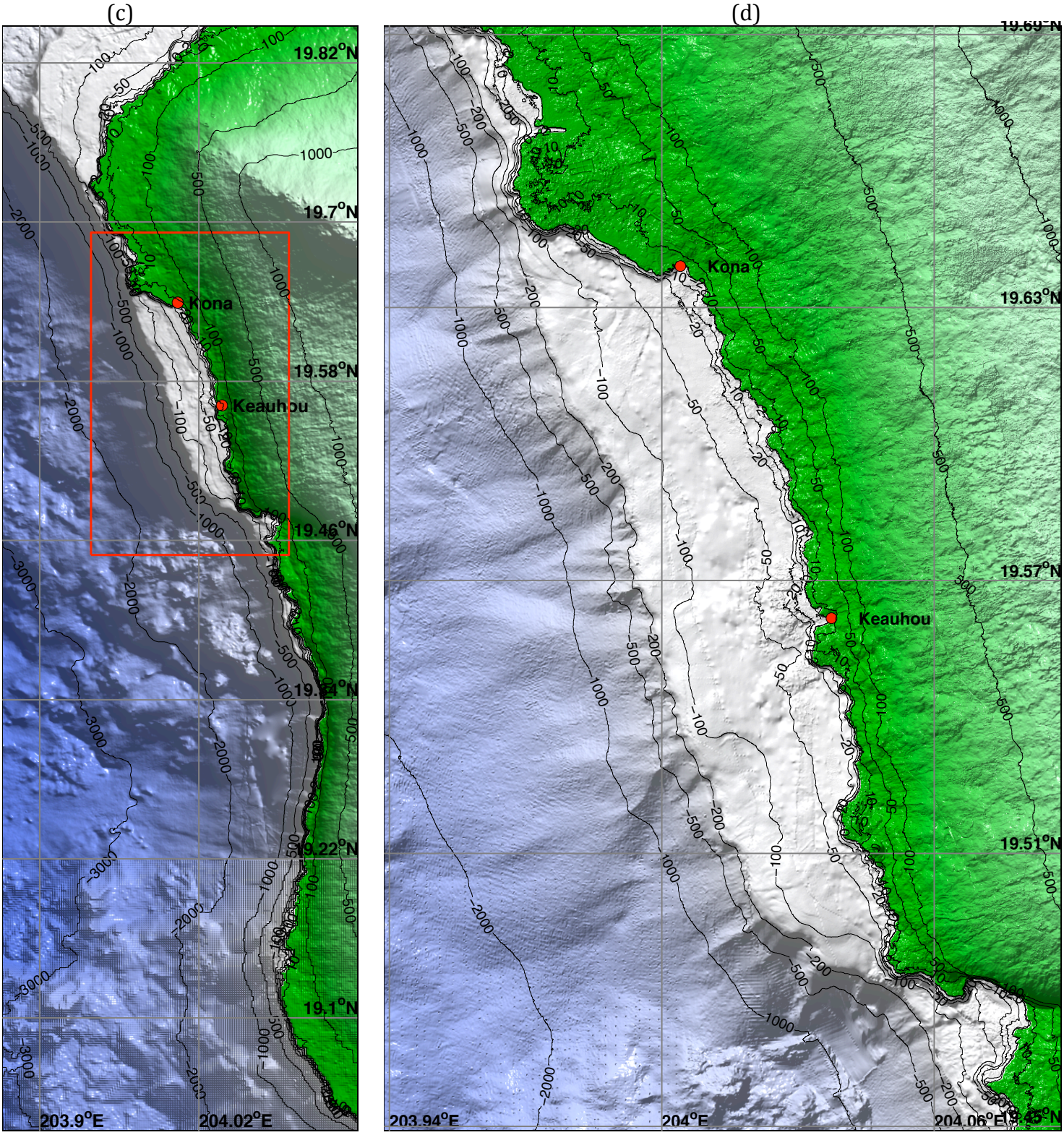

Figure 9 The Kailua-Kona reference model includes four layers of grids with increasing resolutions of (a) 60” (1800m), (b) 6” (180m),(c) 2” (60m) and (d) 2/3” (20m). □, nested grid boundary; ● warning points .

(a)

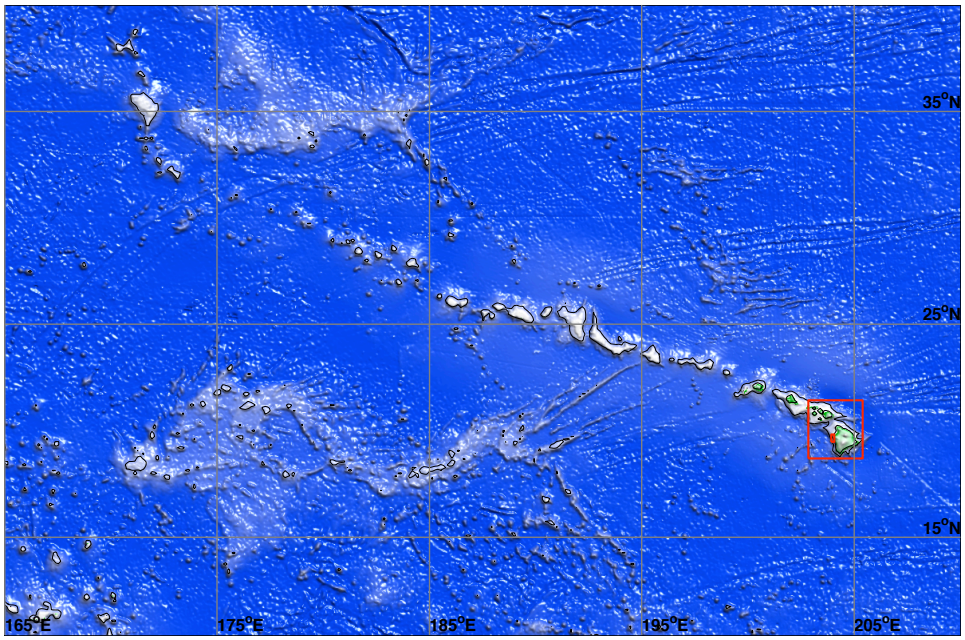
35°N
25°N
15°N
165°E
175°E
185°E
195°E
205°E

(b)

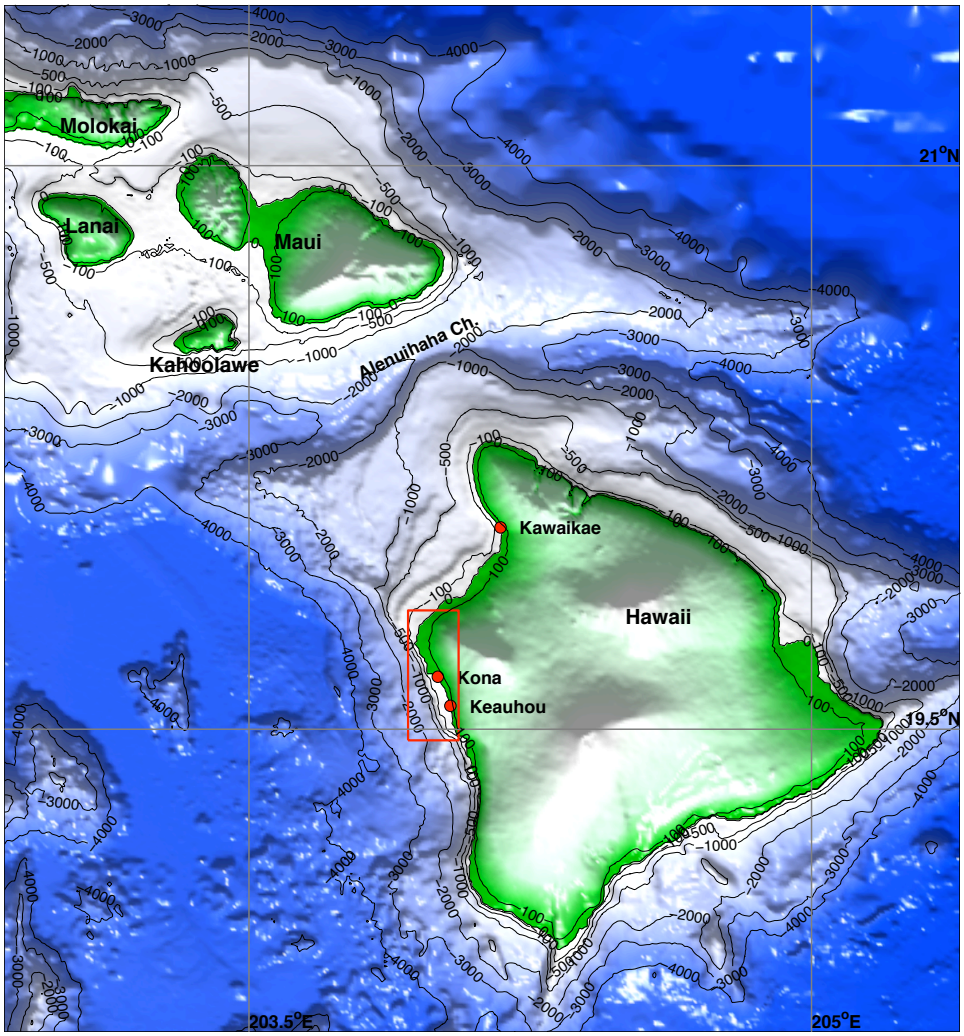
Molokai
Lanai
Maui
Kahoolawe
Alenuihaha Ch.
Kawaikae
Hawaii
Kona
Keauhou
21°N
19.5°N
203.5°E
205°E

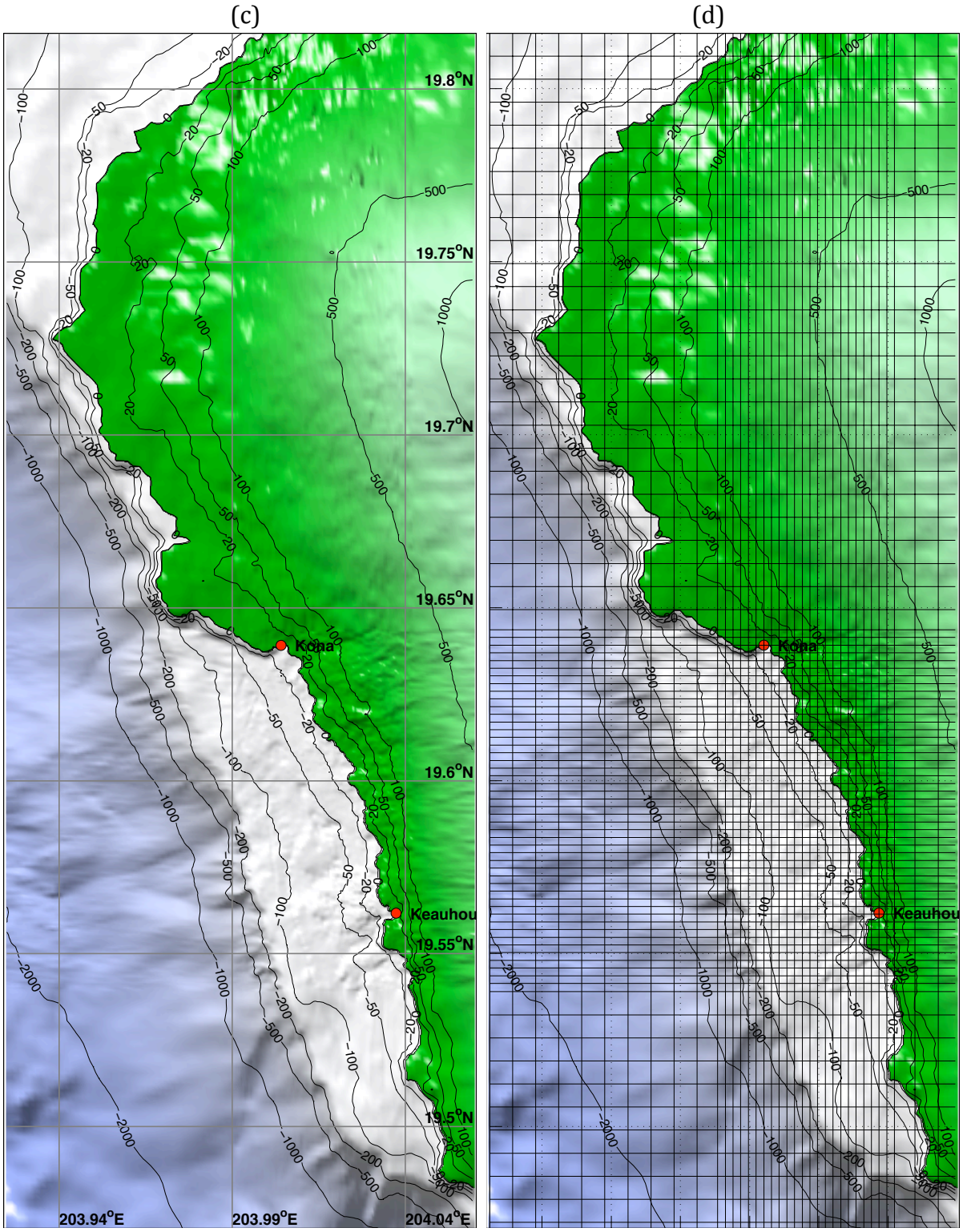

Figure 10 The Kailua-Kona forecast model include three layer of grids with increasing resolutions of (a) 120" (3600m), (b) 24" (720m) and (c) 2- 6 "(60-180m). (d) Each line represents every 4th node in C-grid. □, nested grid boundary; ●, Kailua-Kona warning point at 204.0046 °E, 19.6397 °N, water depth of 2.3 m.

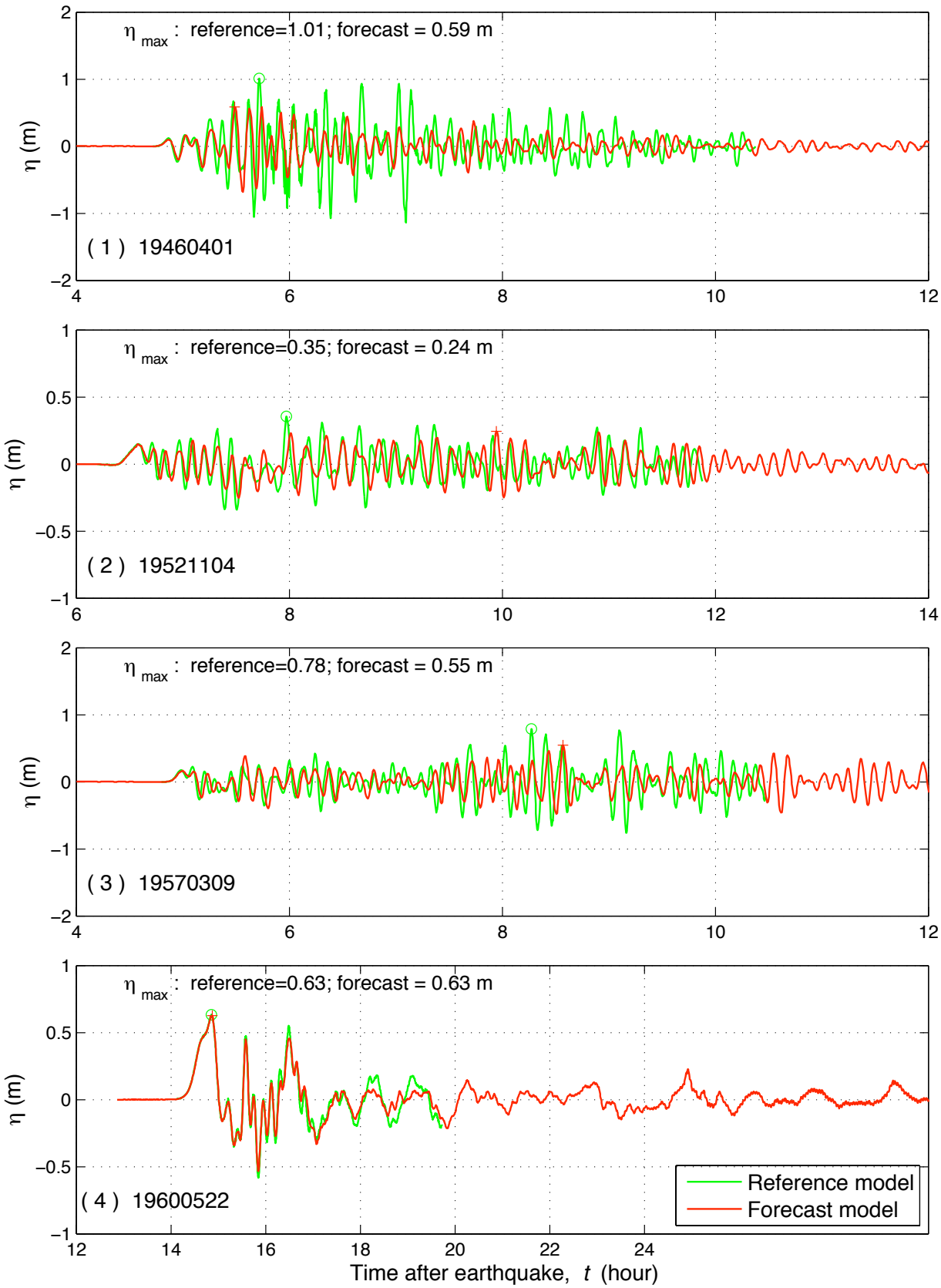
η max : reference=1.01; forecast = 0.59 m
(1) 19460401
η max : reference=0.35; forecast = 0.24 m
(2) 19521104
η max : reference=0.78; forecast = 0.55 m
(3) 19570309
η max : reference=0.63; forecast = 0.63 m
(4) 19600522
η (m)
Reference model
Forecast model
Time after earthquake, t (hour)

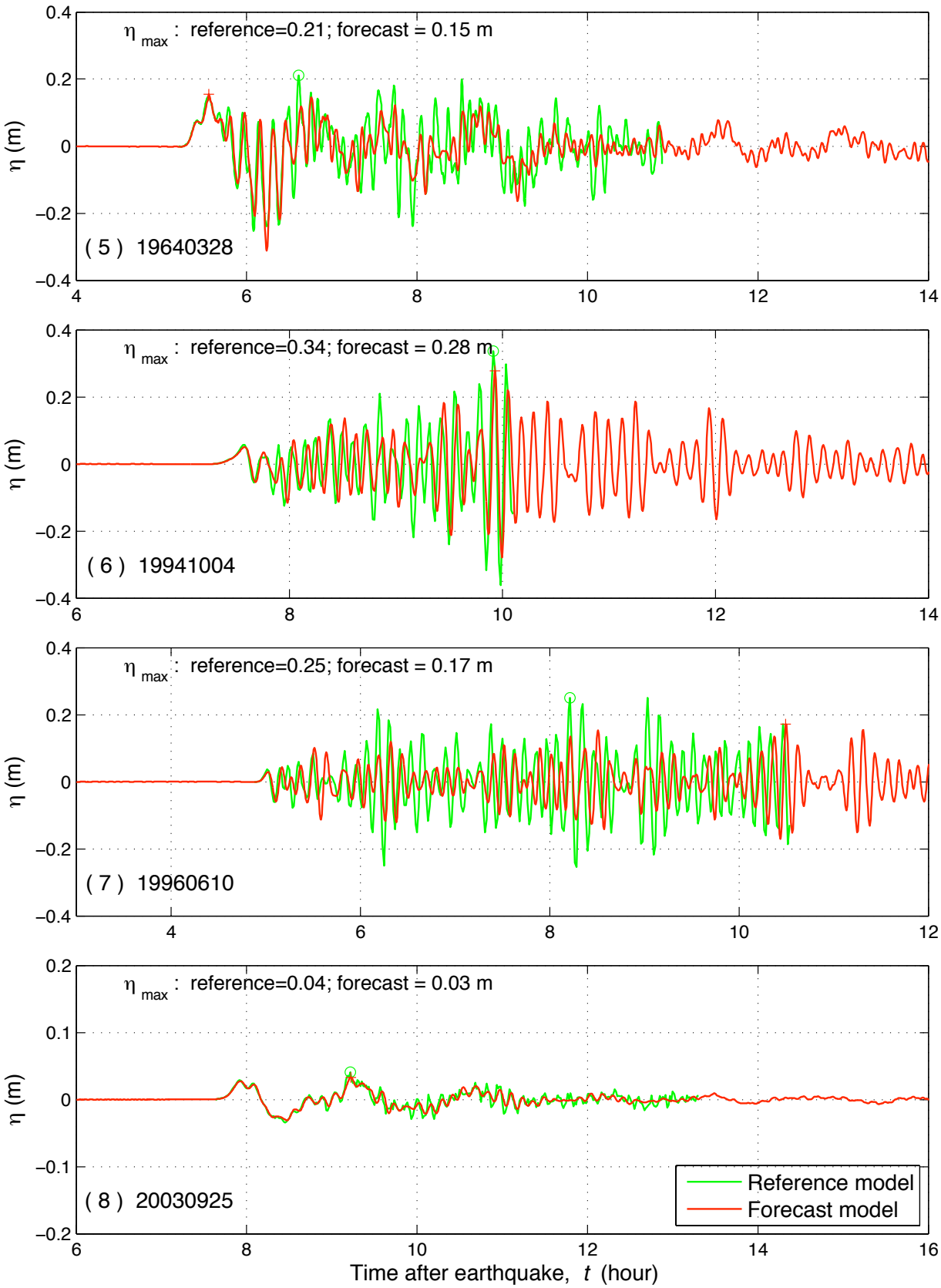
η max : reference=0.21; forecast = 0.15 m
(5) 19640328
η max : reference=0.34; forecast = 0.28 m
(6) 19941004
η max : reference=0.25; forecast = 0.17 m
(7) 19960610
η max : reference=0.04; forecast = 0.03 m
(8) 20030925
Reference model
Forecast model
η (m)
Time after earthquake, t (hour)

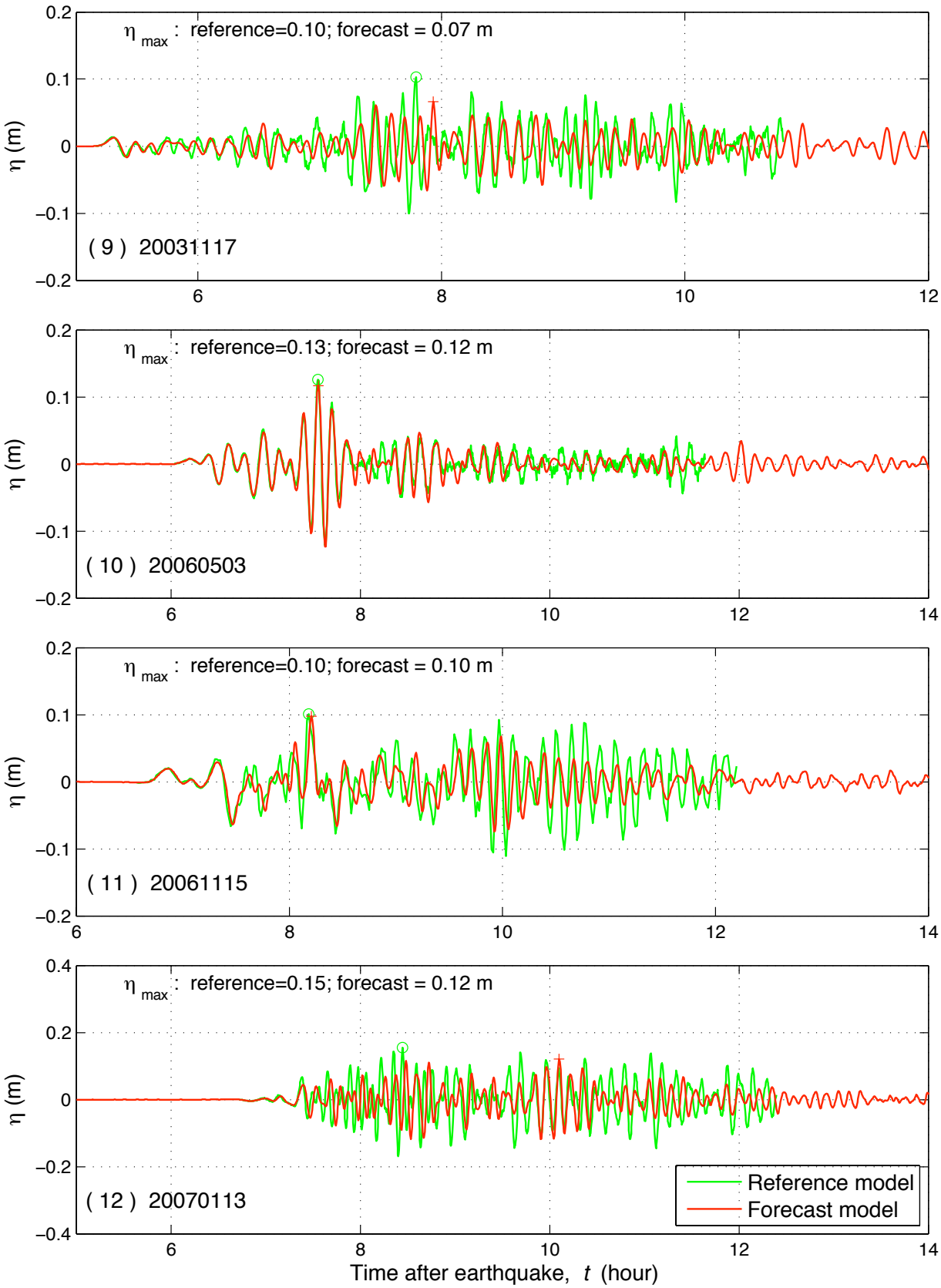
η max : reference=0.10; forecast = 0.07 m
(9) 20031117
η max : reference=0.13; forecast = 0.12 m
(10) 20060503
η max : reference=0.10; forecast = 0.10 m
(11) 20061115
η max : reference=0.15; forecast = 0.12 m
(12) 20070113
Reference model
Forecast model
η (m)
Time after earthquake, t (hour)

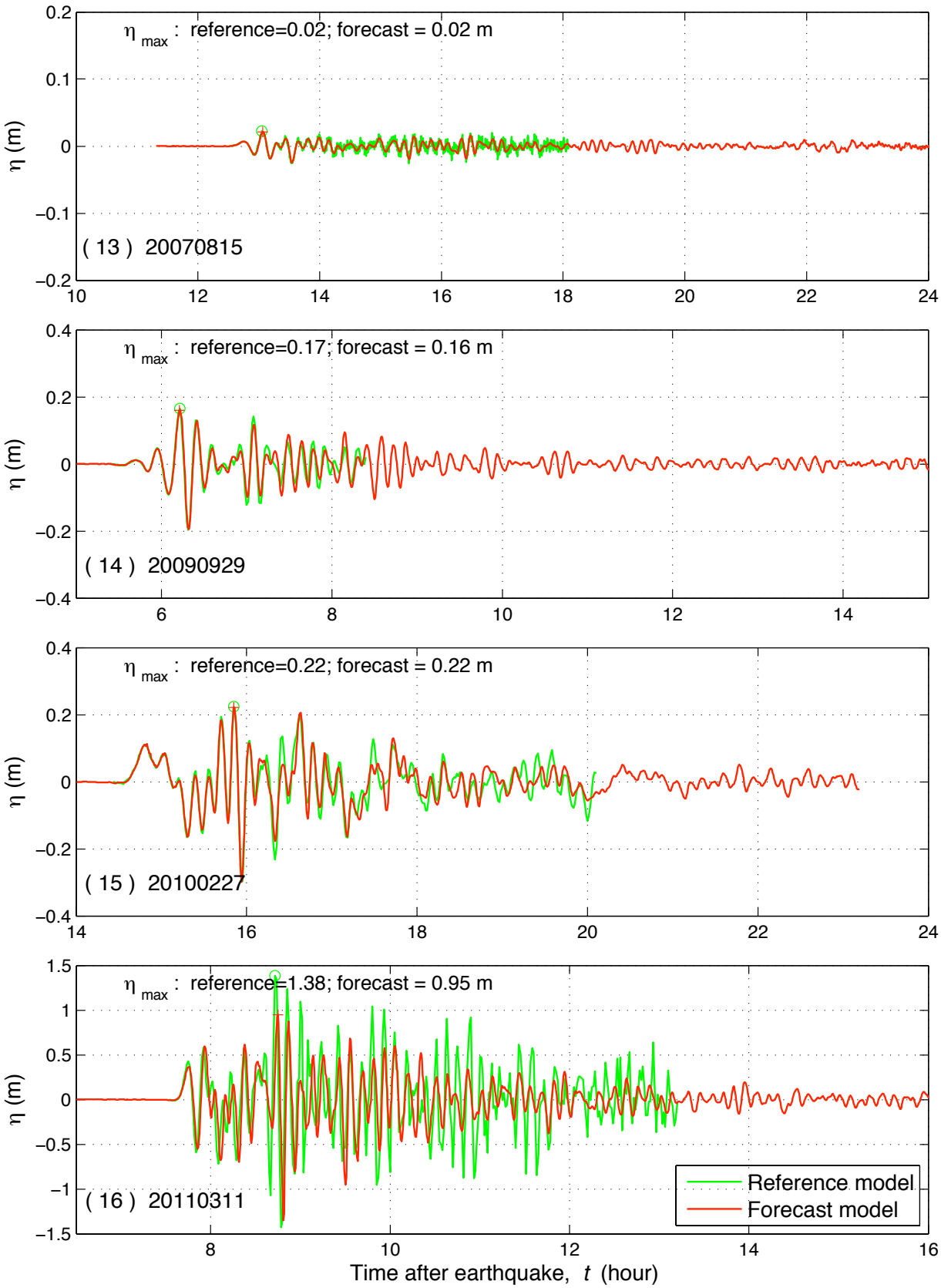

Figure 11 Modeled time series of sea surface elevation η at Kailua-Kona warning point for the past 16 tsunamis. o and + η_{max} , computed by the reference and forecast models respectively.

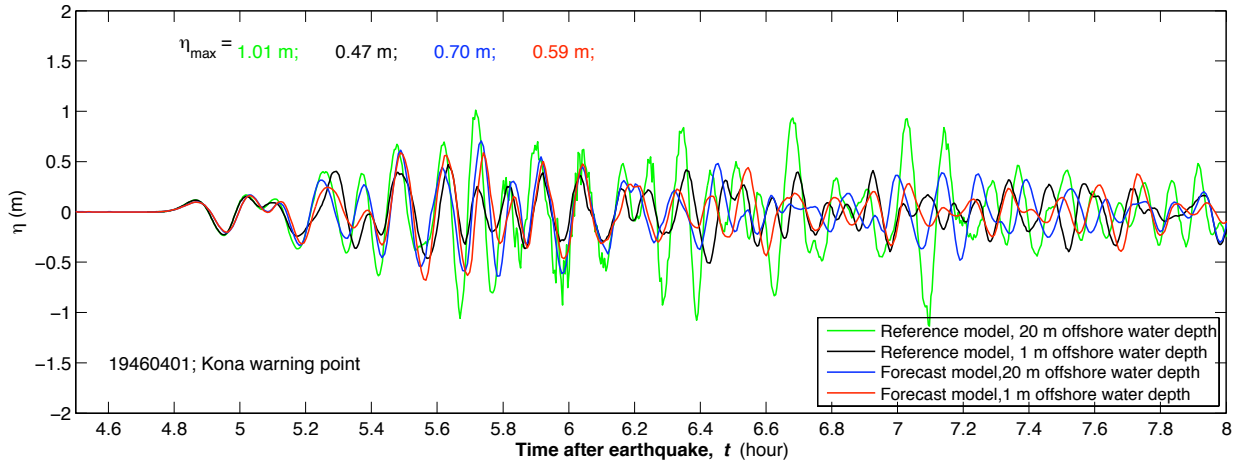

Figure 12 Computed η with different model setups for the 1946 Unimak tsunami.

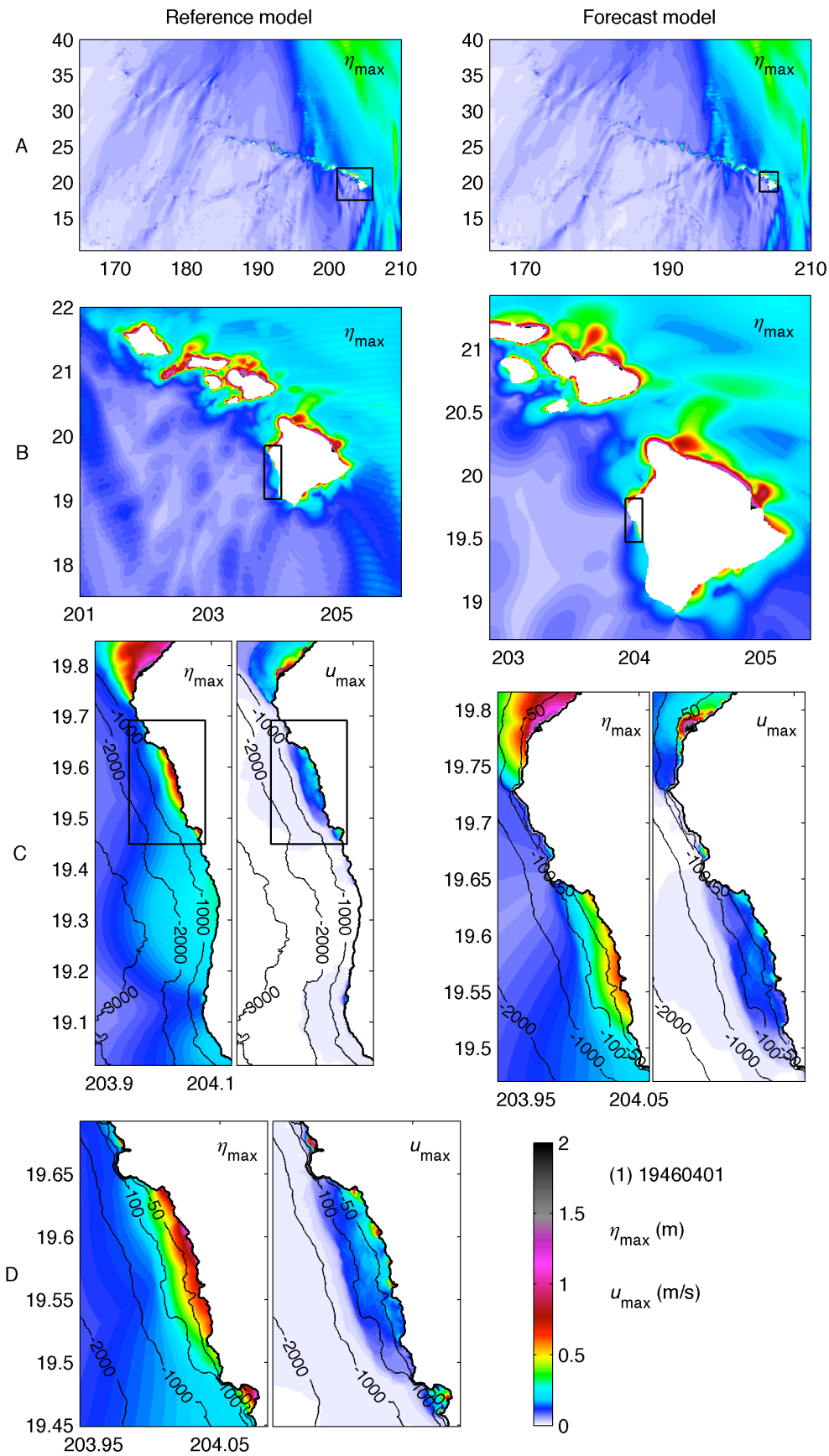
Reference model
Forecast model
A
B
C
D
η_{max}
u_{max}
(1) 19460401
η_{max} (m)
u_{max} (m/s)

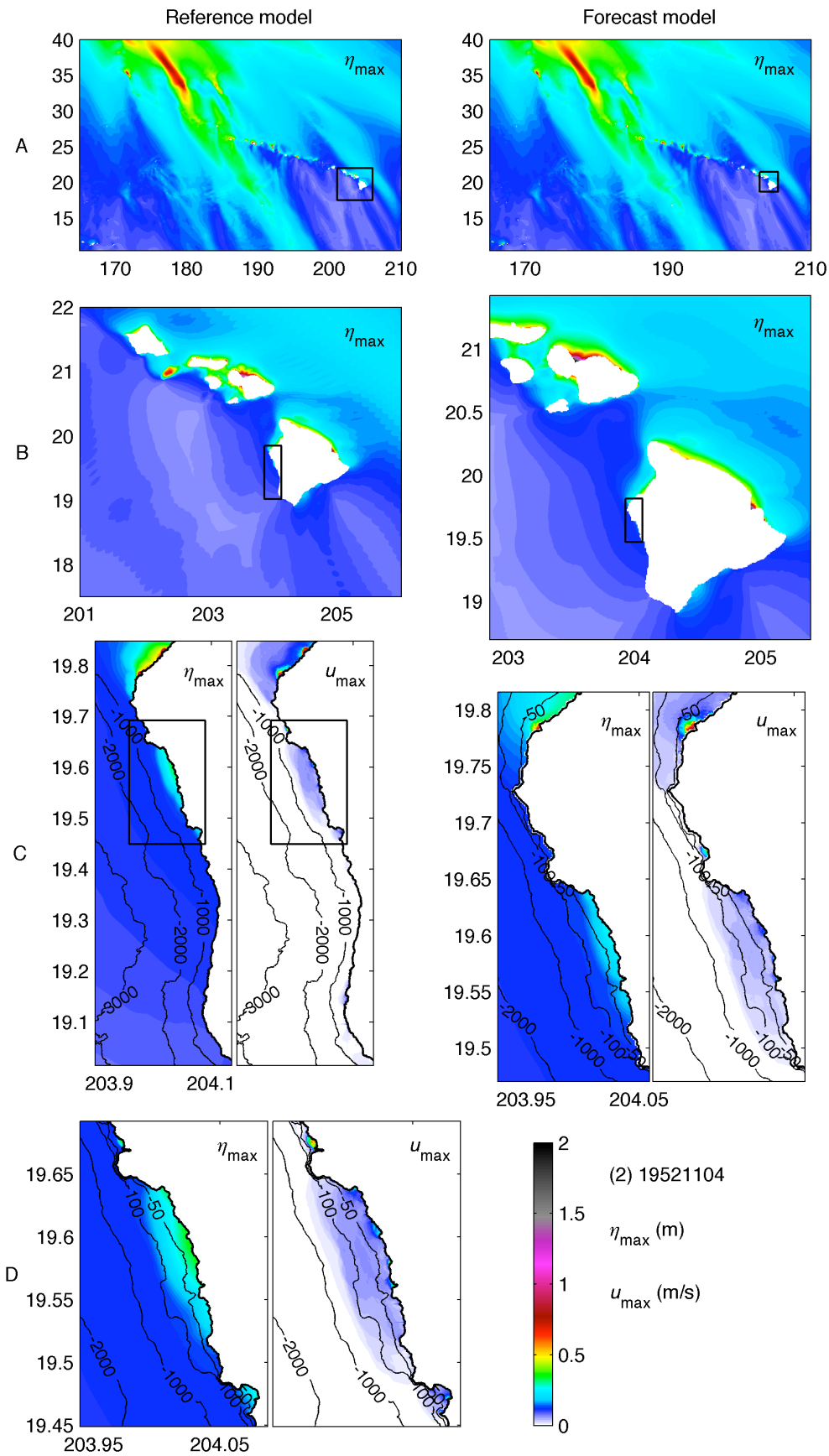
Reference model
Forecast model
A
B
C
D
η_{max}
u_{max}
(2) 19521104
η_{max} (m)
u_{max} (m/s)

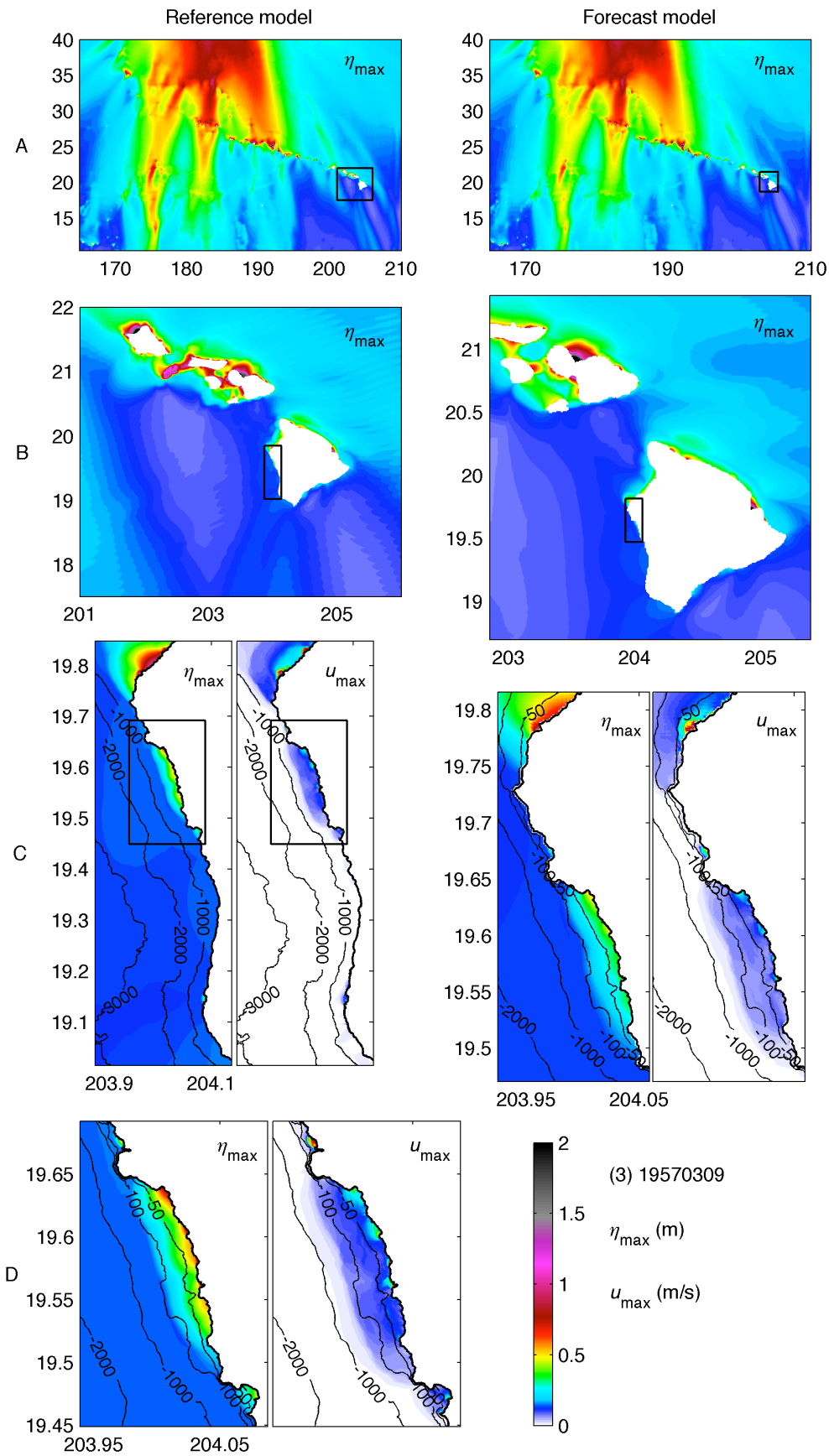
Reference model
Forecast model
A
B
C
D
η_{max}
u_{max}
(3) 19570309
η_{max} (m)
u_{max} (m/s)

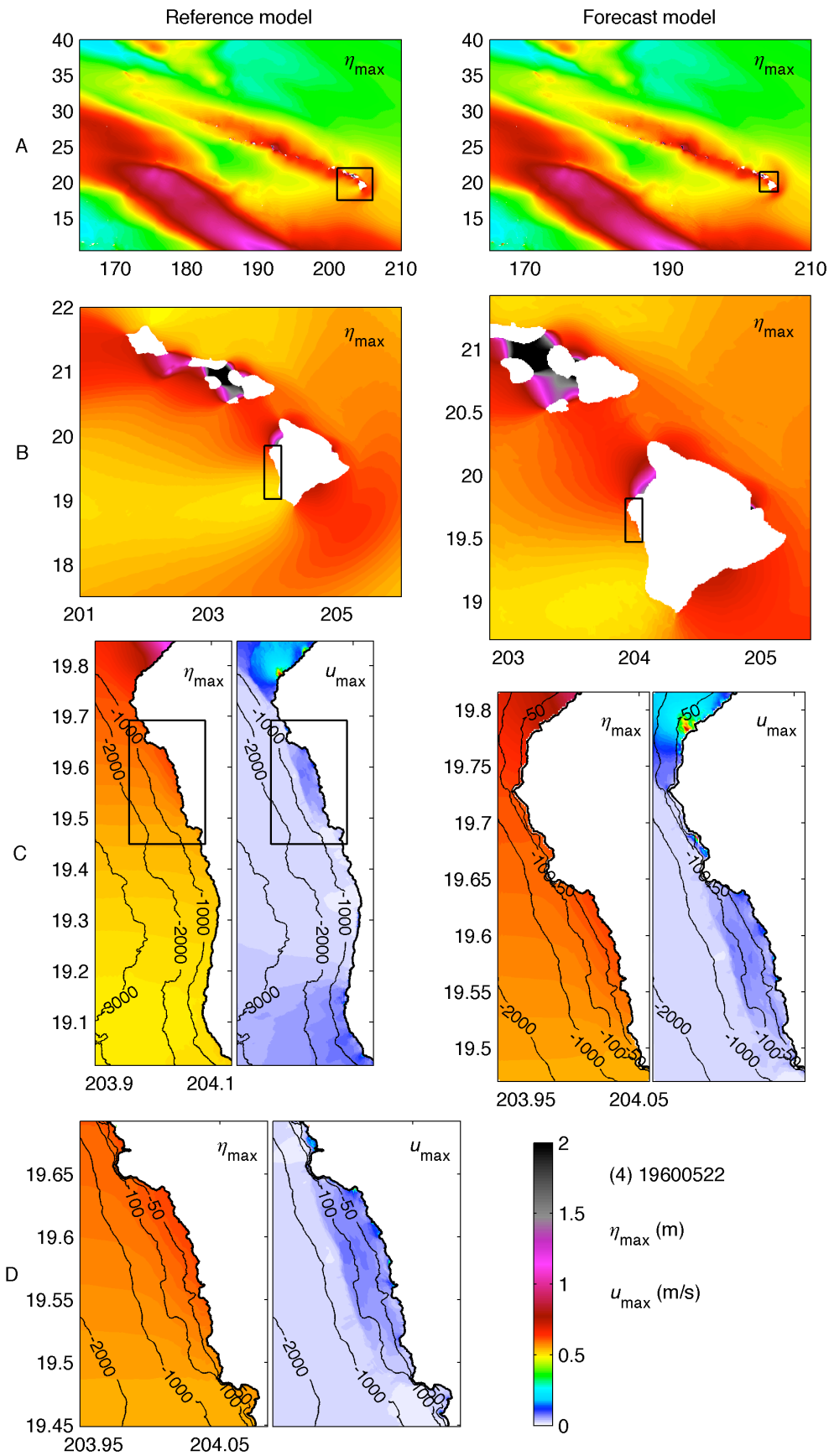
Reference model
Forecast model
A
B
C
D
η_{max}
u_{max}
(4) 19600522
η_{max} (m)
u_{max} (m/s)

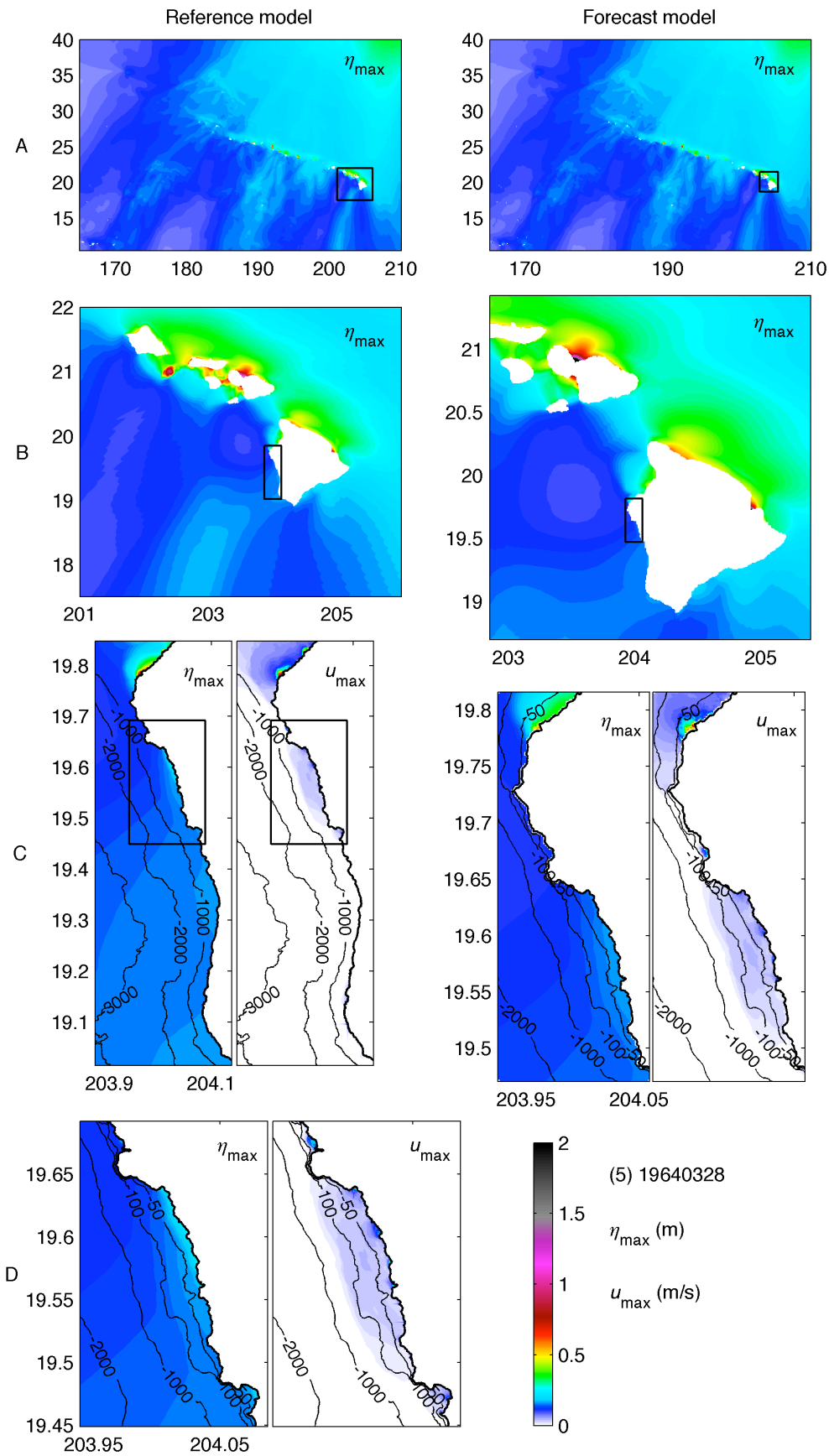
Reference model
Forecast model
A
B
C
D
η_{max}
u_{max}
(5) 19640328
η_{max} (m)
u_{max} (m/s)

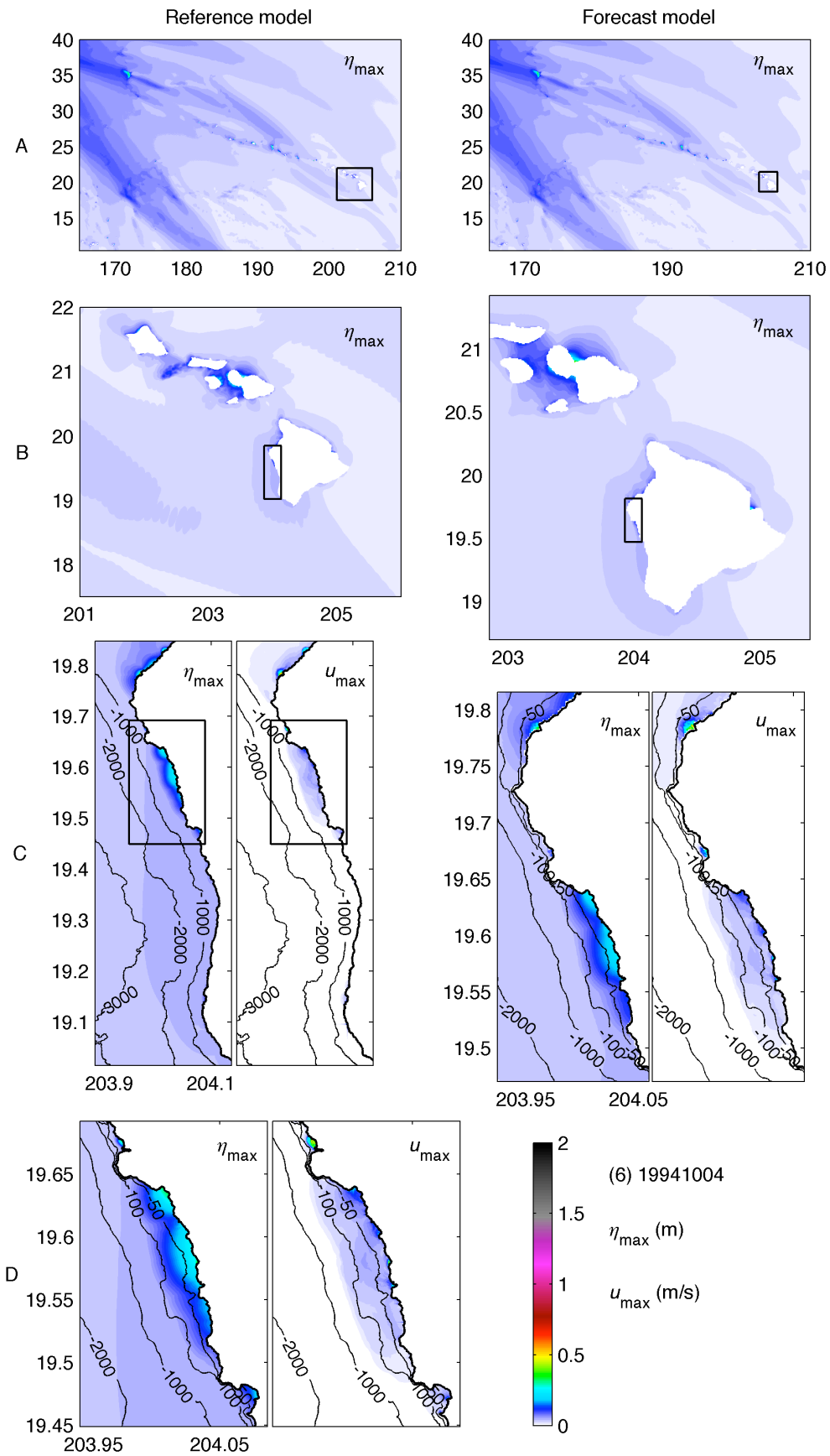
Reference model
Forecast model
A
B
C
D
η_{max}
u_{max}
(6) 19941004
η_{max} (m)
u_{max} (m/s)

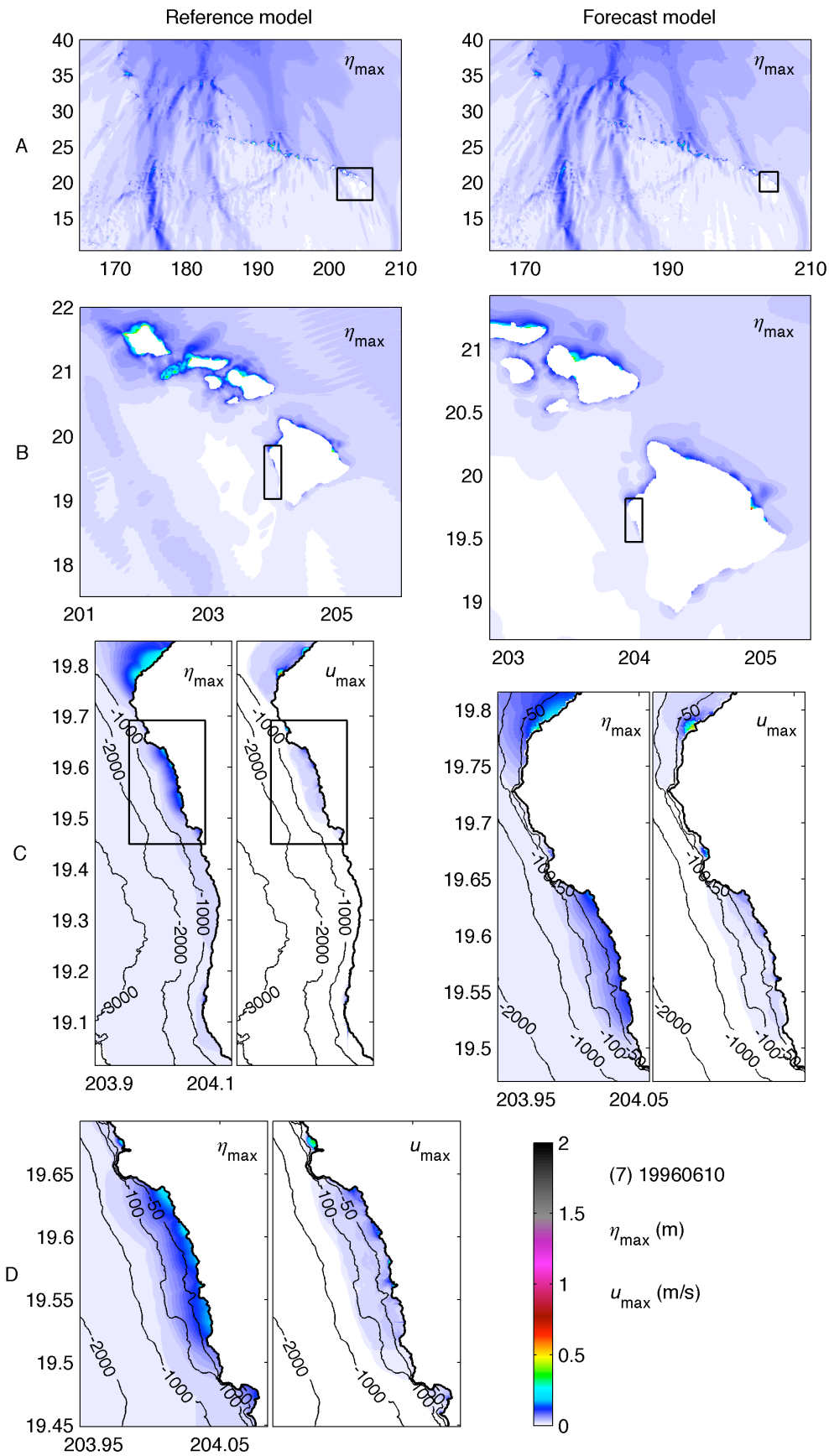
Reference model
Forecast model
A
B
C
D
η_{max}
u_{max}
(7) 19960610
η_{max} (m)
u_{max} (m/s)

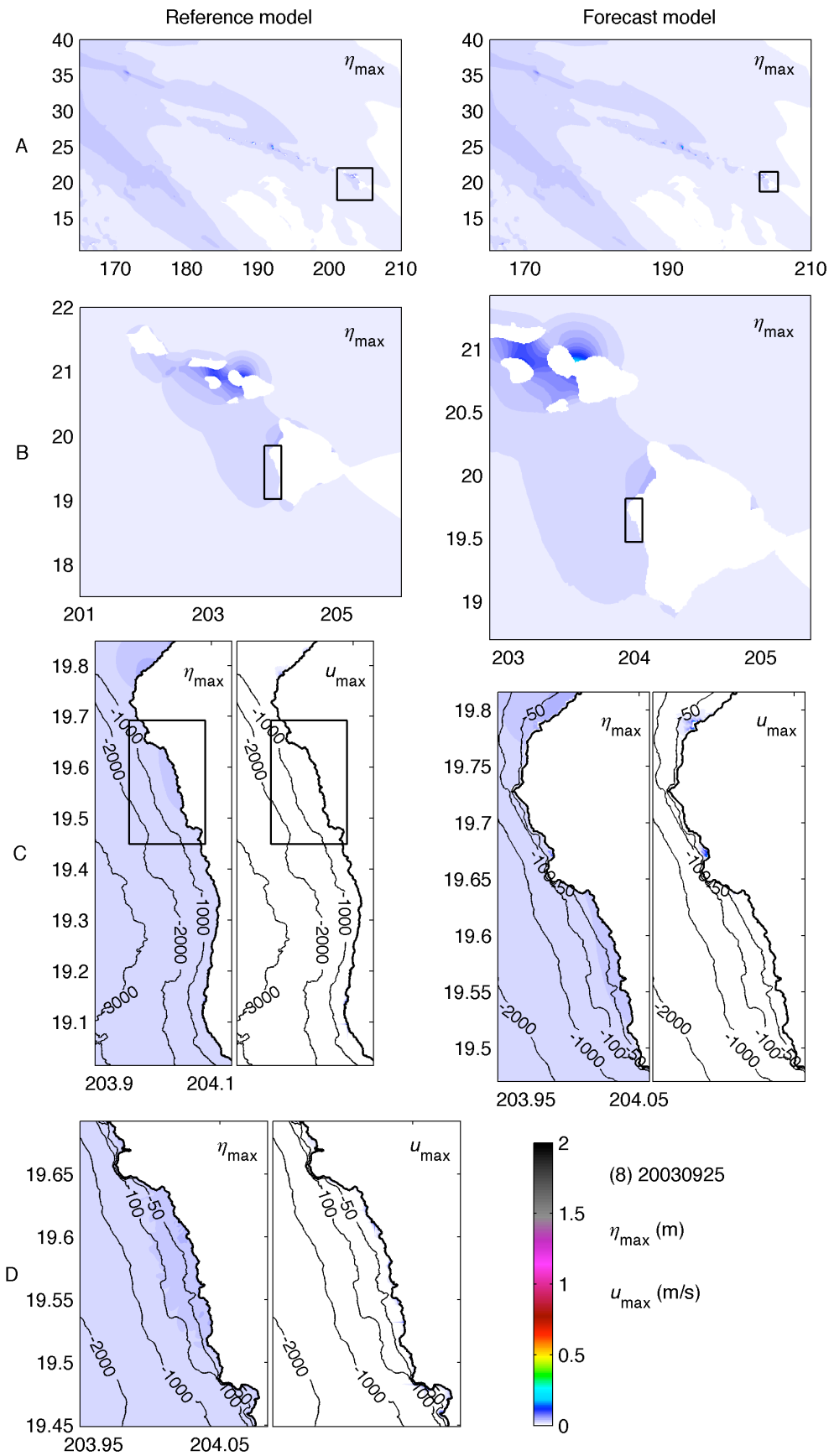
Reference model
Forecast model
A
B
C
D
η_{max}
u_{max}
(8) 20030925
η_{max} (m)
u_{max} (m/s)

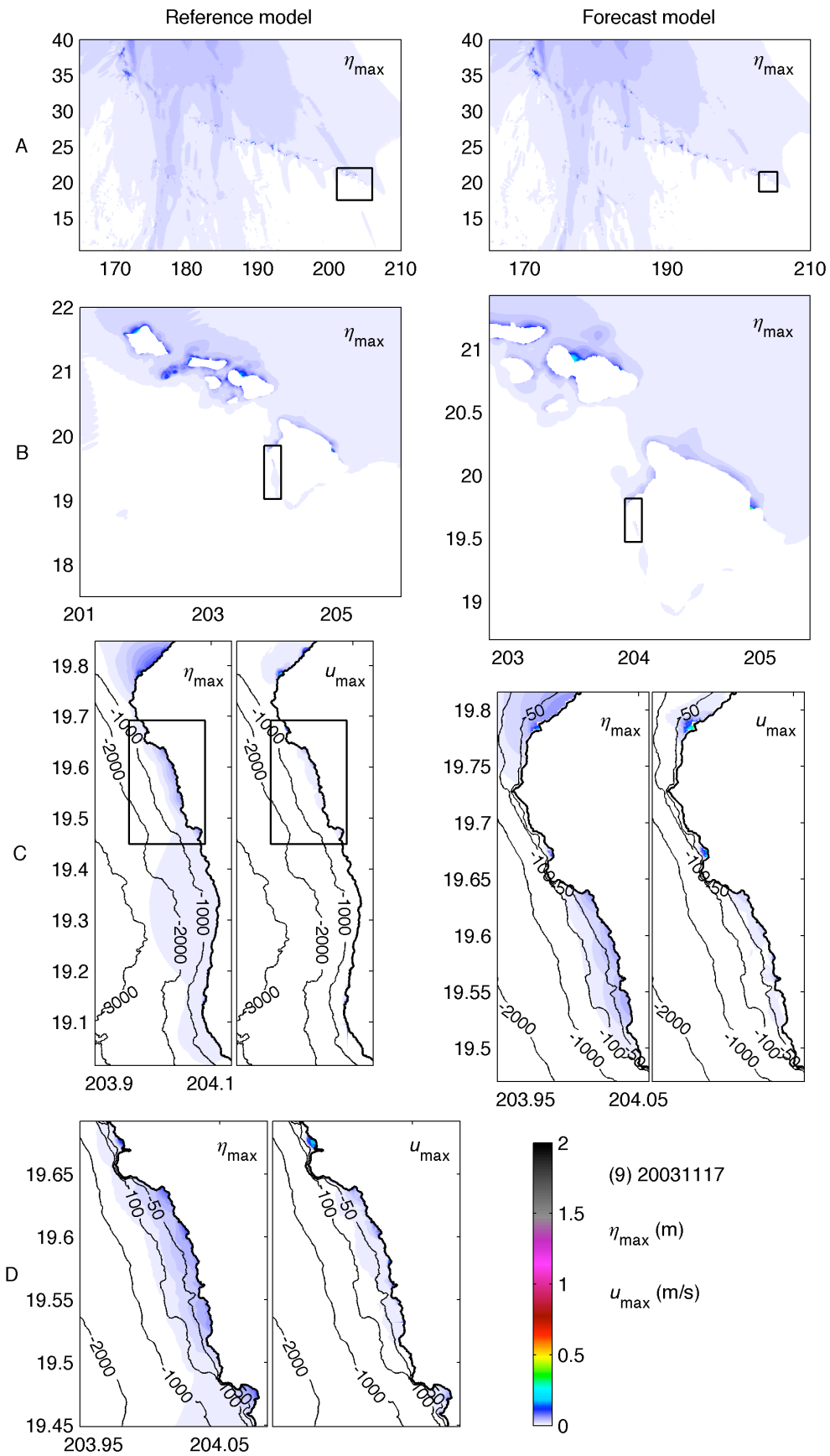
Reference model
Forecast model
A
B
C
D
η_{max}
u_{max}
(9) 20031117
η_{max} (m)
u_{max} (m/s)

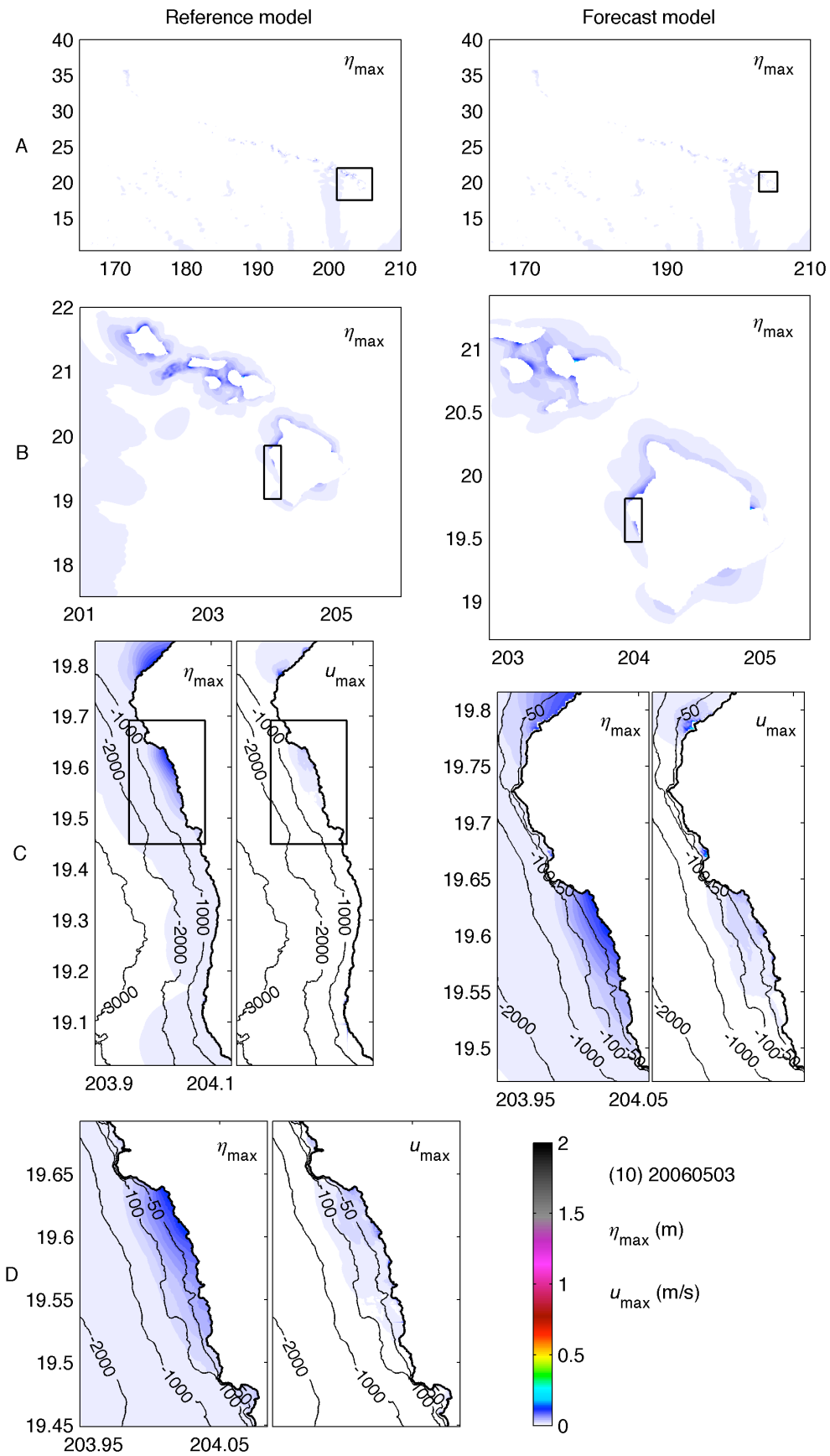
Reference model
Forecast model
A
B
C
D
η_{max}
u_{max}
(10) 20060503
η_{max} (m)
u_{max} (m/s)

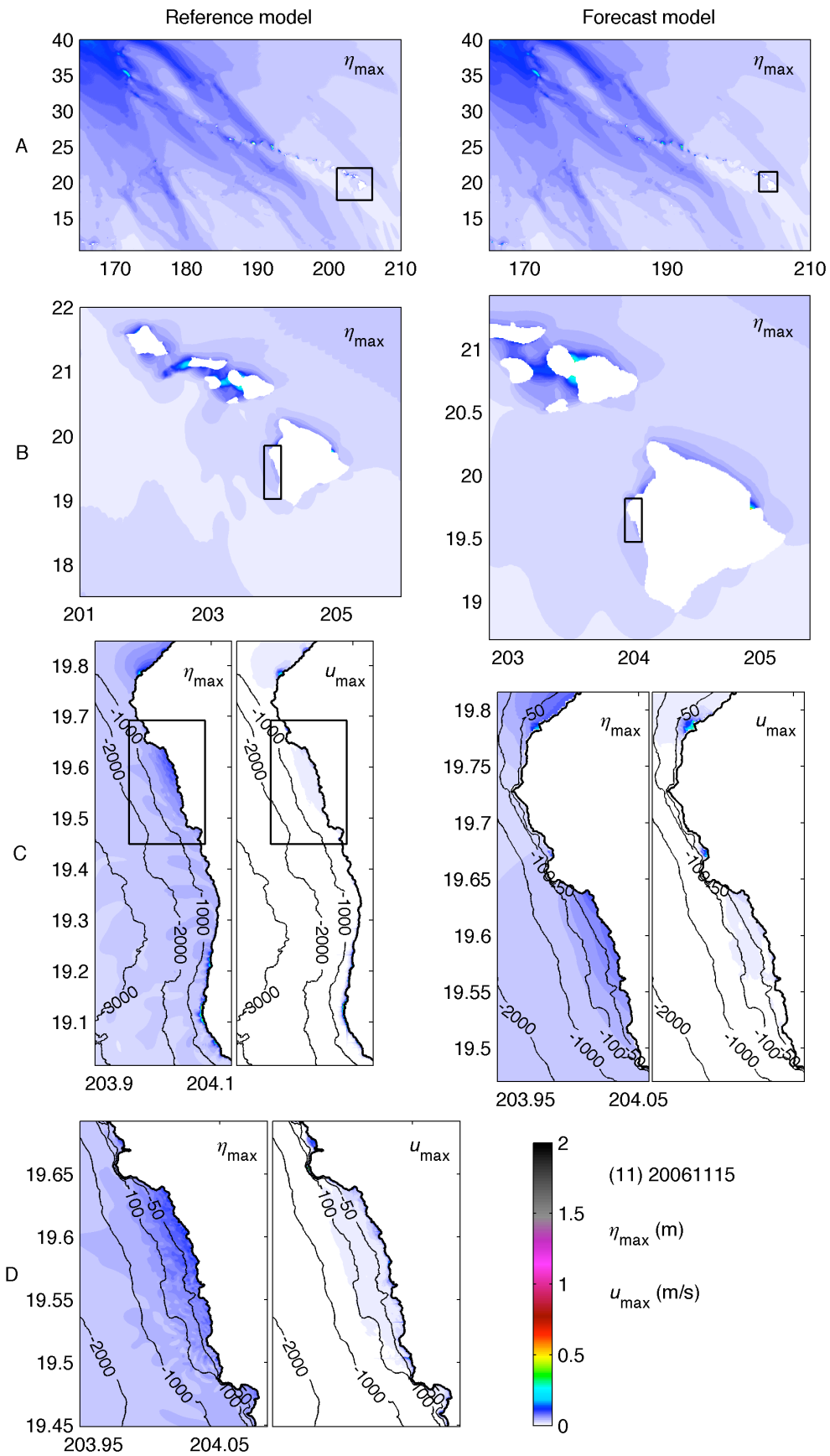
Reference model
Forecast model
A
B
C
D
η_{max}
u_{max}
(11) 20061115
η_{max} (m)
u_{max} (m/s)

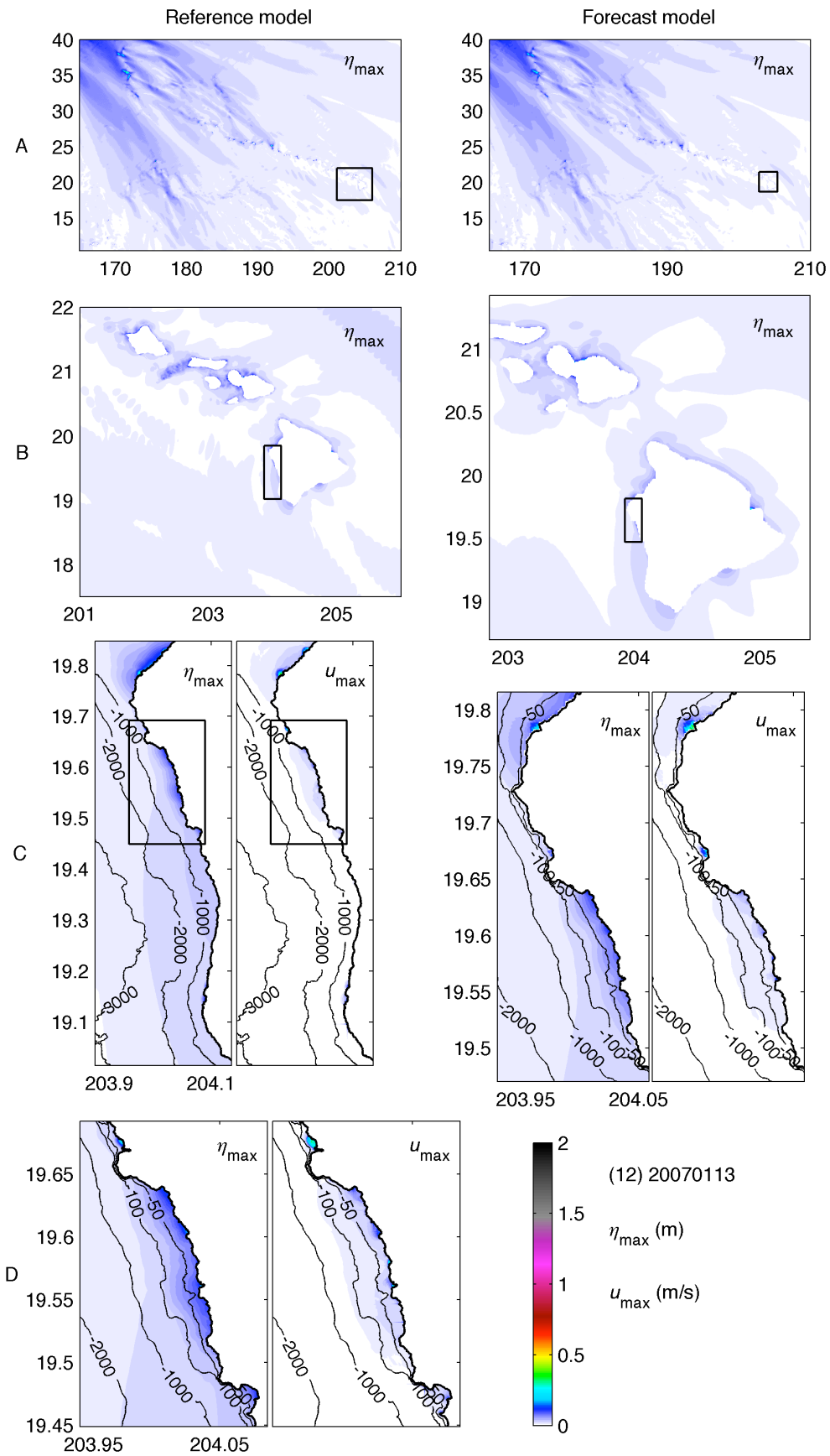
Reference model
Forecast model
A
B
C
D
η_{max}
u_{max}
(12) 20070113
η_{max} (m)
u_{max} (m/s)

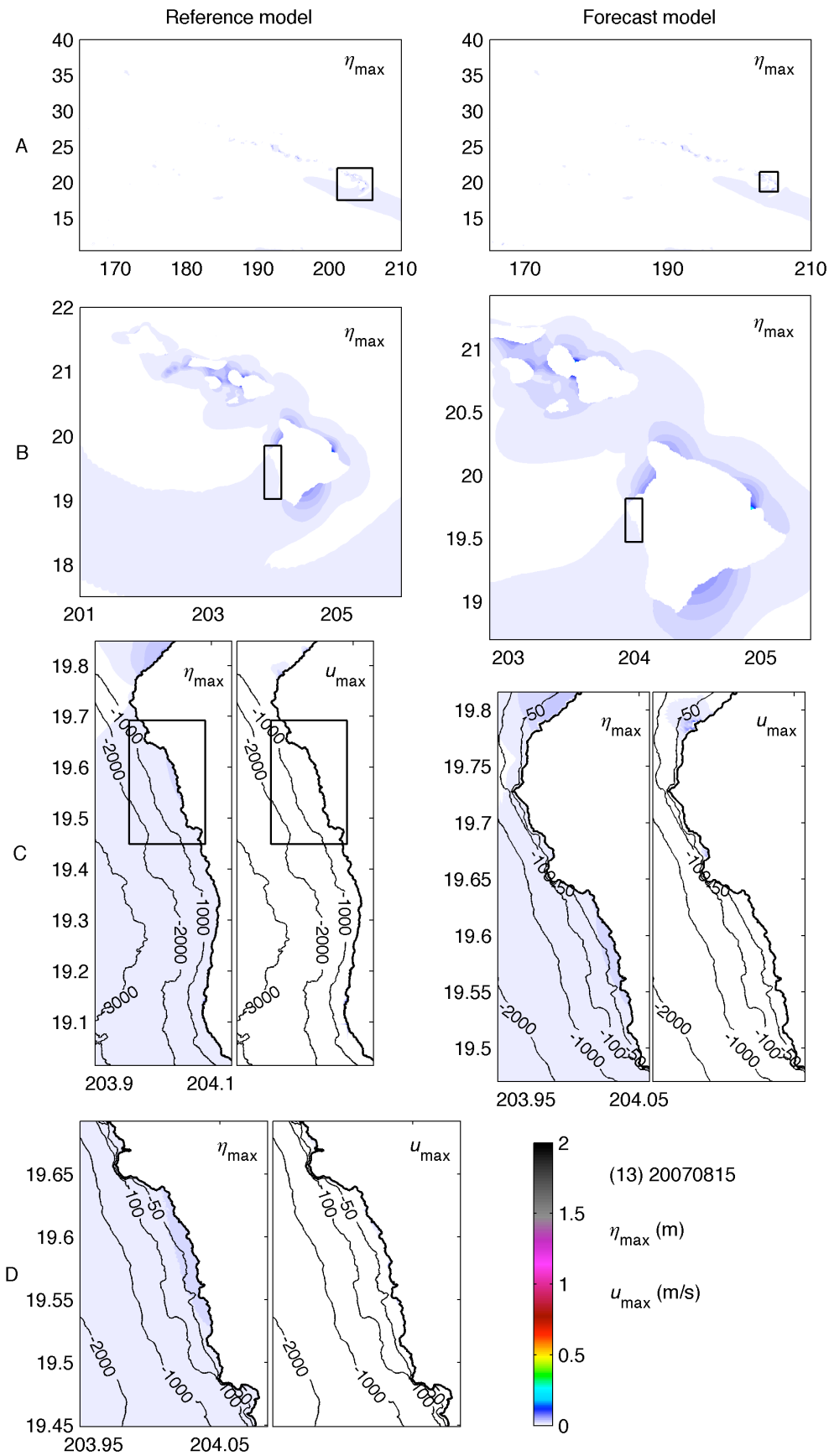
Reference model
Forecast model
A
B
C
D
η_{max}
u_{max}
(13) 20070815
η_{max} (m)
u_{max} (m/s)

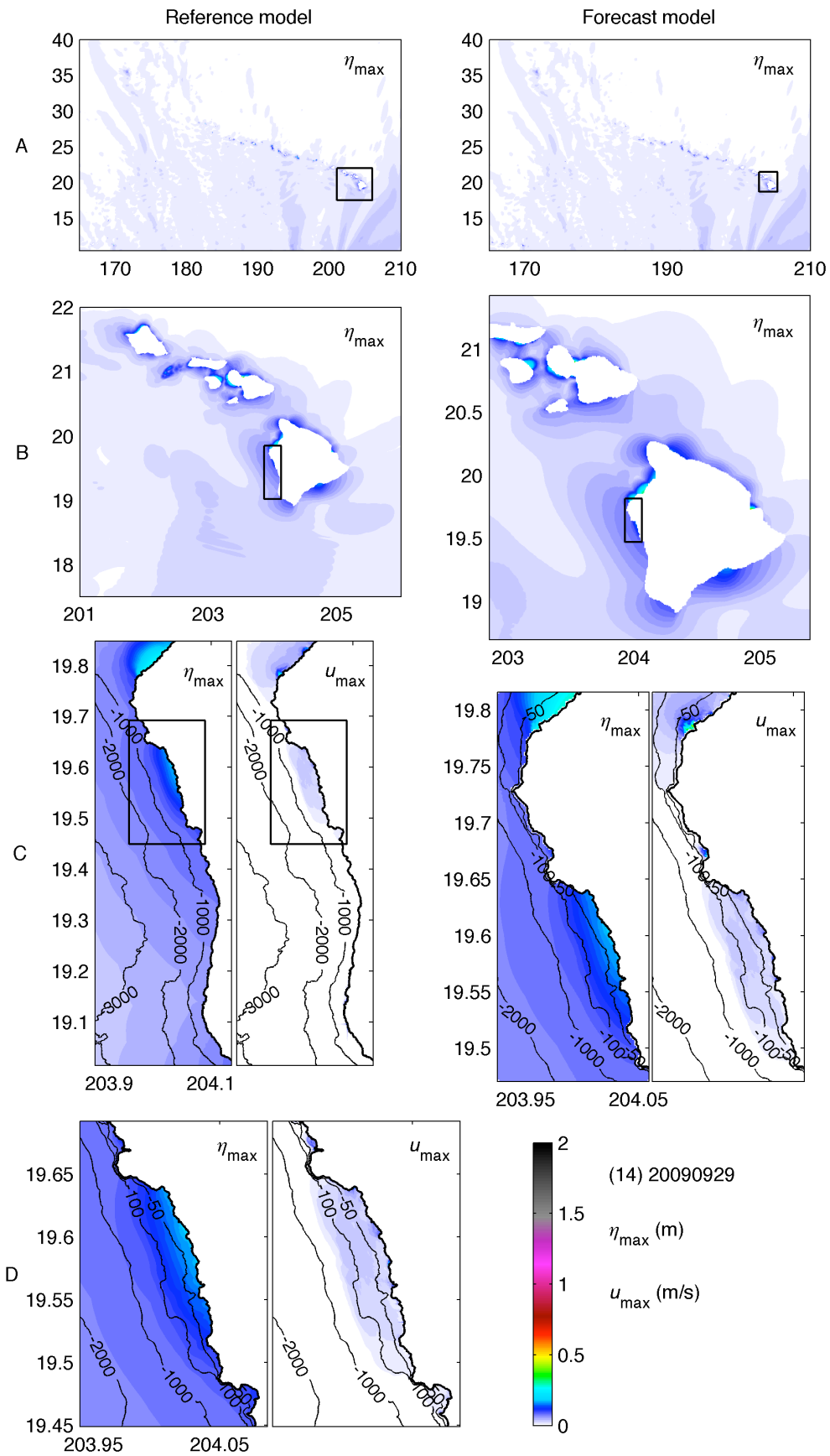
Reference model
Forecast model
A
B
C
D
η_{max}
u_{max}
(14) 20090929
η_{max} (m)
u_{max} (m/s)

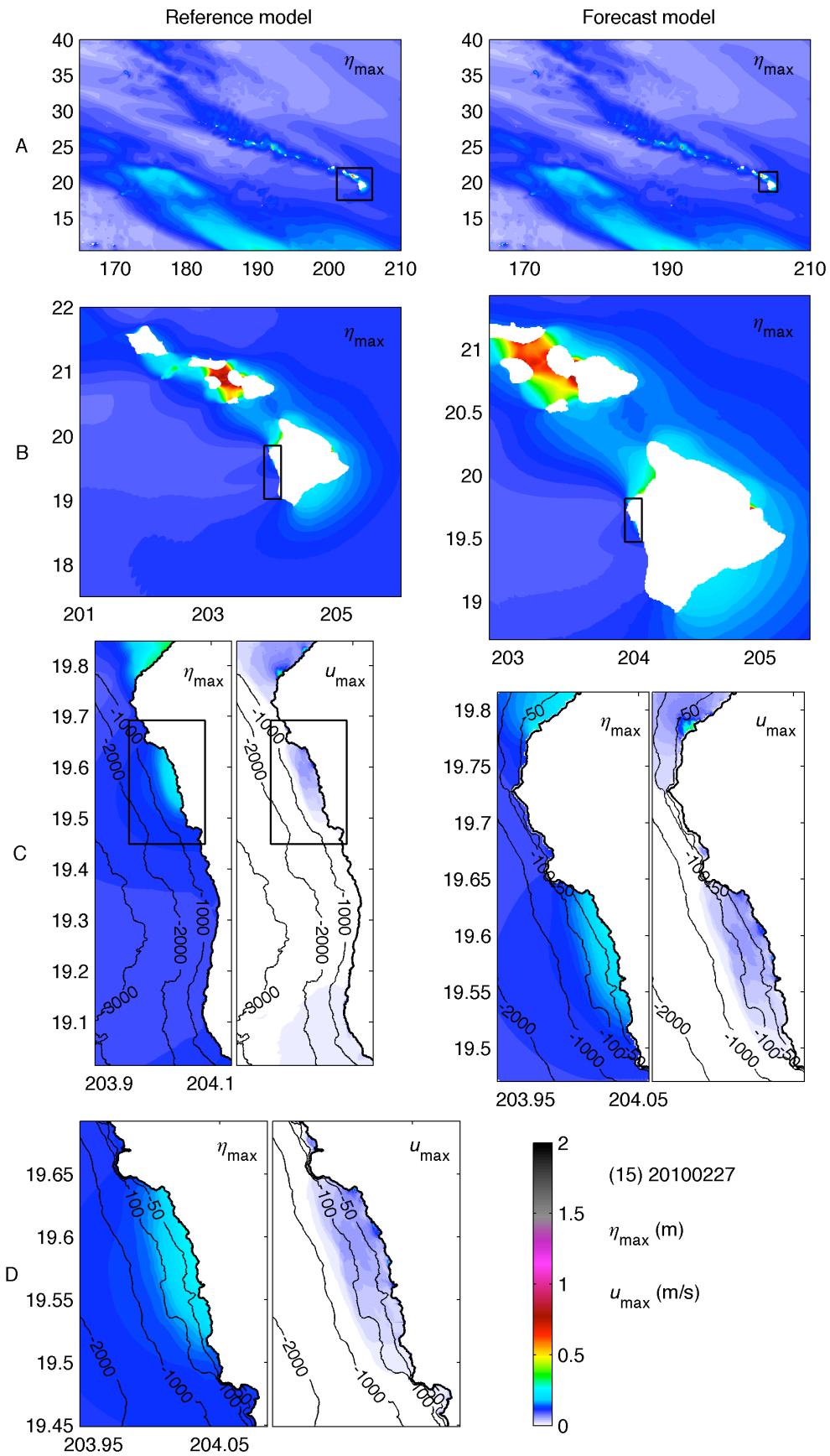
Reference model
Forecast model
A
B
C
D
η_{max}
u_{max}
(15) 20100227
η_{max} (m)
u_{max} (m/s)

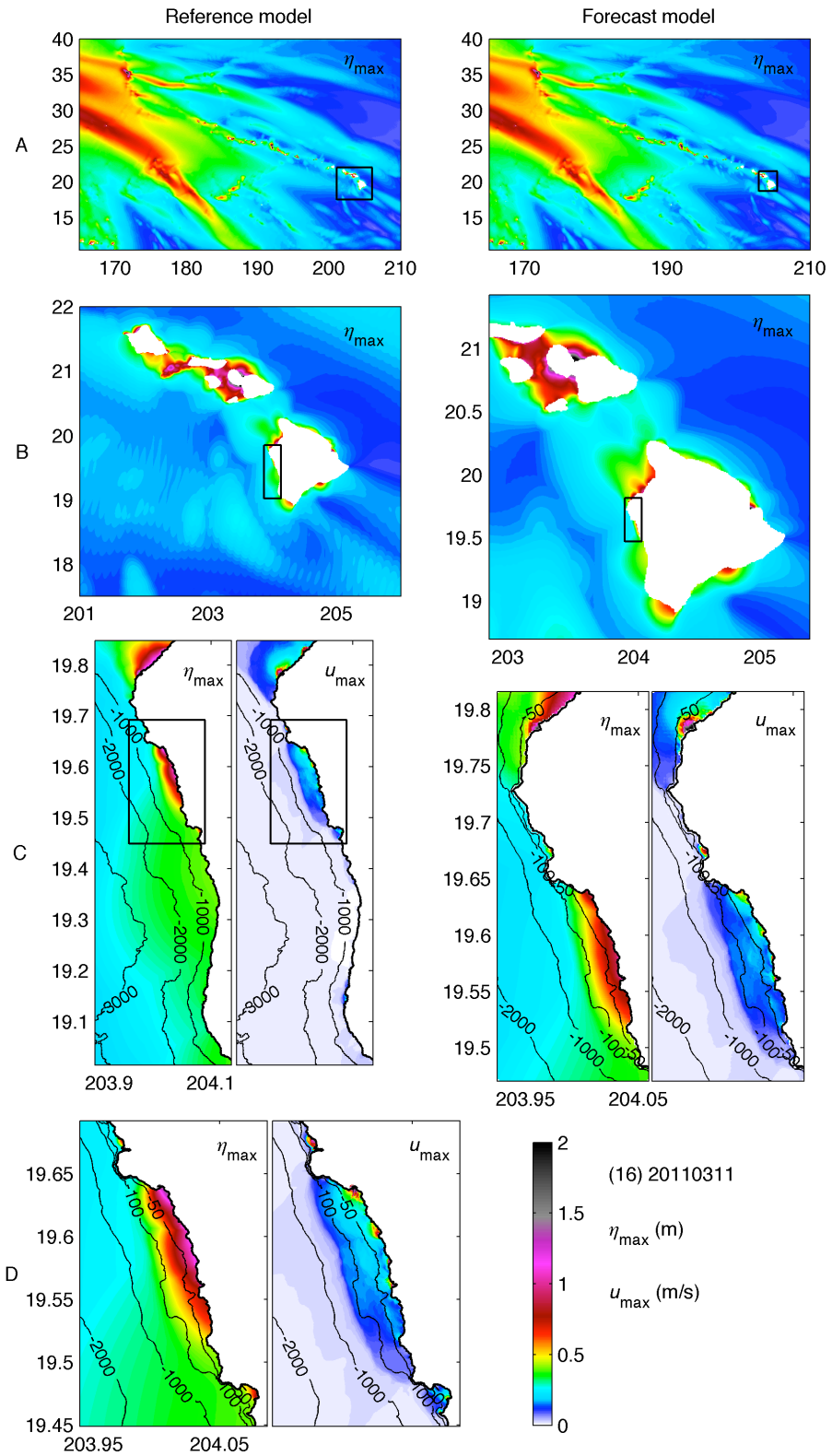

Figure 13 Computed maximum sea surface elevation and current by the Kailua-Kona reference and forecast models for the sixteen past tsunami

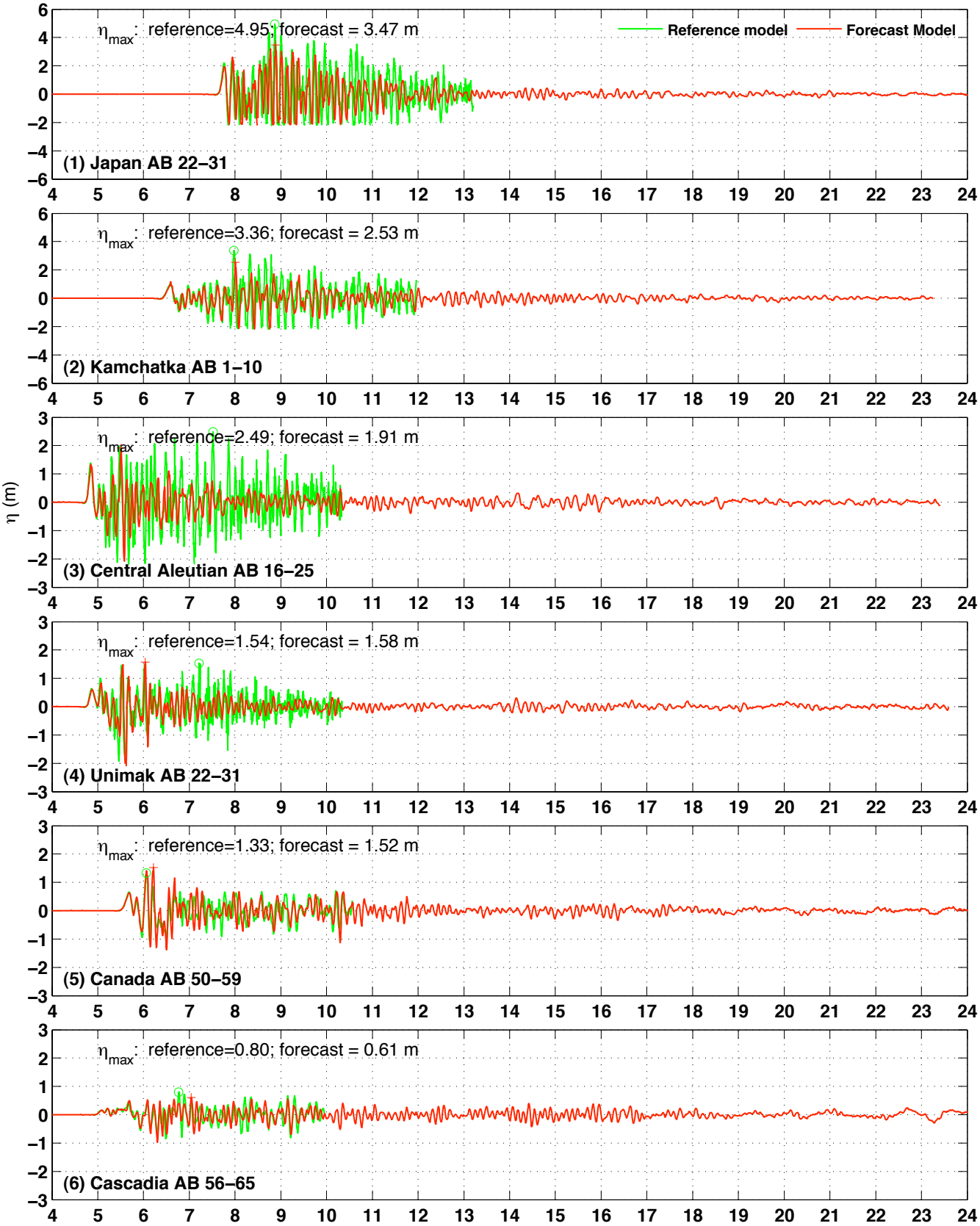
Reference model
Forecast Model
η_{max}: reference=4.95; forecast = 3.47 m
(1) Japan AB 22–31
η_{max}: reference=3.36; forecast = 2.53 m
(2) Kamchatka AB 1–10
η_{max}: reference=2.49; forecast = 1.91 m
(3) Central Aleutian AB 16–25
η_{max}: reference=1.54; forecast = 1.58 m
(4) Unimak AB 22–31
η_{max}: reference=1.33; forecast = 1.52 m
(5) Canada AB 50–59
η_{max}: reference=0.80; forecast = 0.61 m
(6) Cascadia AB 56–65
η (m)

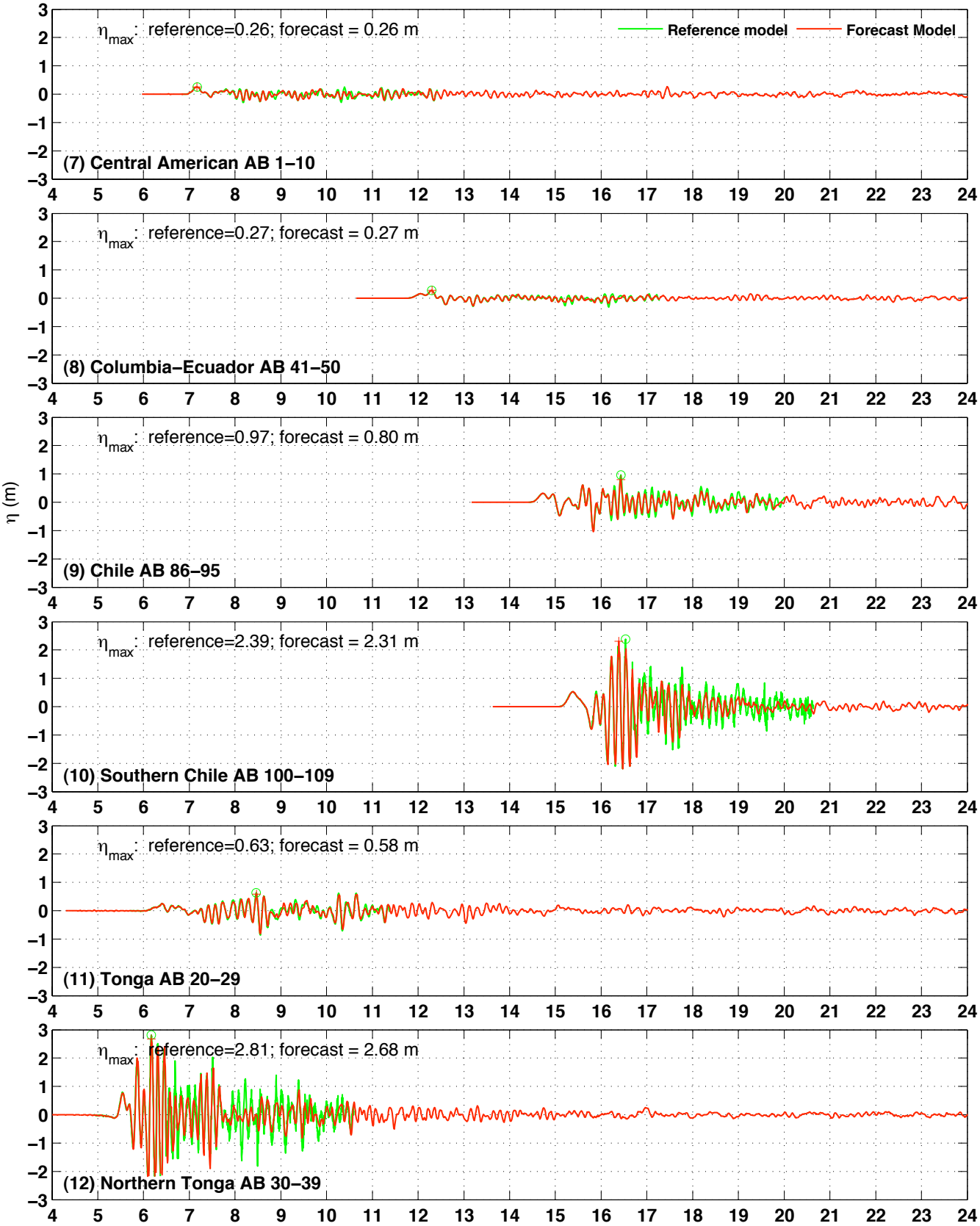
Reference model
Forecast Model
η (m)
ηmax: reference=0.26; forecast = 0.26 m
(7) Central American AB 1–10
ηmax: reference=0.27; forecast = 0.27 m
(8) Columbia–Ecuador AB 41–50
ηmax: reference=0.97; forecast = 0.80 m
(9) Chile AB 86–95
ηmax: reference=2.39; forecast = 2.31 m
(10) Southern Chile AB 100–109
ηmax: reference=0.63; forecast = 0.58 m
(11) Tonga AB 20–29
ηmax: reference=2.81; forecast = 2.68 m
(12) Northern Tonga AB 30–39

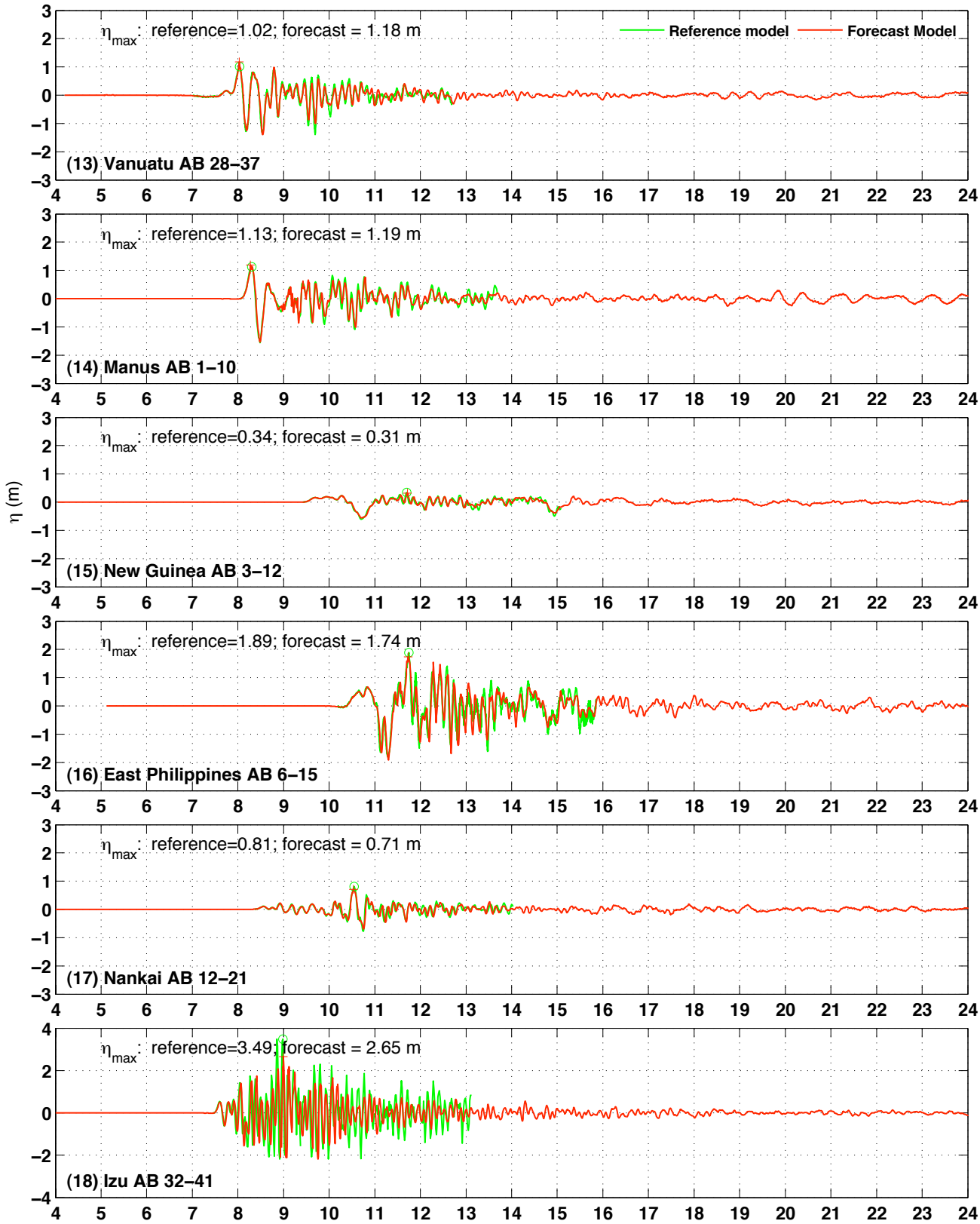

Figure 14 Modeled time series of sea surface elevation η at Kailua-Kona warning point for the eighteen simulated magnitude 9.3 tsunamis. o and + $\eta_{\max}$, computed by the reference and forecast models respectively.

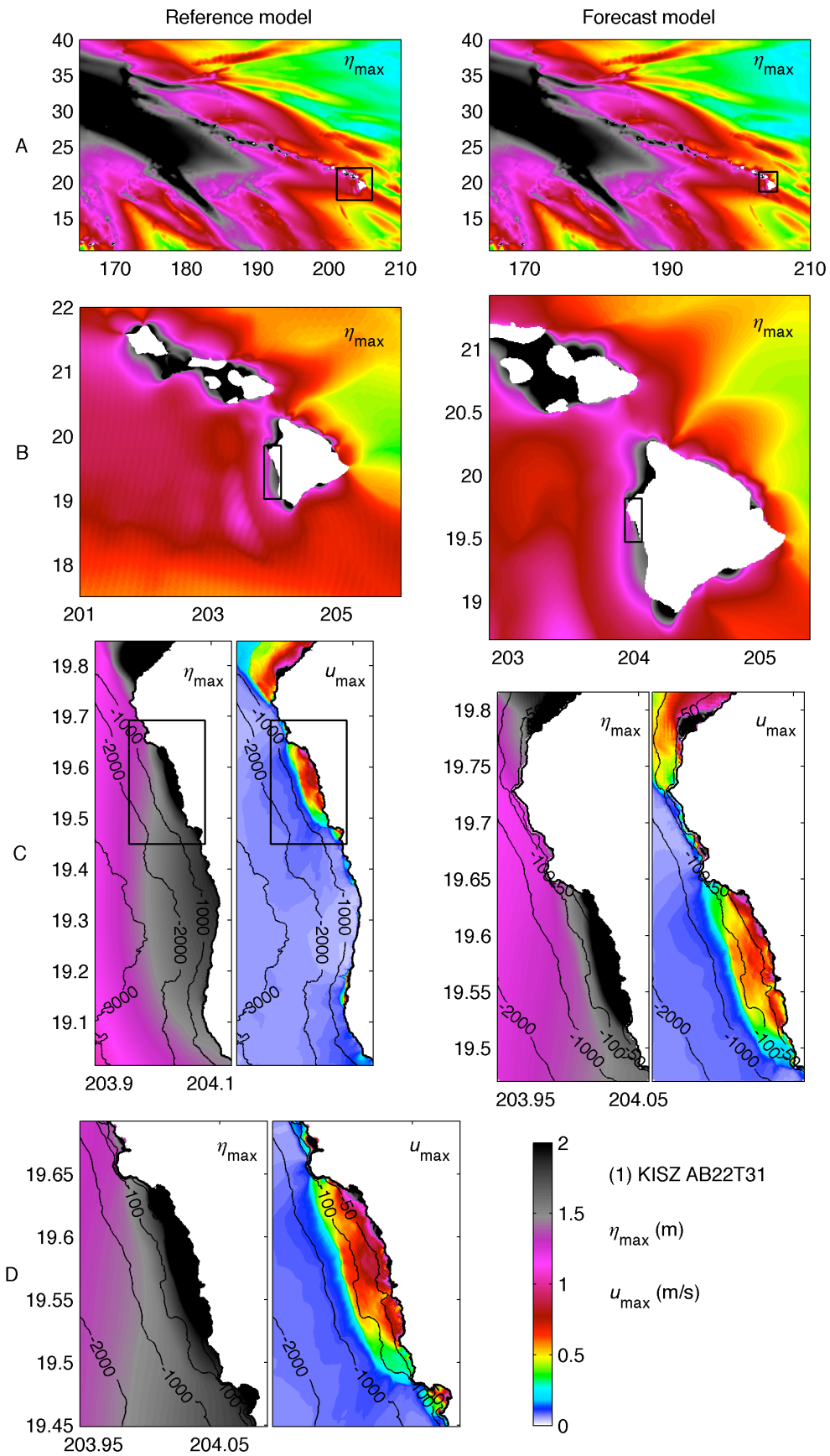
Reference model
Forecast model
A
B
C
D
η_{max}
u_{max}
(1) KISZ AB22T31
η_{max} (m)
u_{max} (m/s)

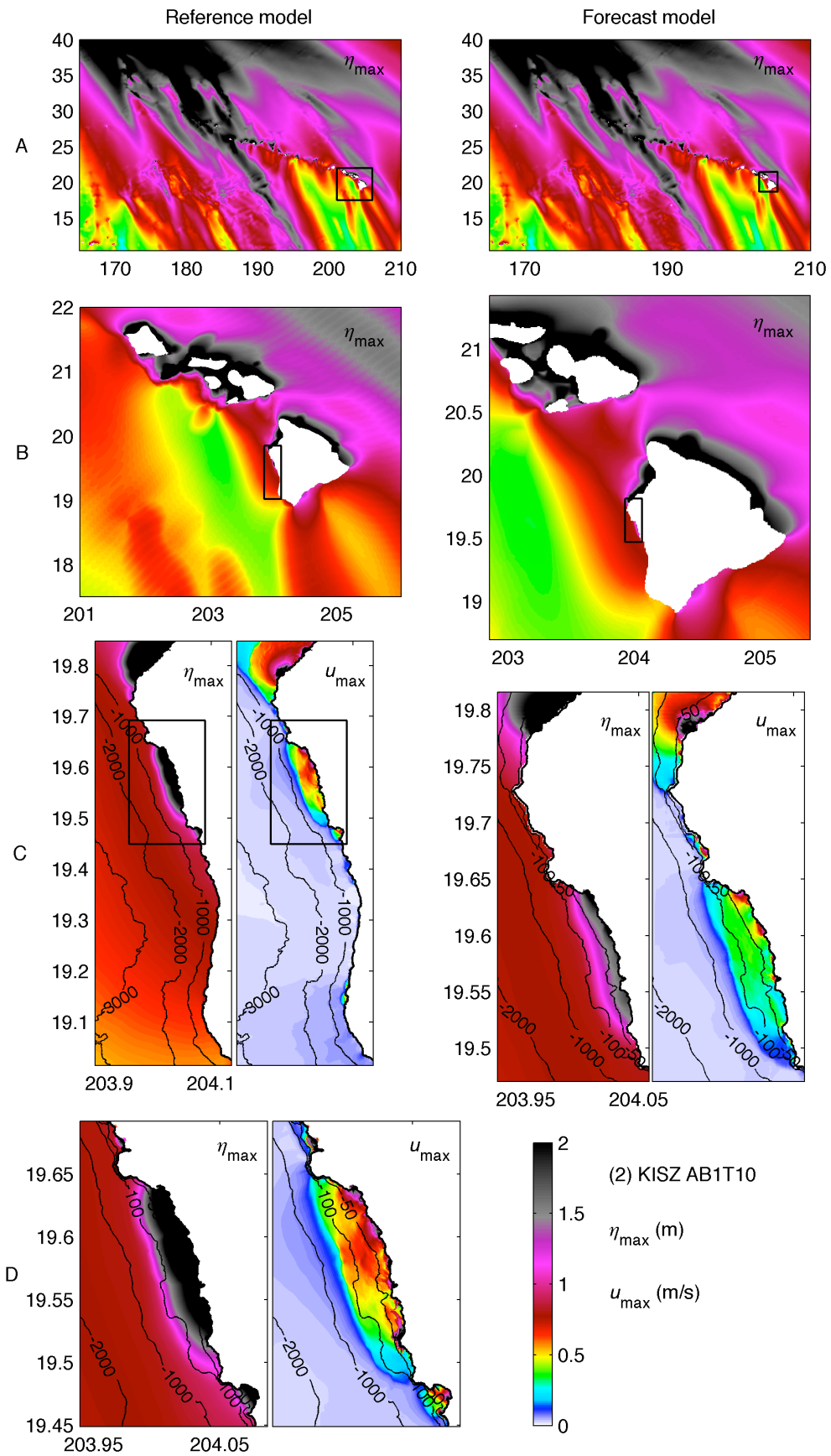
Reference model
Forecast model
A
B
C
D
η_{max}
u_{max}
(2) KISZ AB1T10
η_{max} (m)
u_{max} (m/s)

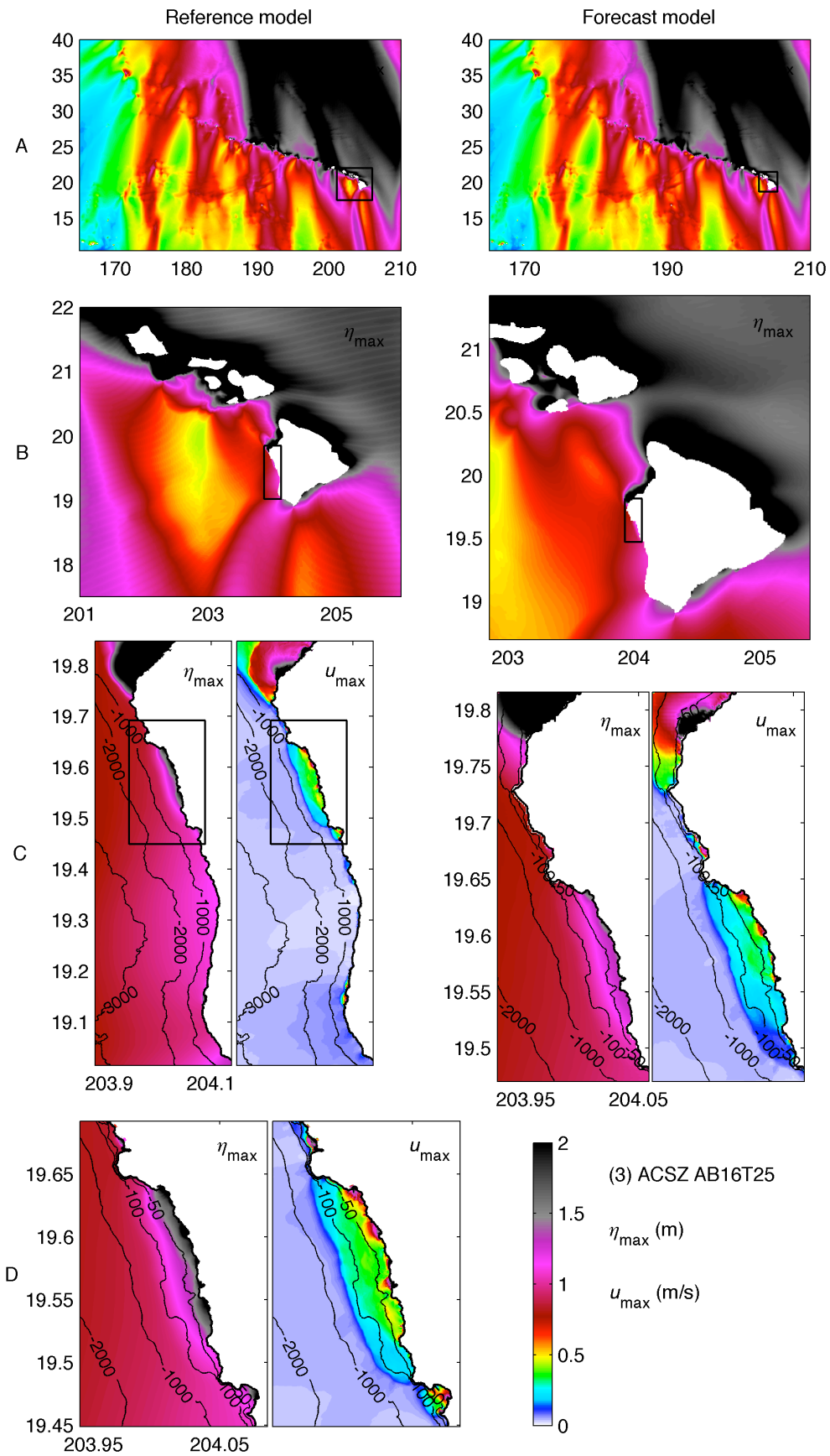
Reference model
Forecast model
A
B
C
D
η_{max}
u_{max}
(3) ACSZ AB16T25
η_{max} (m)
u_{max} (m/s)

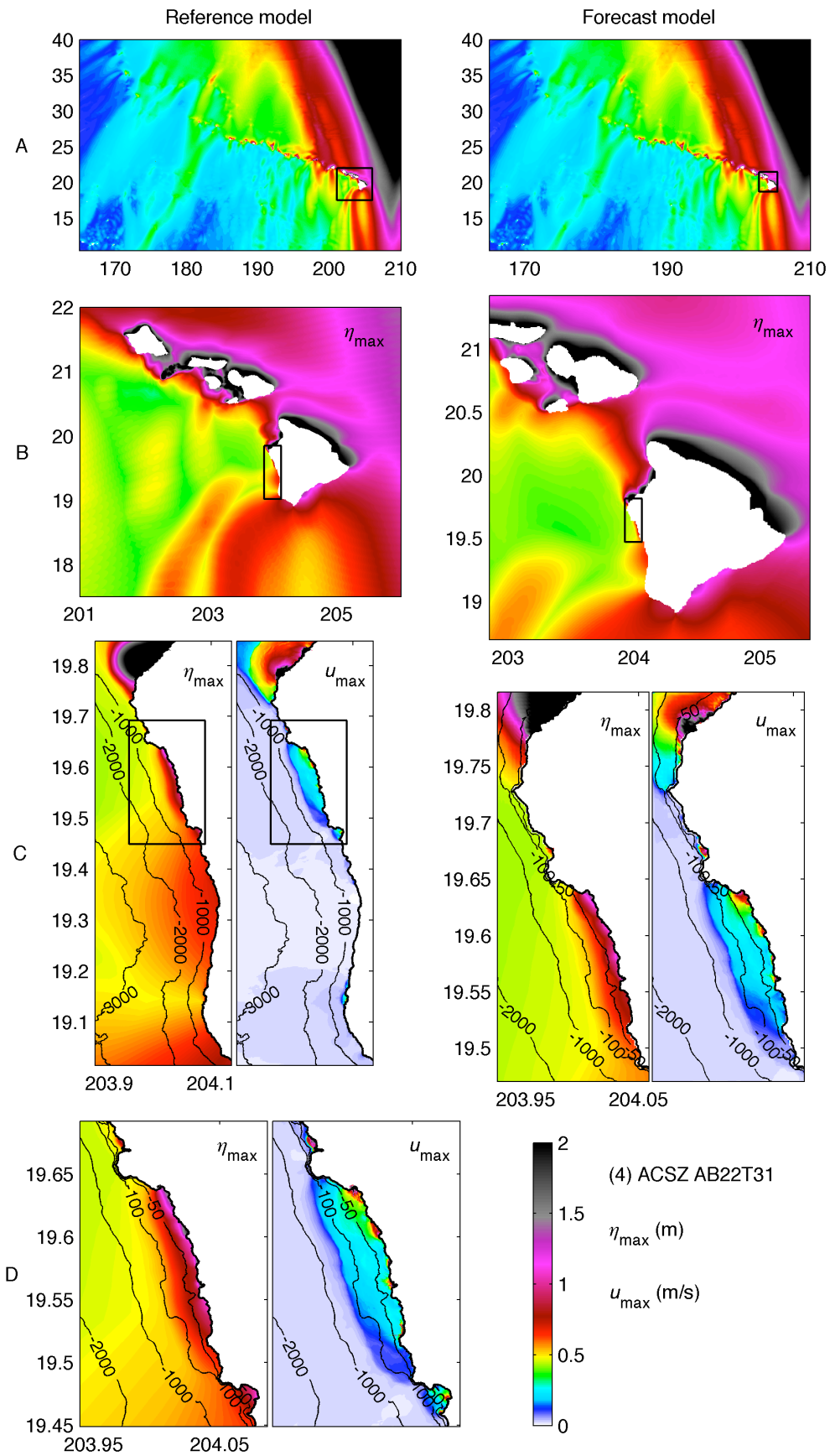
Reference model
Forecast model
A
B
C
D
η_{max}
u_{max}
(4) ACSZ AB22T31
η_{max} (m)
u_{max} (m/s)

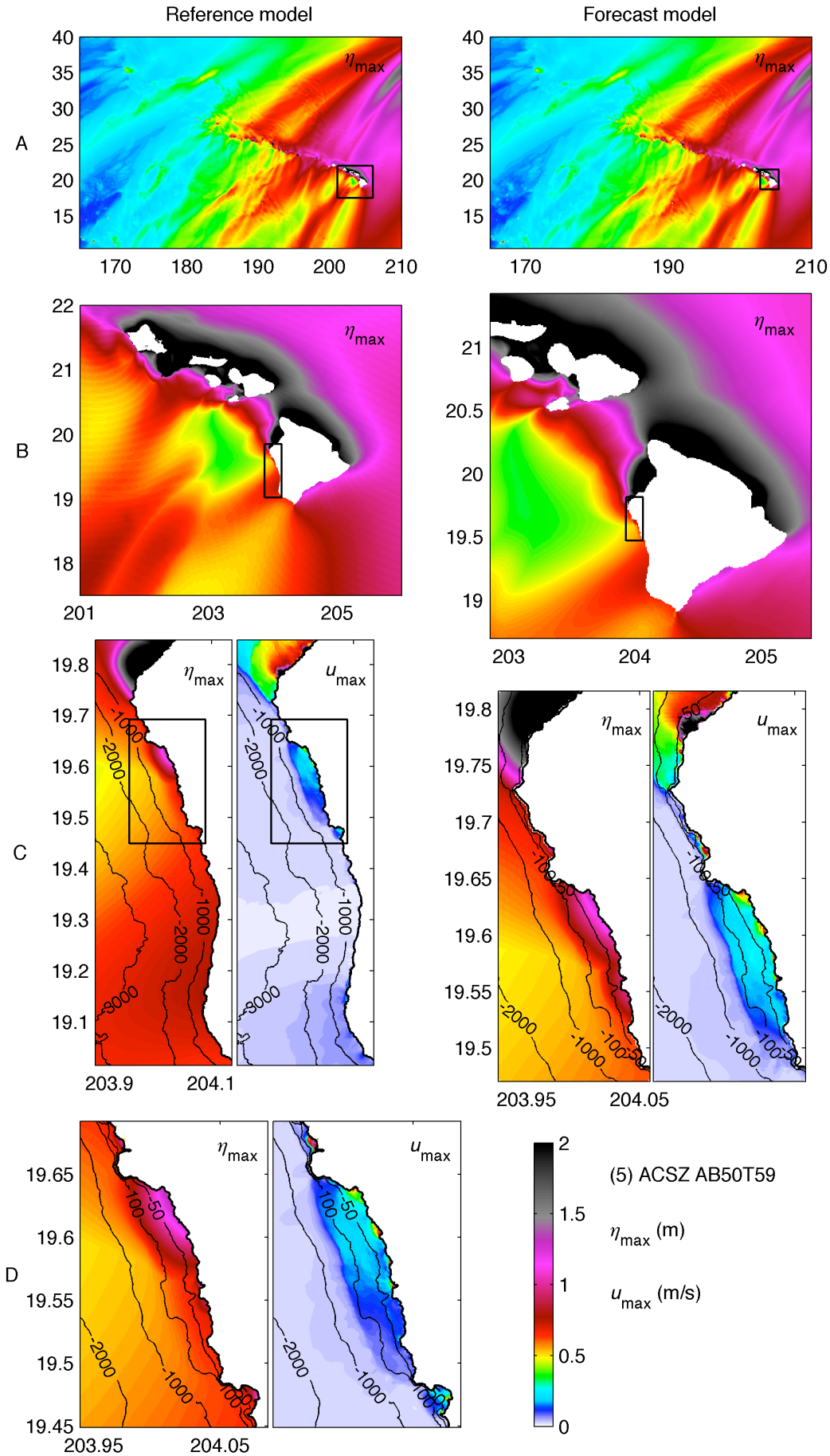
Reference model
Forecast model
A
B
C
D
η_{max}
u_{max}
(5) ACSZ AB50T59
η_{max} (m)
u_{max} (m/s)

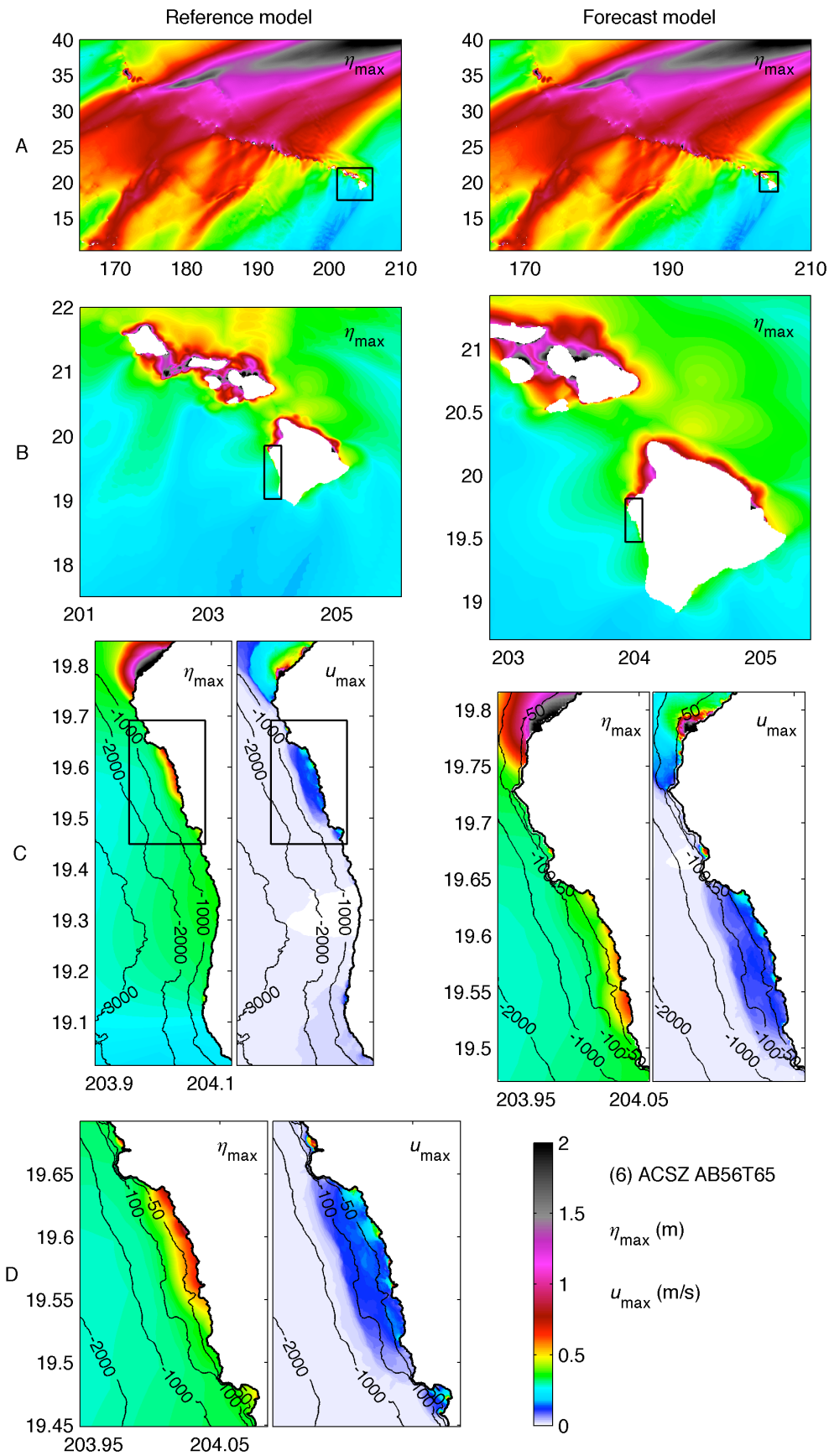
Reference model
Forecast model
A
B
C
D
η_{max}
u_{max}
(6) ACSZ AB56T65
η_{max} (m)
u_{max} (m/s)

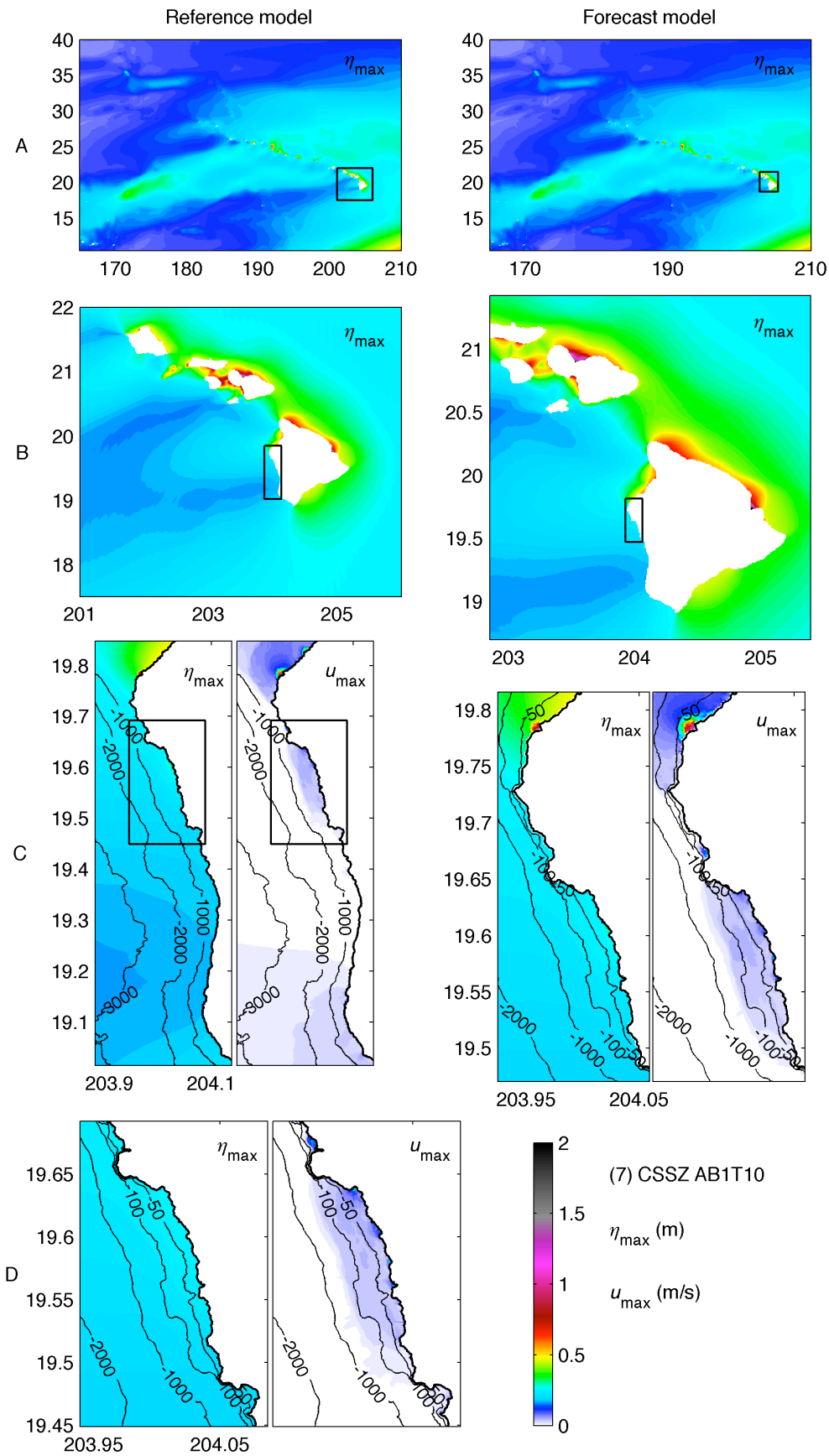
Reference model
Forecast model
A
B
C
D
η_{max}
u_{max}
(7) CSSZ AB1T10
η_{max} (m)
u_{max} (m/s)

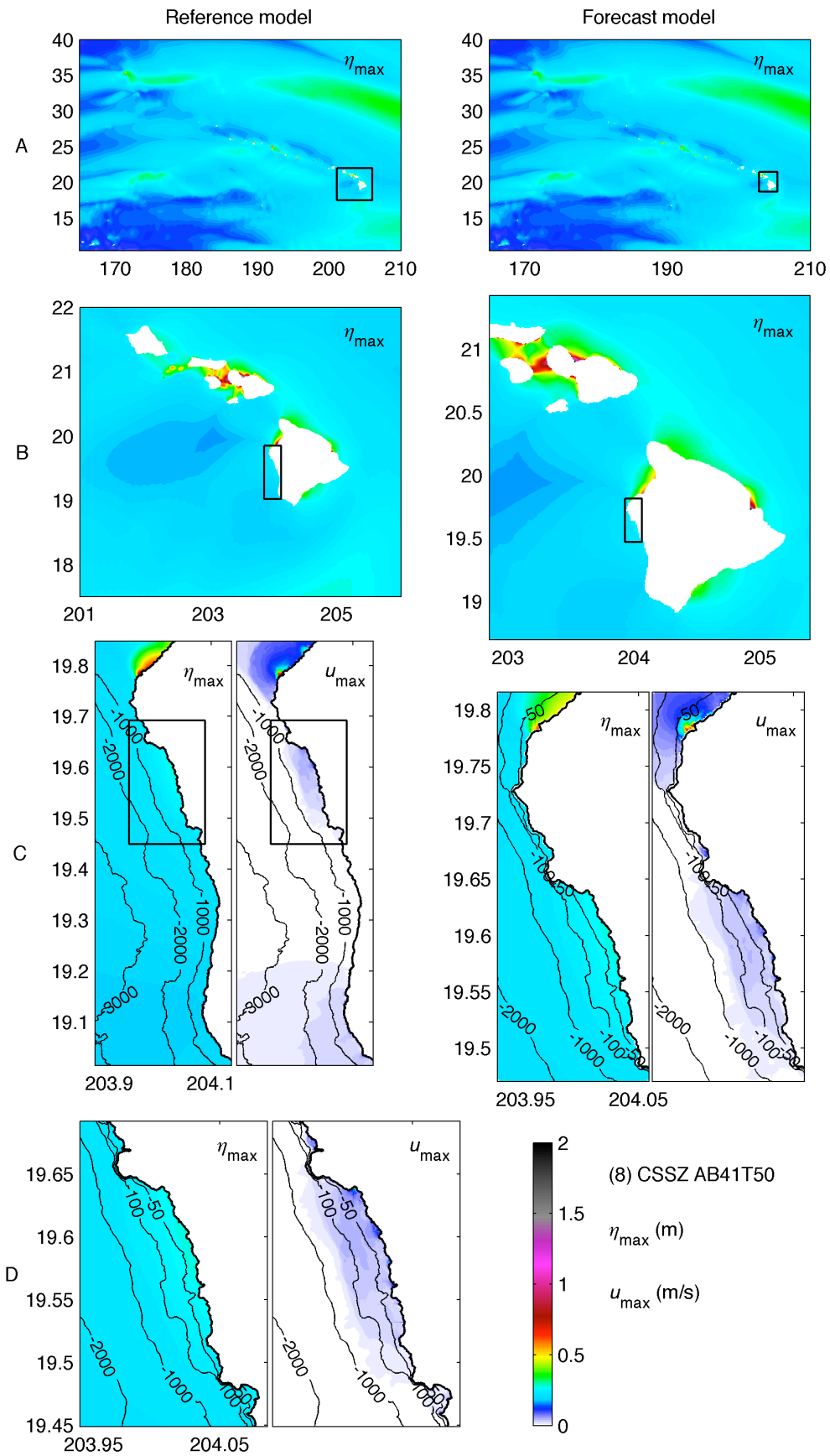
Reference model
Forecast model
A
B
C
D
η_{max}
u_{max}
(8) CSSZ AB41T50
η_{max} (m)
u_{max} (m/s)

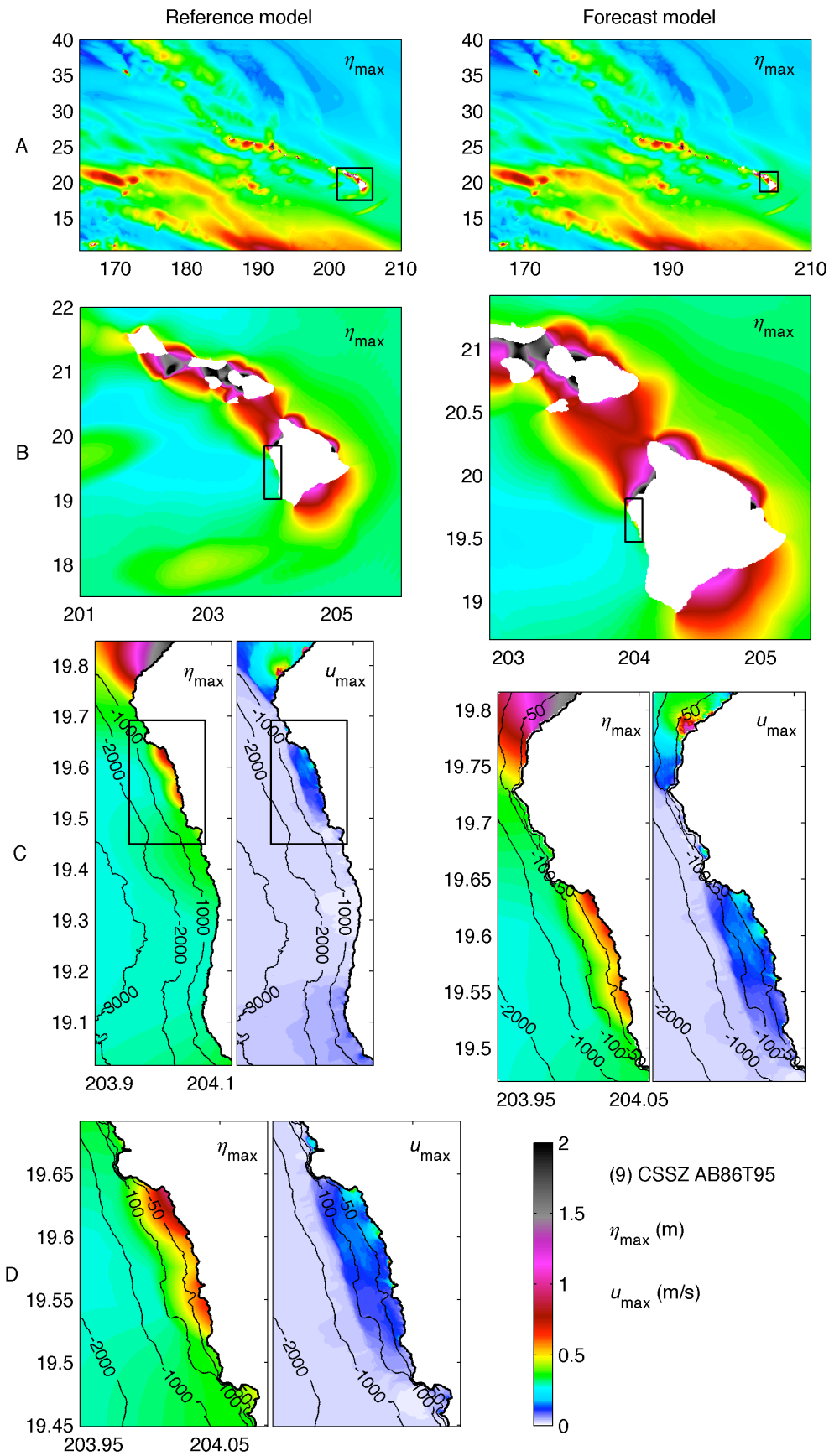
Reference model
Forecast model
A
B
C
D
η_{max}
u_{max}
(9) CSSZ AB86T95
η_{max} (m)
u_{max} (m/s)

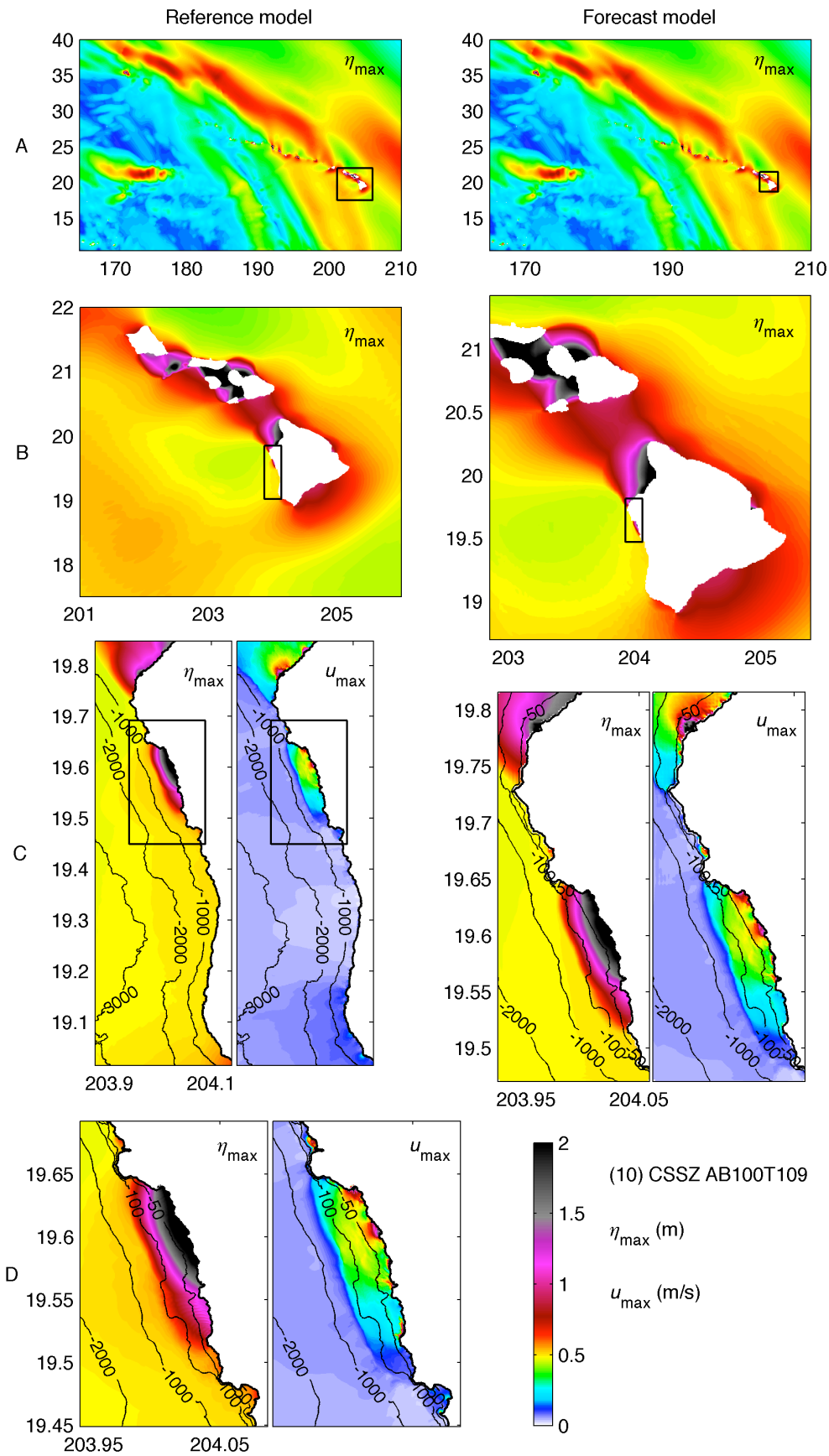
Reference model
Forecast model
A
B
C
D
η_{max}
u_{max}
(10) CSSZ AB100T109
η_{max} (m)
u_{max} (m/s)

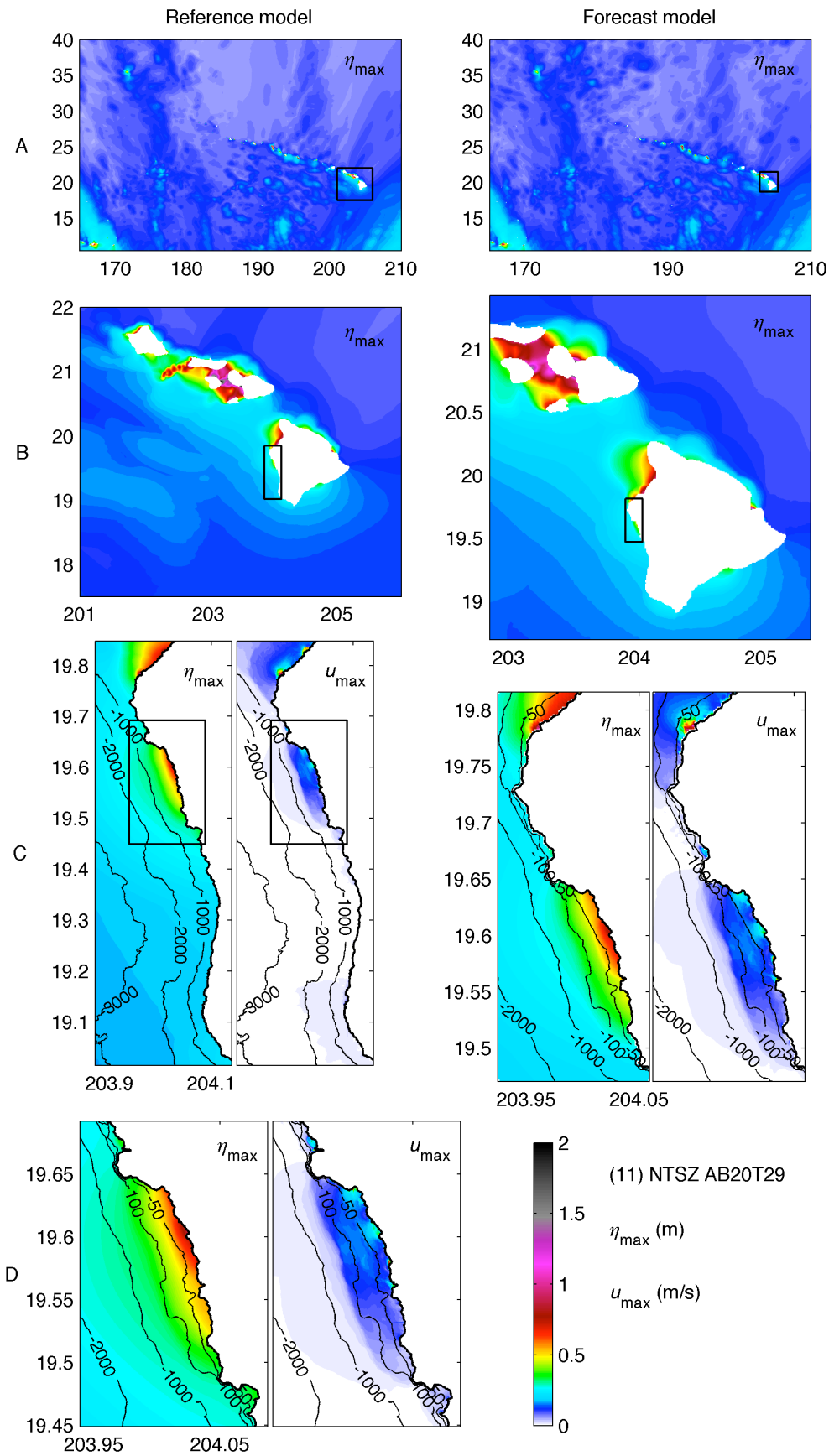
Reference model
Forecast model
A
B
C
D
η_{max}
u_{max}
(11) NTSZ AB20T29
η_{max} (m)
u_{max} (m/s)

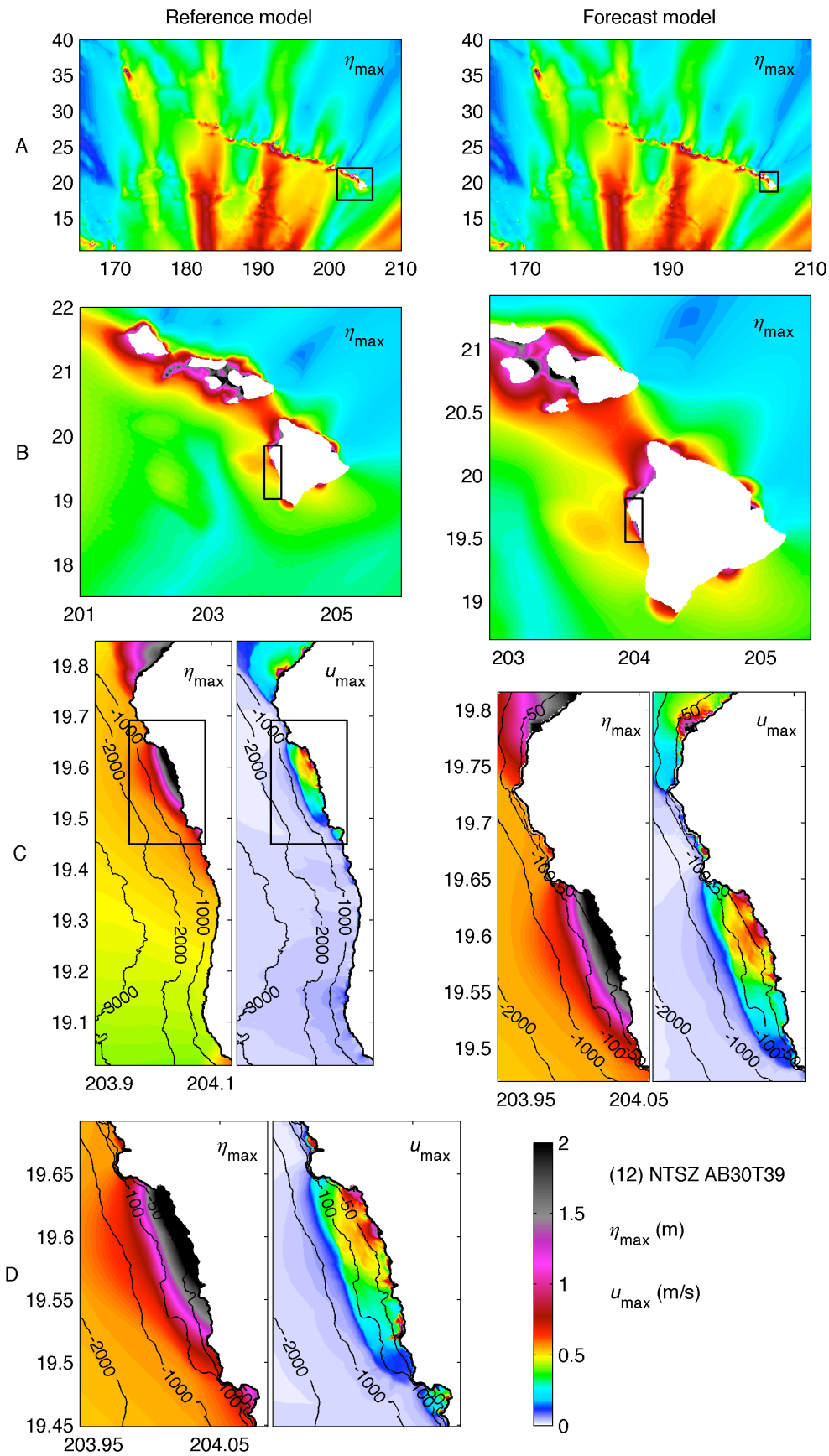
Reference model
Forecast model
A
B
C
D
η_{max}
u_{max}
(12) NTSZ AB30T39
η_{max} (m)
u_{max} (m/s)

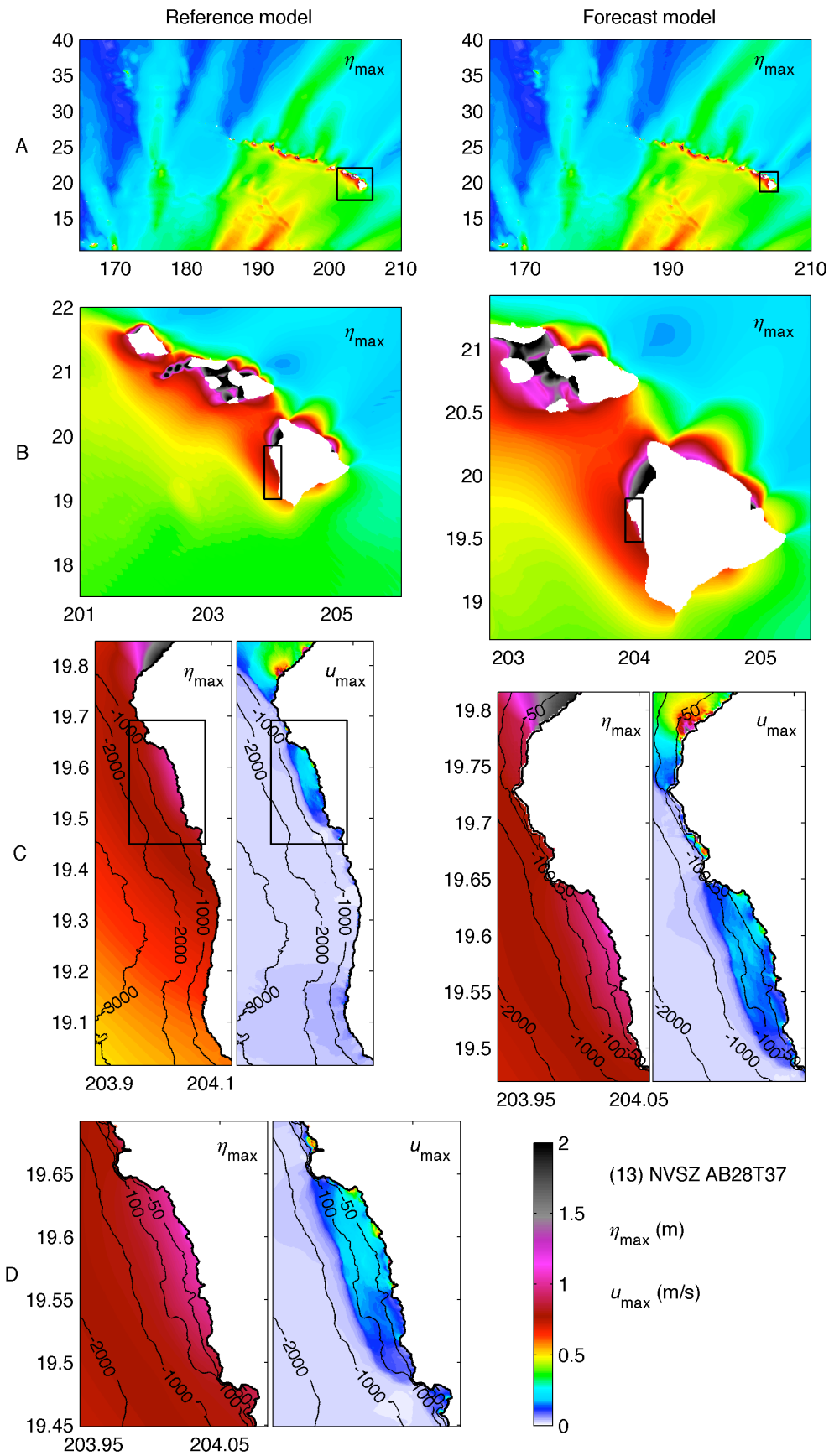
Reference model
Forecast model
A
B
C
D
η_{max}
u_{max}
(13) NVSZ AB28T37
η_{max} (m)
u_{max} (m/s)

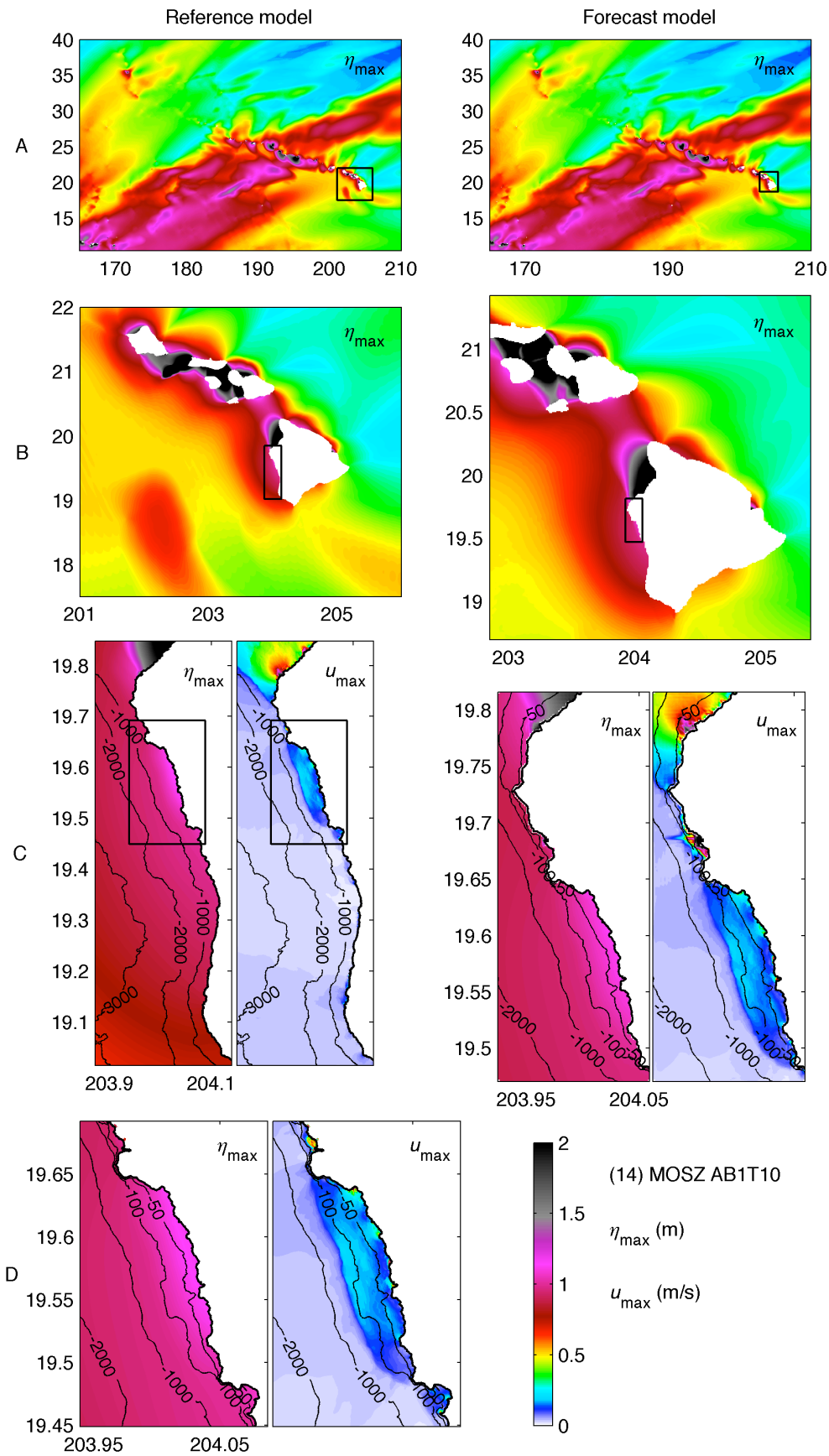
Reference model
Forecast model
A
B
C
D
η_{max}
u_{max}
(14) MOSZ AB1T10
η_{max} (m)
u_{max} (m/s)

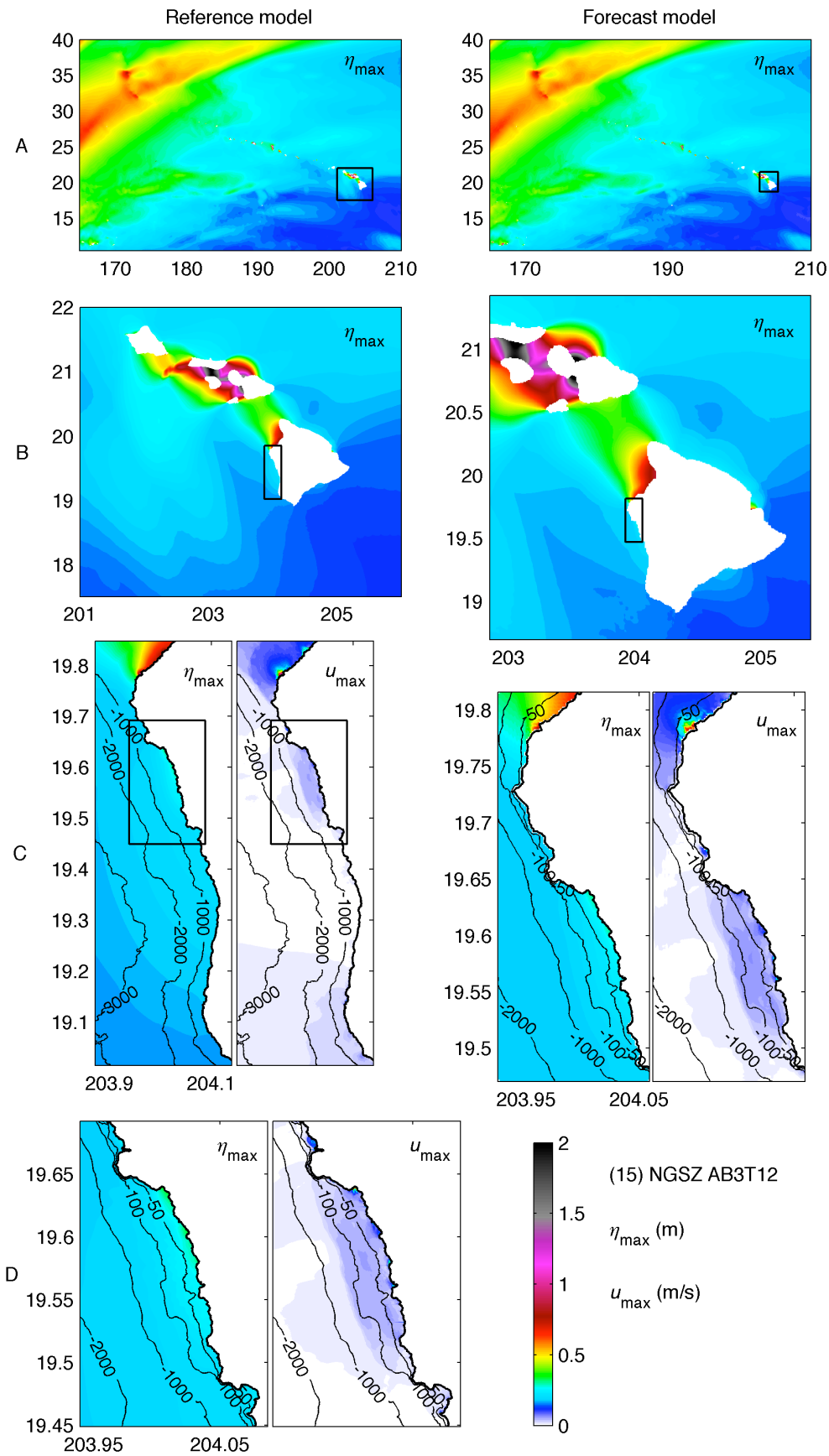
Reference model
Forecast model
A
B
C
D
η_{max}
u_{max}
(15) NGSZ AB3T12
η_{max} (m)
u_{max} (m/s)

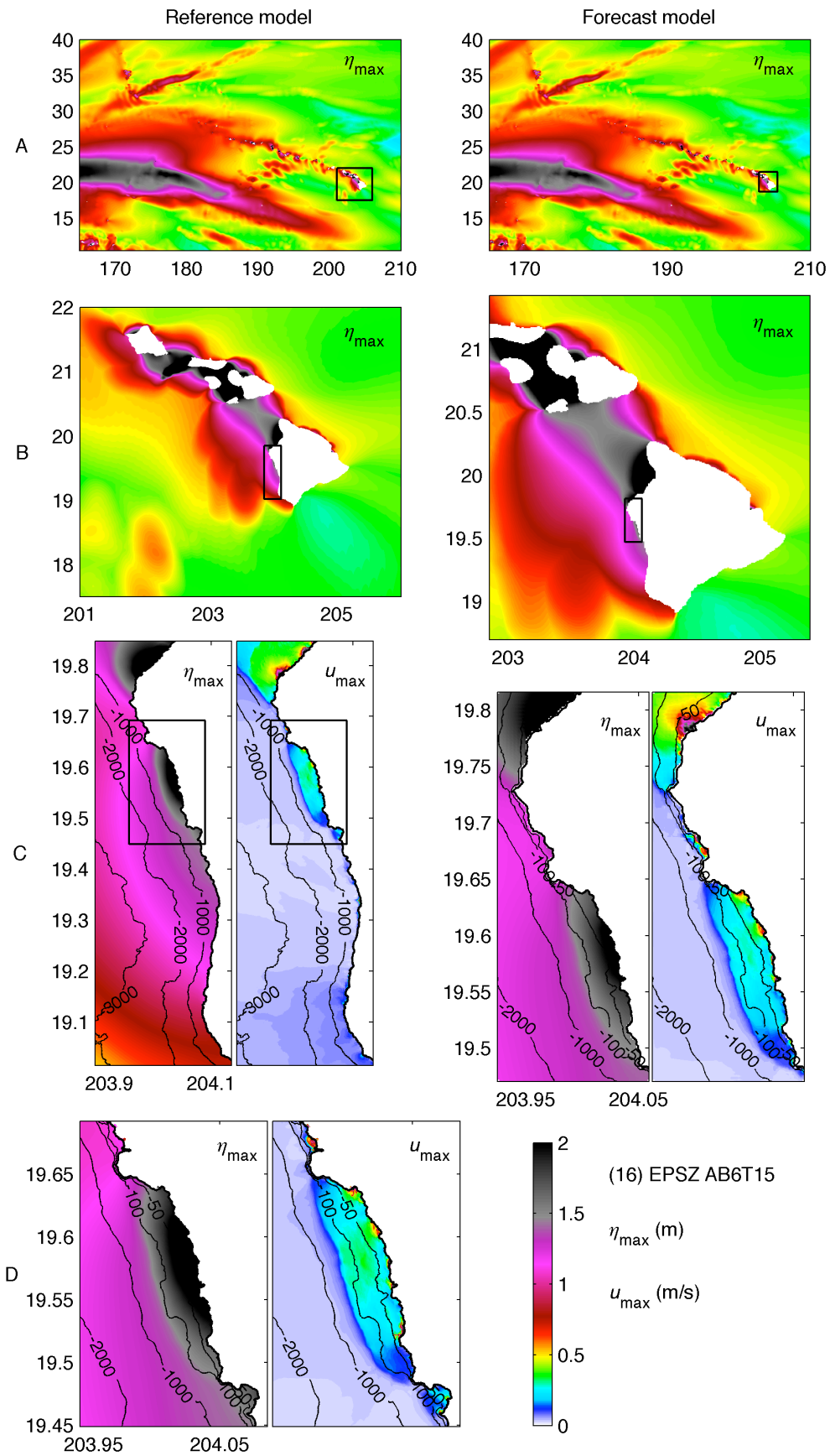
Reference model
Forecast model
A
B
C
D
η_{max}
u_{max}
(16) EPSZ AB6T15
η_{max} (m)
u_{max} (m/s)

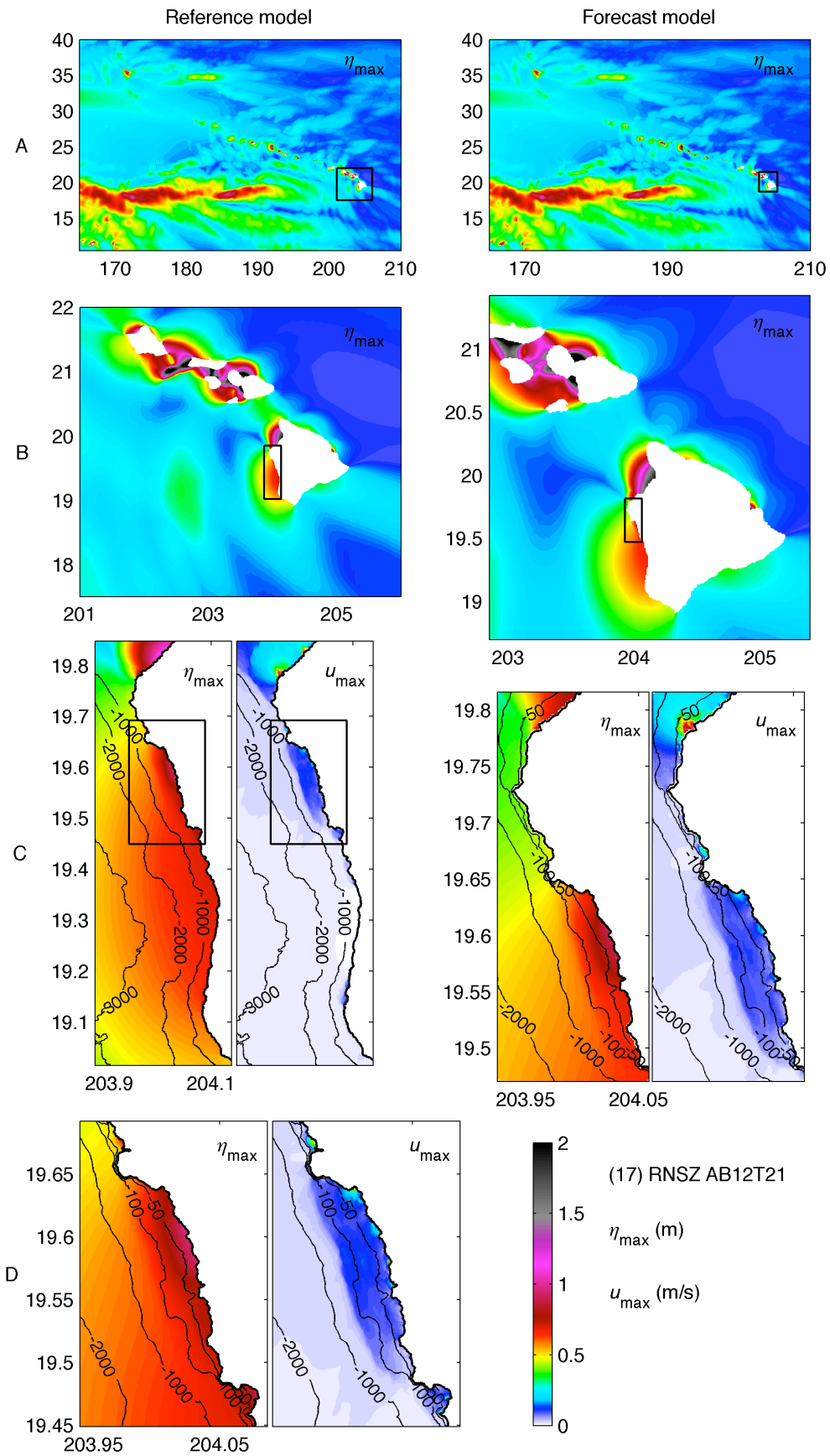
Reference model
Forecast model
A
B
C
D
η_{max}
u_{max}
(17) RNSZ AB12T21
η_{max} (m)
u_{max} (m/s)

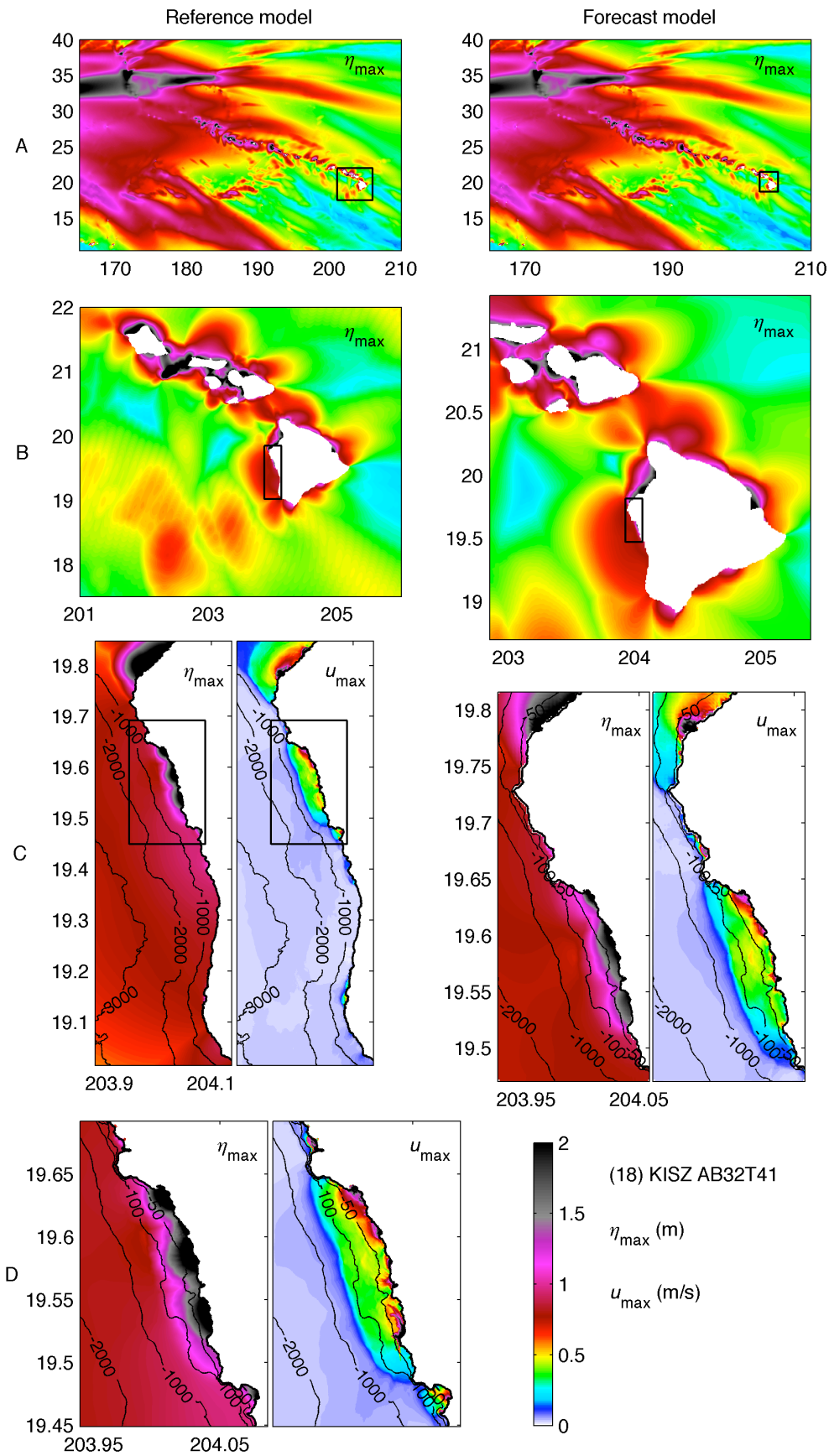
Reference model
Forecast model
A
B
C
D
η_{max}
u_{max}
(18) KISZ AB32T41
η_{max} (m)
u_{max} (m/s)

Figure 15 Computed maximum sea surface elevation and current by the Kailua-Kona reference and forecast models for the eighteen simulated magnitude 9.3 tsunami.

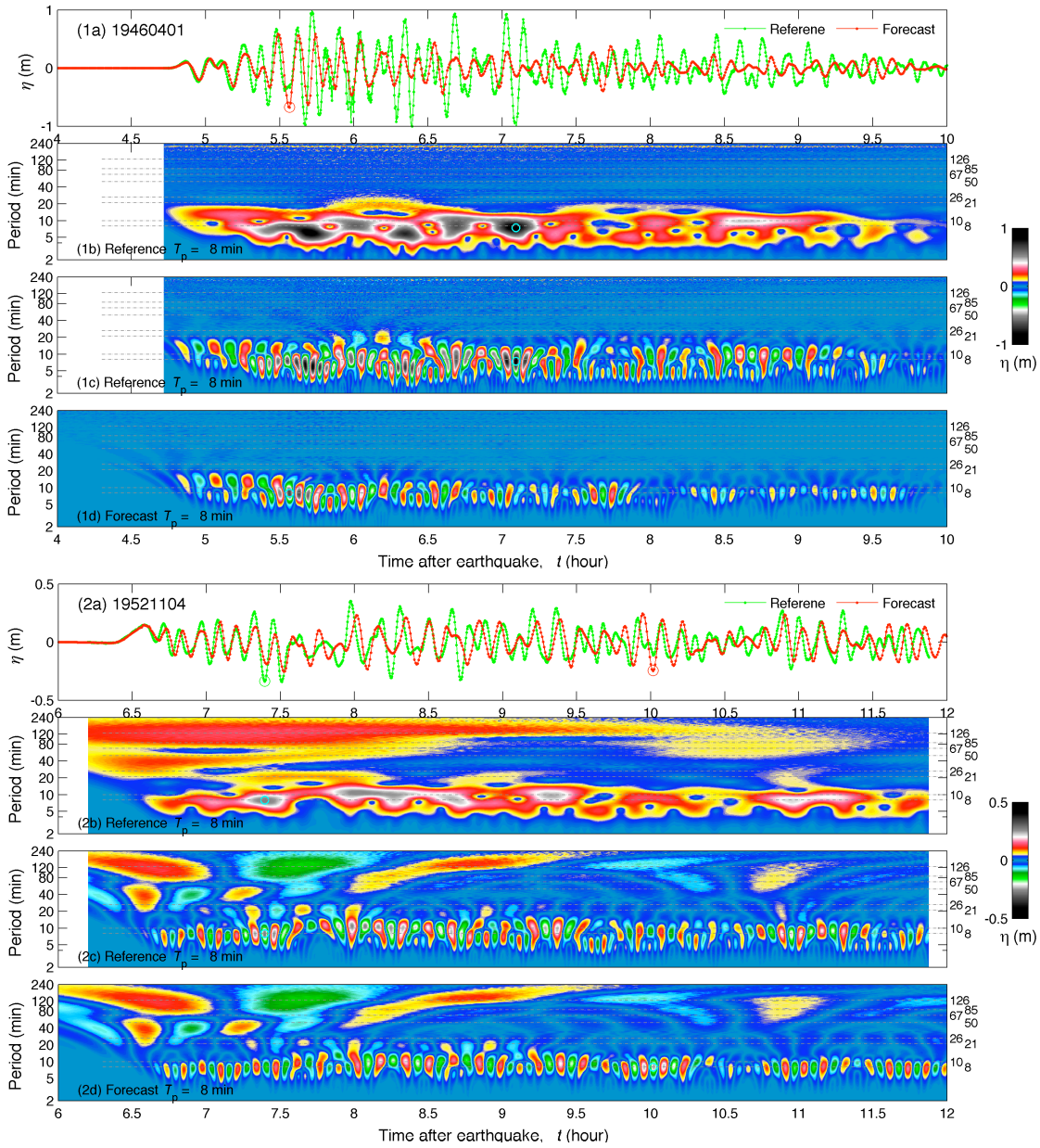
(1a) 19460401
Referene
Forecast
η (m)
Period (min)
(1b) Reference T_p = 8 min
(1c) Reference T_p = 8 min
(1d) Forecast T_p = 8 min
η (m)
Time after earthquake, t (hour)
(2a) 19521104
Referene
Forecast
η (m)
Period (min)
(2b) Reference T_p = 8 min
(2c) Reference T_p = 8 min
(2d) Forecast T_p = 8 min
η (m)
Time after earthquake, t (hour)

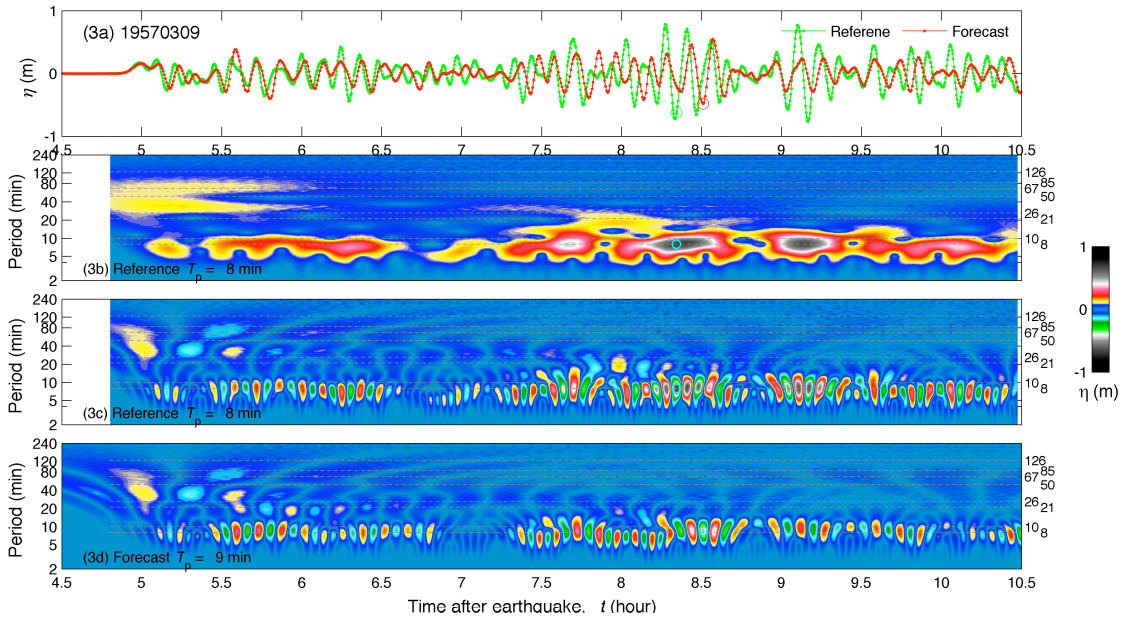
(3a) 19570309
Referene
Forecast
η (m)
(3b) Reference T_p = 8 min
(3c) Reference T_p = 8 min
(3d) Forecast T_p = 9 min
Period (min)
η (m)
Time after earthquake, t (hour)

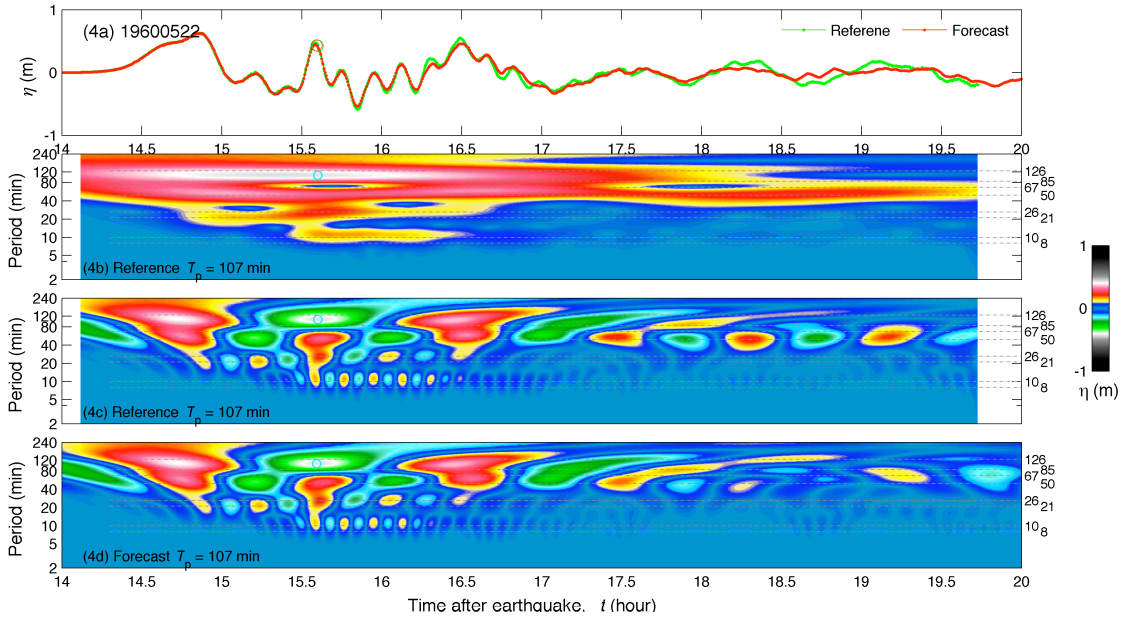
(4a) 19600522
Referene
Forecast
η (m)
(4b) Reference T_p = 107 min
(4c) Reference T_p = 107 min
(4d) Forecast T_p = 107 min
Period (min)
η (m)
Time after earthquake, t (hour)

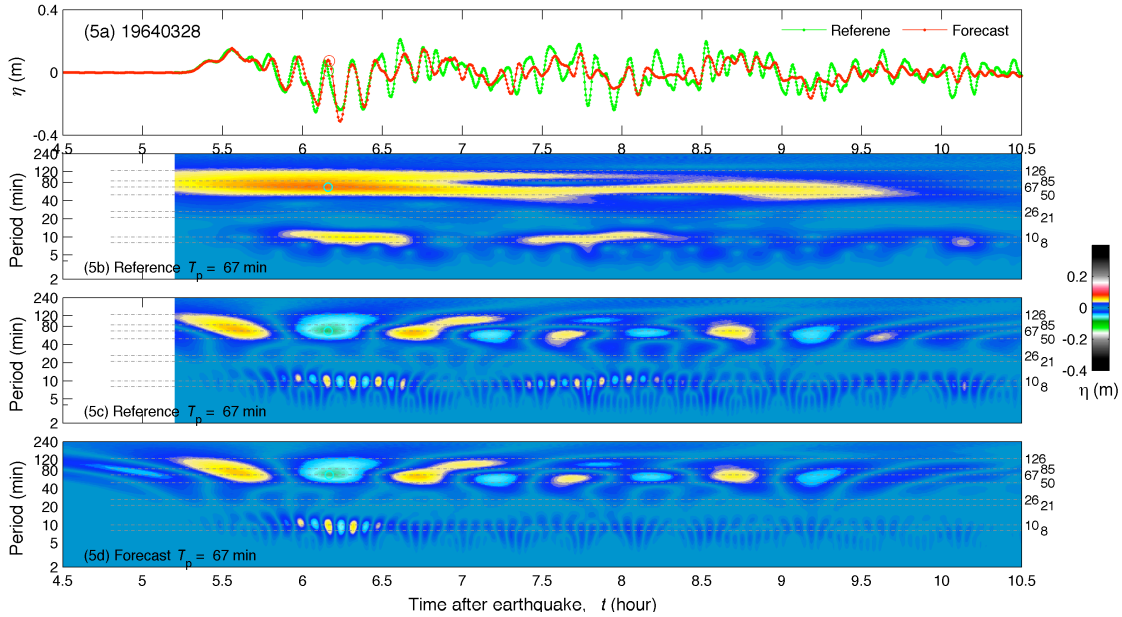
(5a) 19640328
Referene
Forecast
η (m)
(5b) Reference T_p = 67 min
(5c) Reference T_p = 67 min
(5d) Forecast T_p = 67 min
Period (min)
η (m)
Time after earthquake, t (hour)

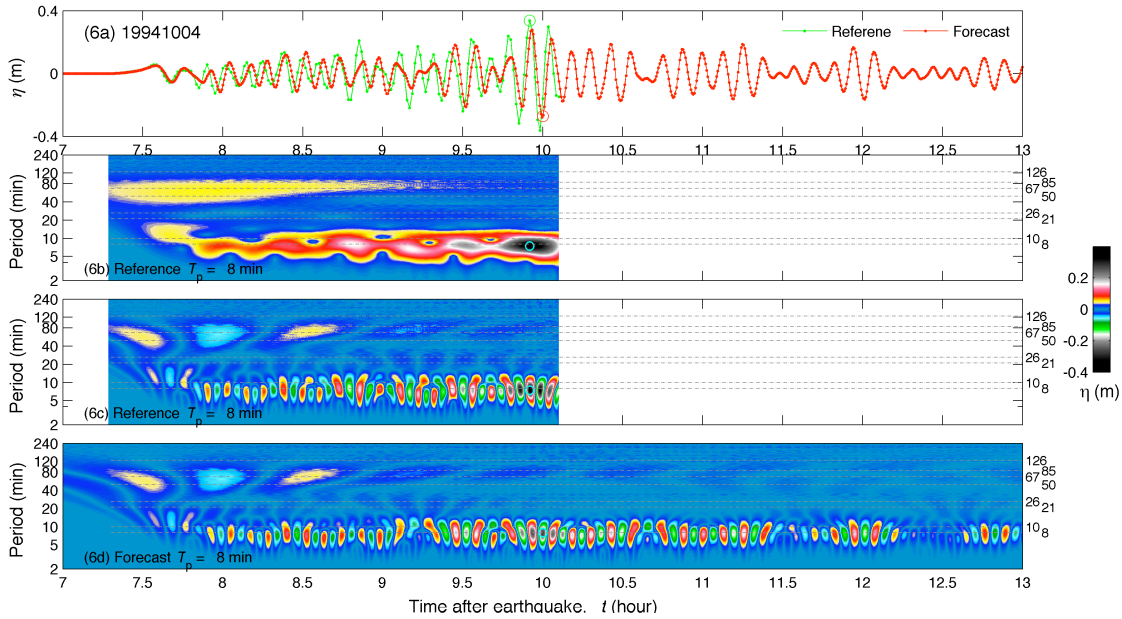
(6a) 19941004
Referene
Forecast
η (m)
Period (min)
(6b) Reference T_p = 8 min
(6c) Reference T_p = 8 min
(6d) Forecast T_p = 8 min
η (m)
Time after earthquake, t (hour)

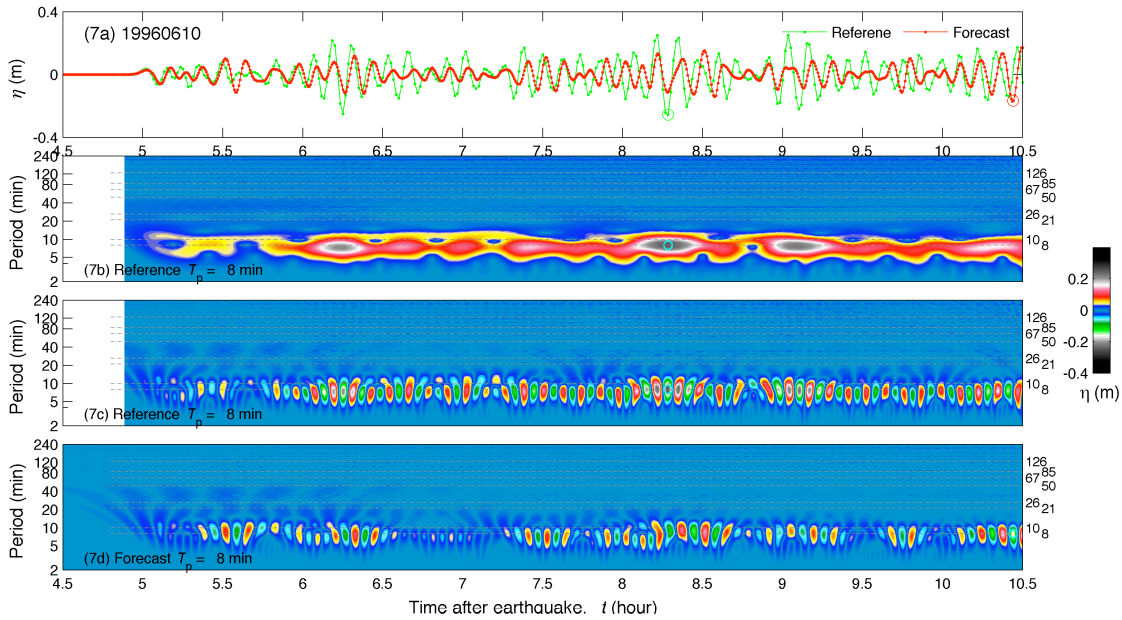
(7a) 19960610
Referene
Forecast
η (m)
Period (min)
(7b) Reference T_p = 8 min
(7c) Reference T_p = 8 min
(7d) Forecast T_p = 8 min
η (m)
Time after earthquake, t (hour)

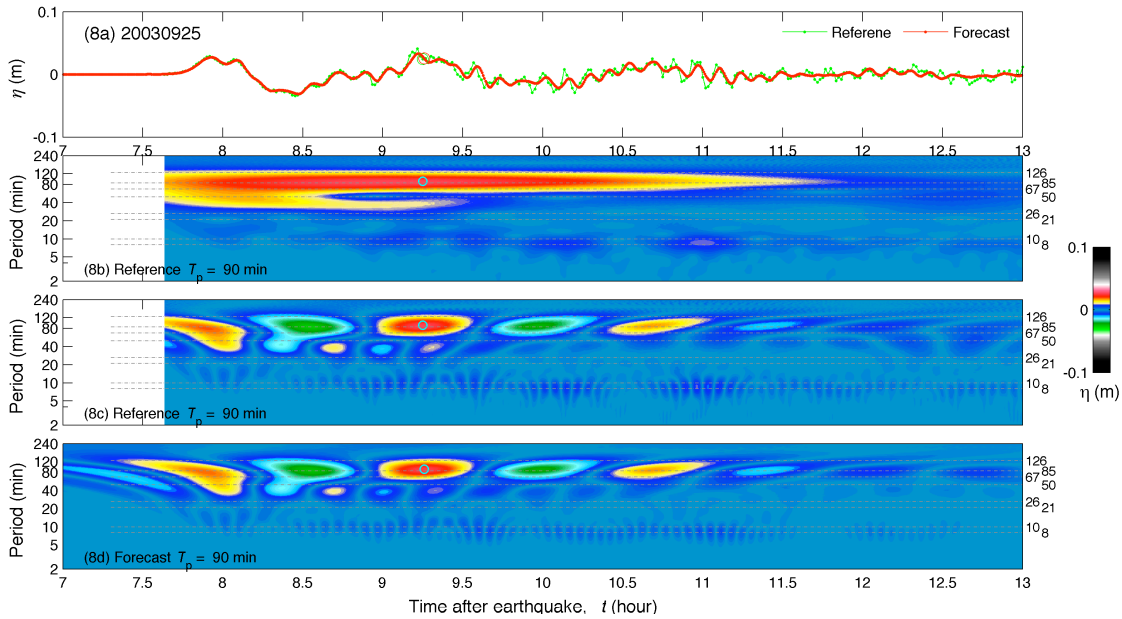
(8a) 20030925
Referene
Forecast
η (m)
Period (min)
(8b) Reference T_p = 90 min
(8c) Reference T_p = 90 min
(8d) Forecast T_p = 90 min
η (m)
Time after earthquake, t (hour)

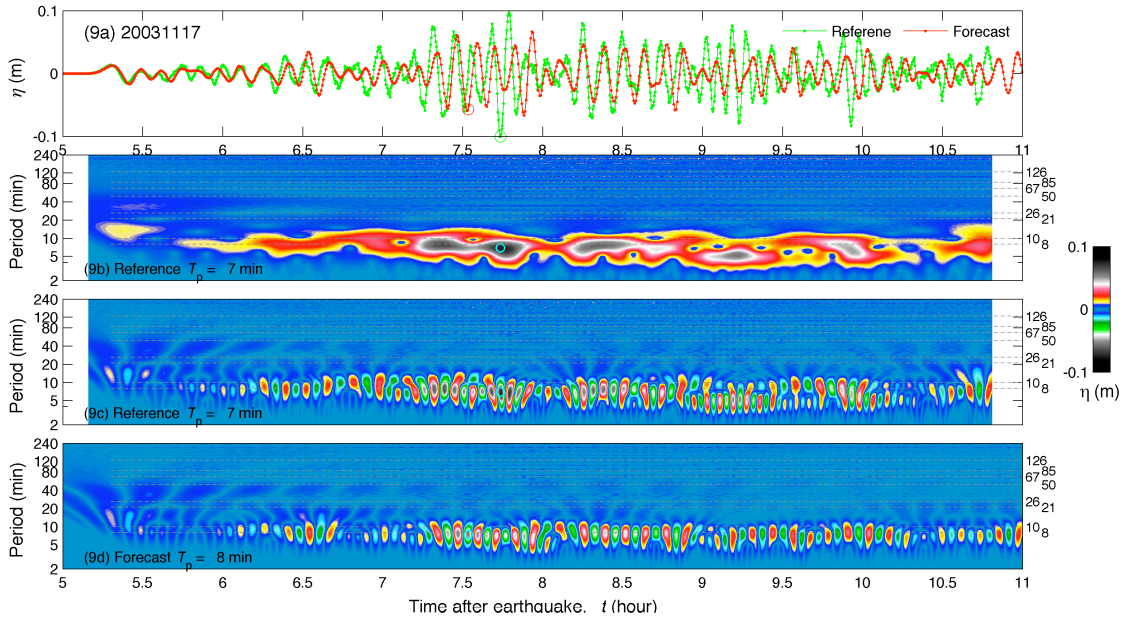
(9a) 20031117
Referene
Forecast
η (m)
Period (min)
(9b) Reference T_p = 7 min
(9c) Reference T_p = 7 min
(9d) Forecast T_p = 8 min
η (m)
Time after earthquake, t (hour)

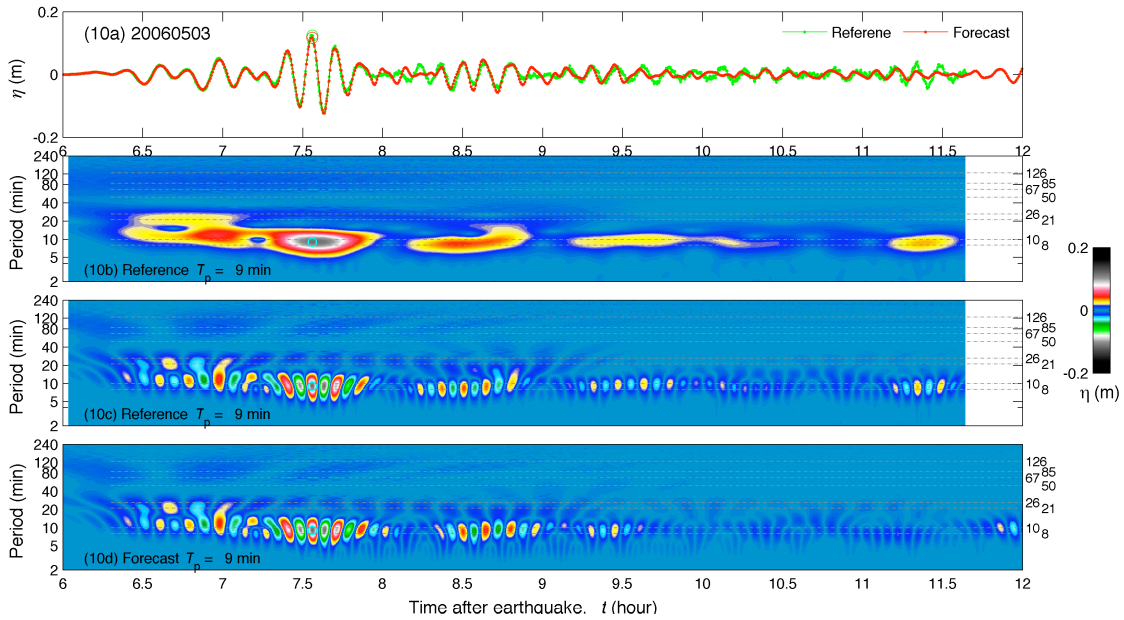
(10a) 20060503
Referene
Forecast
η (m)
Period (min)
(10b) Reference T_p = 9 min
(10c) Reference T_p = 9 min
(10d) Forecast T_p = 9 min
η (m)
Time after earthquake, t (hour)

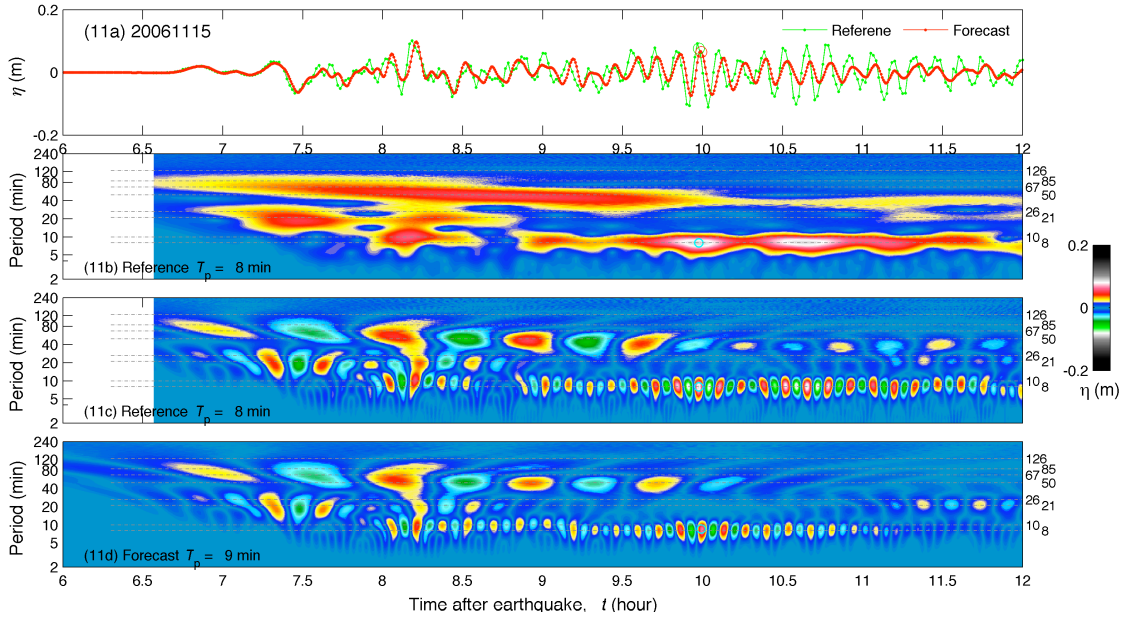
(11a) 20061115
Referene
Forecast
η (m)
Period (min)
(11b) Reference T_p = 8 min
(11c) Reference T_p = 8 min
(11d) Forecast T_p = 9 min
η (m)
Time after earthquake, t (hour)

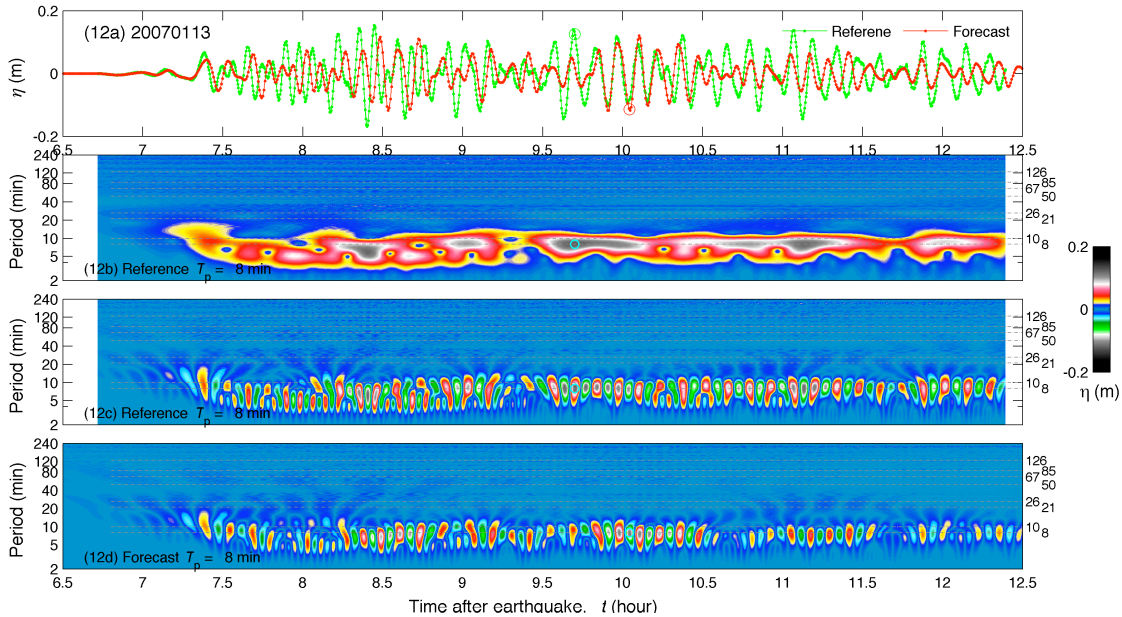
(12a) 20070113
Referene
Forecast
η (m)
Period (min)
(12b) Reference T_p = 8 min
(12c) Reference T_p = 8 min
(12d) Forecast T_p = 8 min
η (m)
Time after earthquake, t (hour)

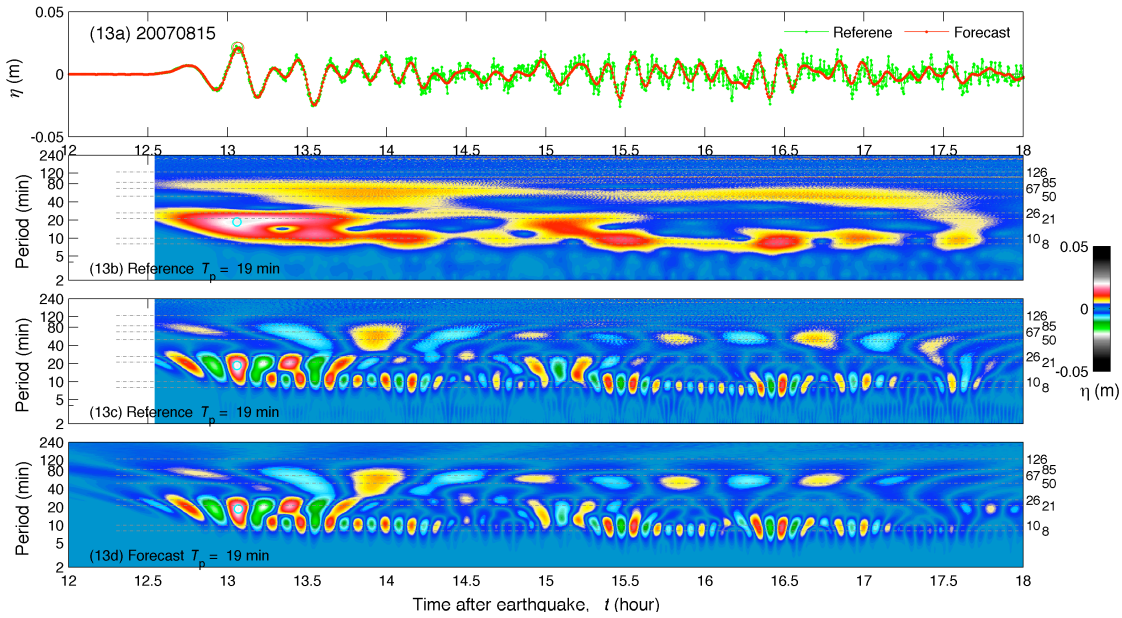
(13a) 20070815
Referene
Forecast
η (m)
Period (min)
(13b) Reference T_p = 19 min
(13c) Reference T_p = 19 min
(13d) Forecast T_p = 19 min
η (m)
Time after earthquake, t (hour)

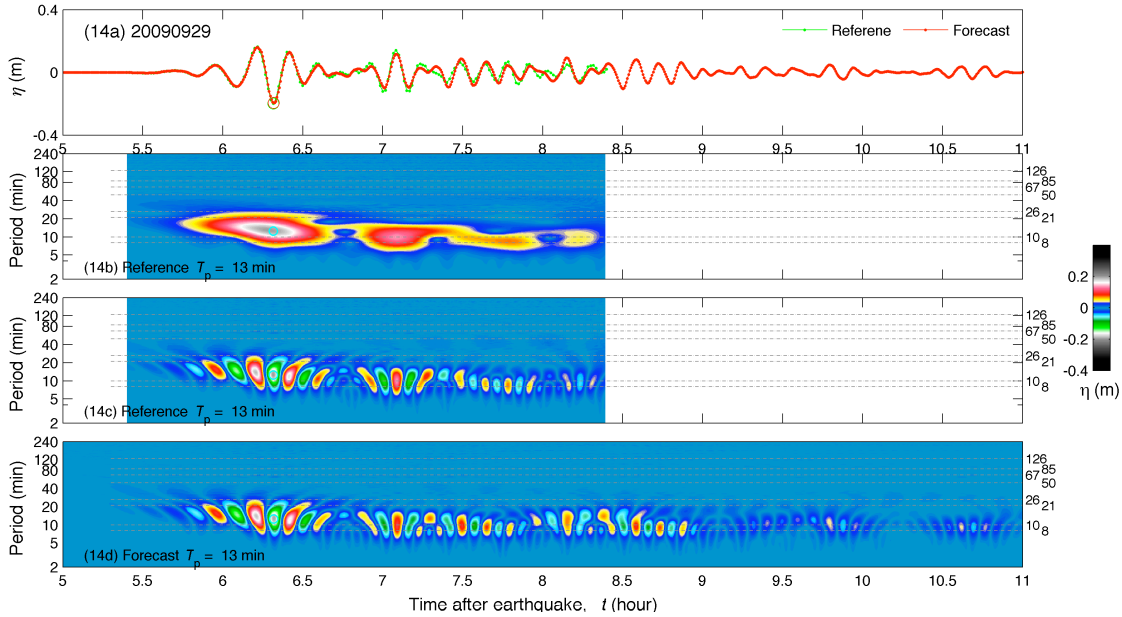
(14a) 20090929
Referene
Forecast
η (m)
Period (min)
(14b) Reference T_p = 13 min
(14c) Reference T_p = 13 min
(14d) Forecast T_p = 13 min
η (m)
Time after earthquake, t (hour)

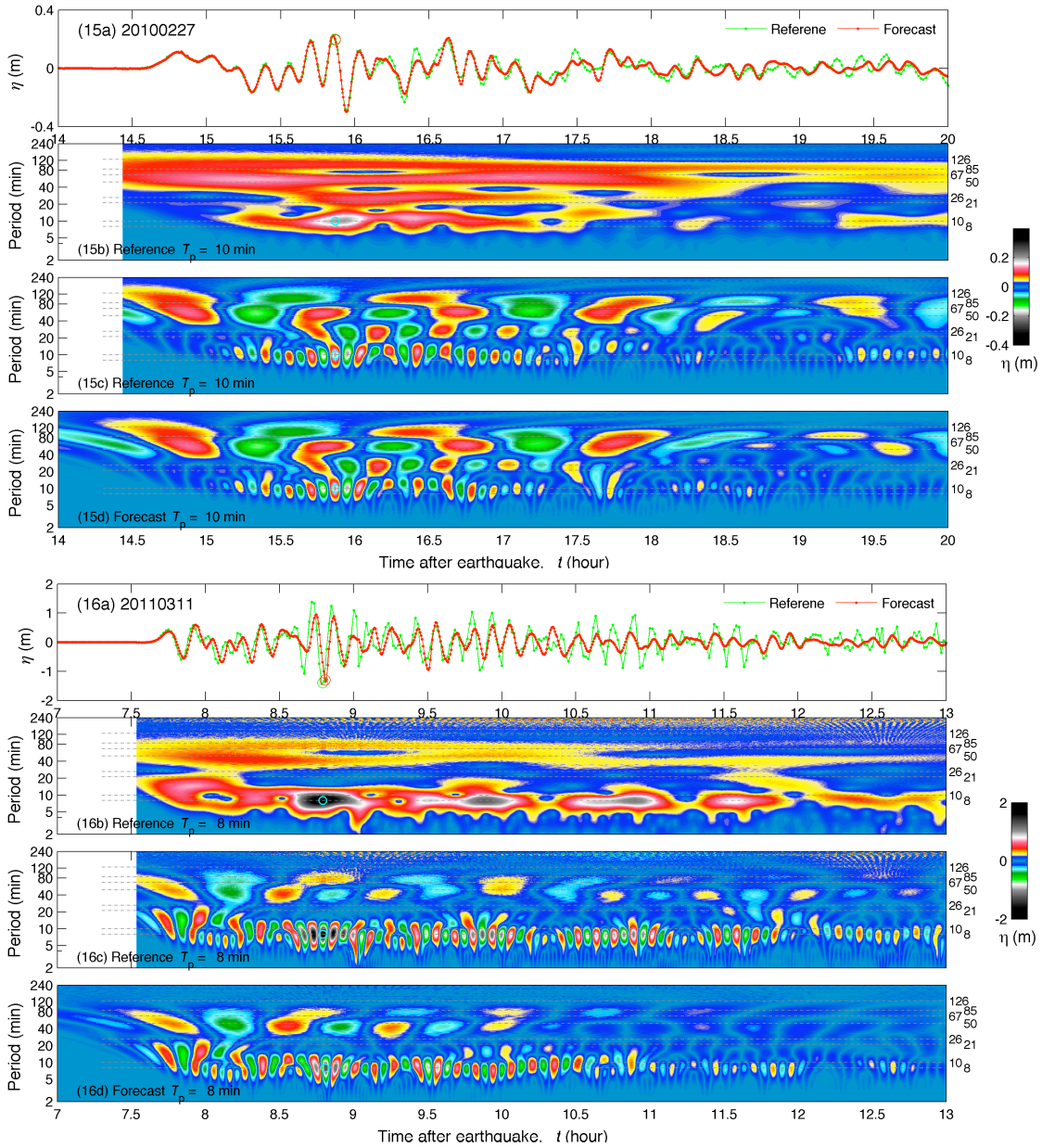

Figure 16 (a) Modeled η time series at Kailua-Kona warning point for the past 16 tsunamis. (b) Wavelet–derived amplitude spectra for the reference model. (c and d) Real part of the spectrograms computed by the reference and forecast models.

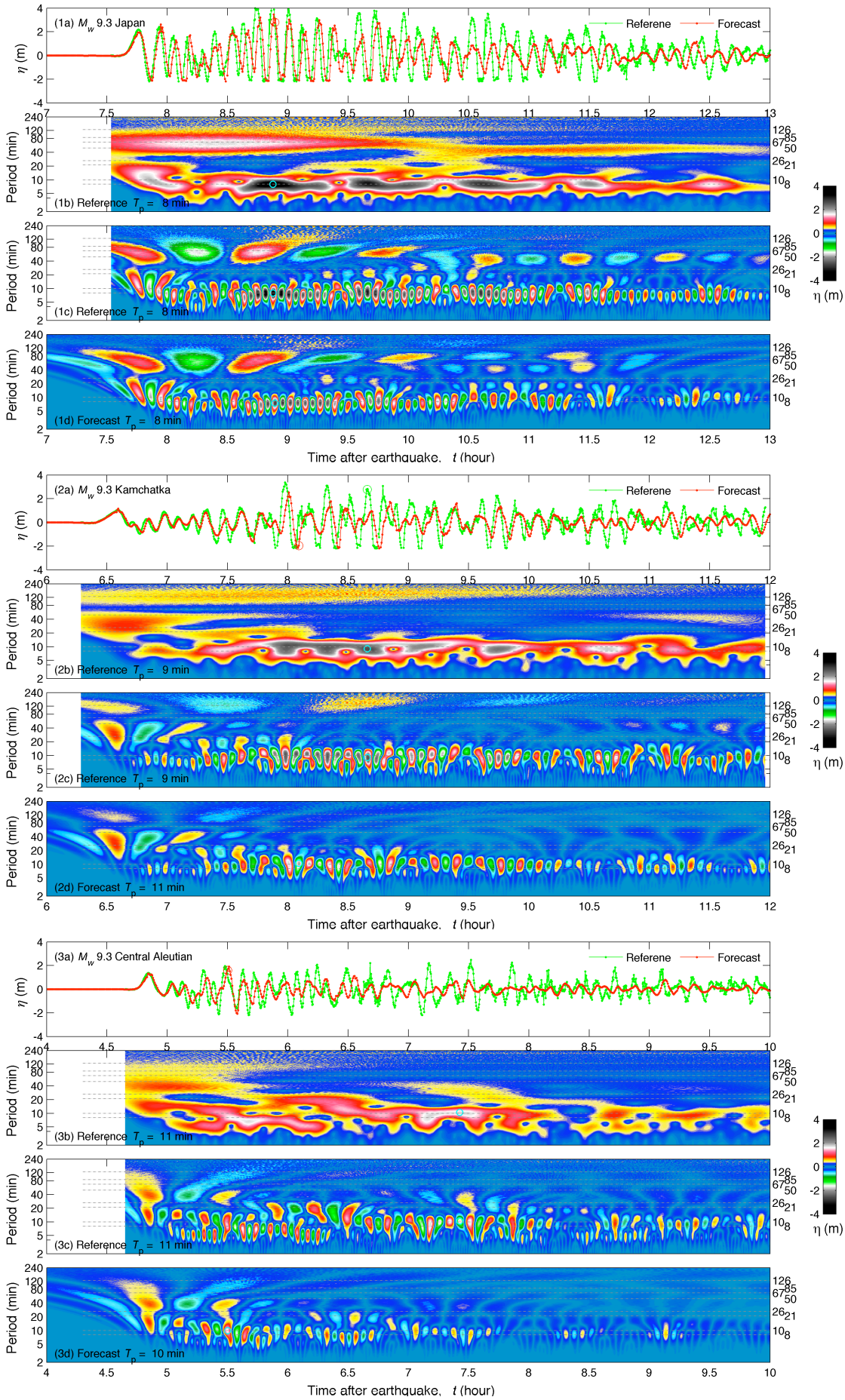
(1a) M_w 9.3 Japan
Referene
Forecast
η (m)
Period (min)
(1b) Reference T_p = 8 min
(1c) Reference T_p = 8 min
(1d) Forecast T_p = 8 min
Time after earthquake, t (hour)
(2a) M_w 9.3 Kamchatka
(2b) Reference T_p = 9 min
(2c) Reference T_p = 9 min
(2d) Forecast T_p = 11 min
(3a) M_w 9.3 Central Aleutian
(3b) Reference T_p = 11 min
(3c) Reference T_p = 11 min
(3d) Forecast T_p = 10 min

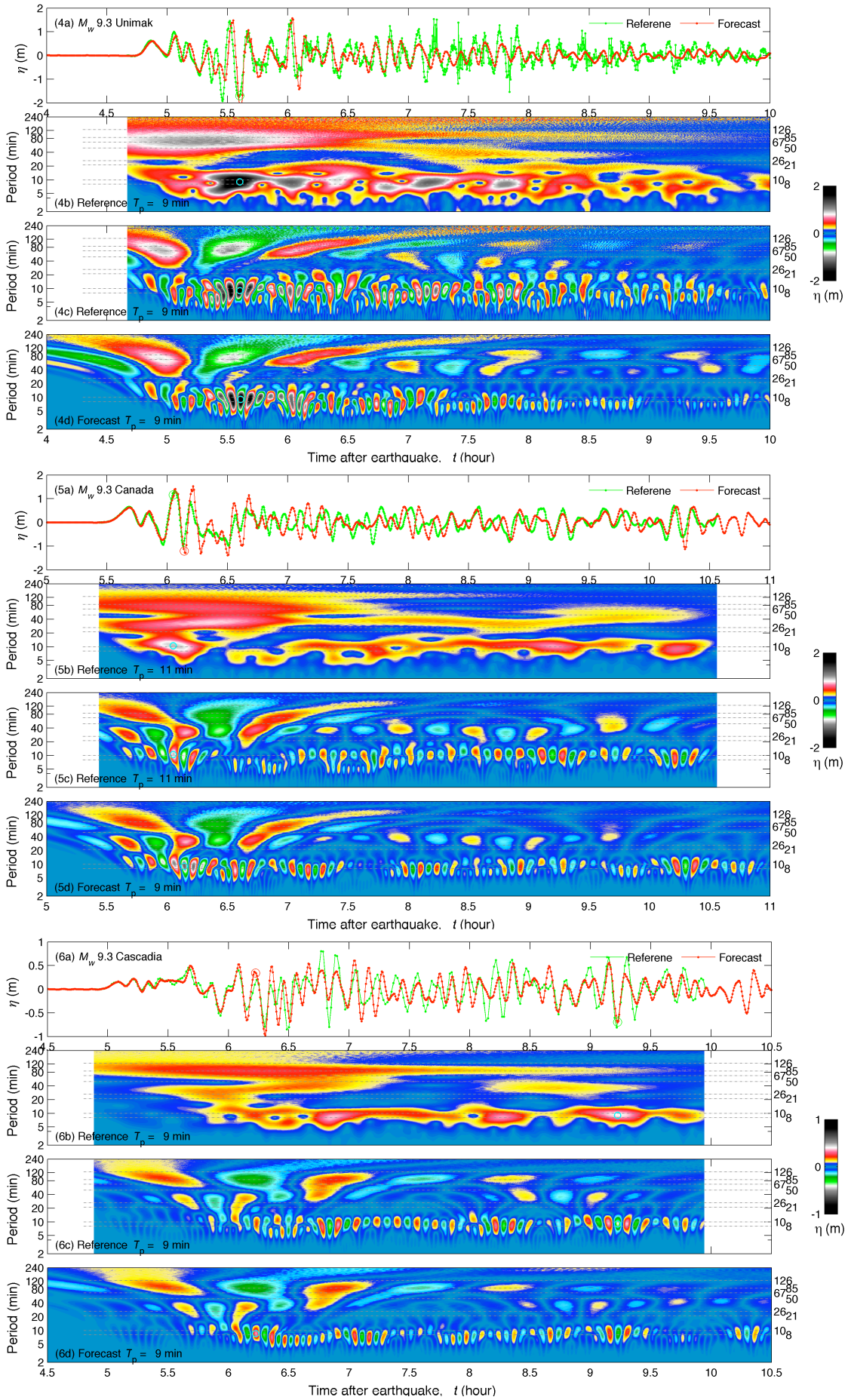
(4a) M_w 9.3 Unimak
Referene
Forecast
η (m)
Period (min)
(4b) Reference T_p = 9 min
(4c) Reference T_p = 9 min
(4d) Forecast T_p = 9 min
η (m)
Time after earthquake, t (hour)
(5a) M_w 9.3 Canada
Referene
Forecast
η (m)
Period (min)
(5b) Reference T_p = 11 min
(5c) Reference T_p = 11 min
(5d) Forecast T_p = 9 min
η (m)
Time after earthquake, t (hour)
(6a) M_w 9.3 Cascadia
Referene
Forecast
η (m)
Period (min)
(6b) Reference T_p = 9 min
(6c) Reference T_p = 9 min
(6d) Forecast T_p = 9 min
η (m)
Time after earthquake, t (hour)

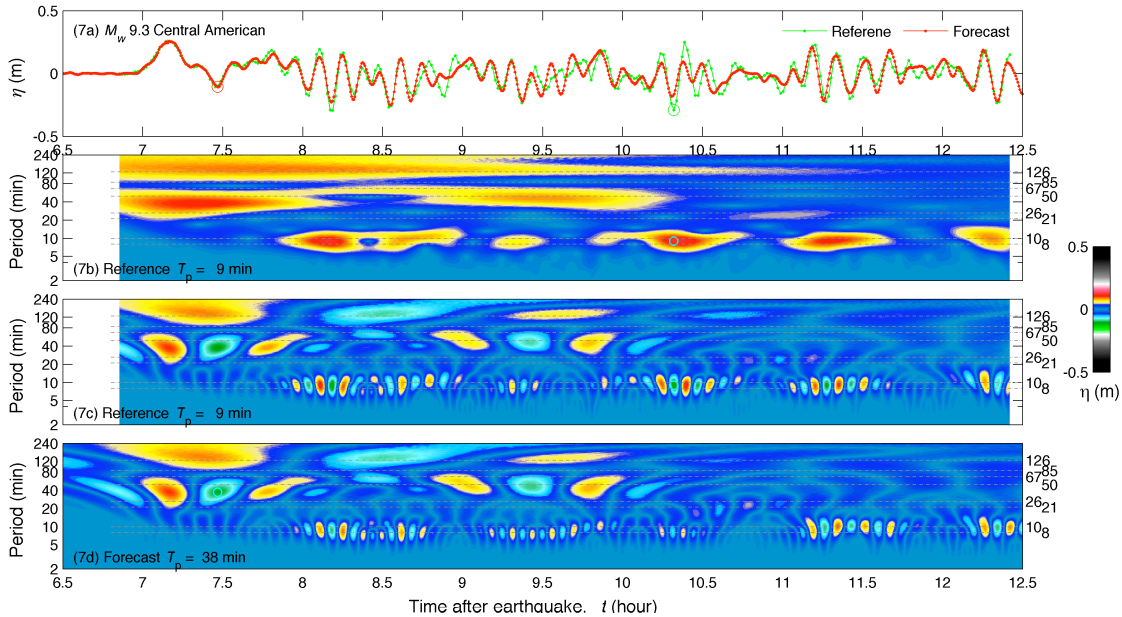
(7a) M_w 9.3 Central American
Referene
Forecast
η (m)
Period (min)
(7b) Reference T_p = 9 min
(7c) Reference T_p = 9 min
(7d) Forecast T_p = 38 min
η (m)
Time after earthquake, t (hour)

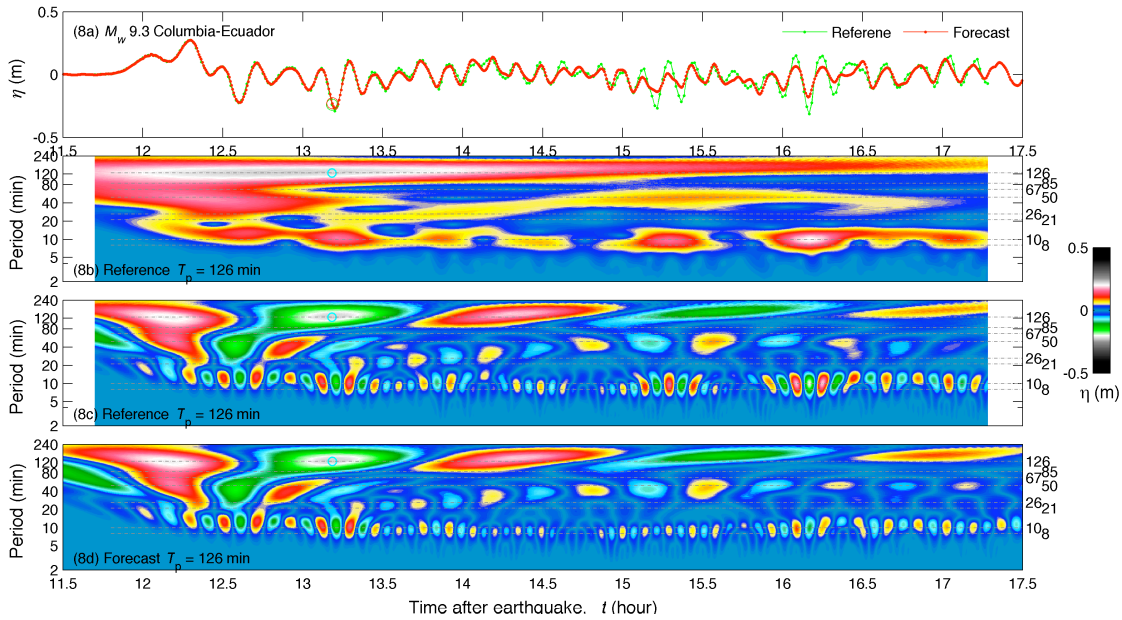
(8a) M_w 9.3 Columbia-Ecuador
Referene
Forecast
η (m)
Period (min)
(8b) Reference T_p = 126 min
(8c) Reference T_p = 126 min
(8d) Forecast T_p = 126 min
η (m)
Time after earthquake, t (hour)

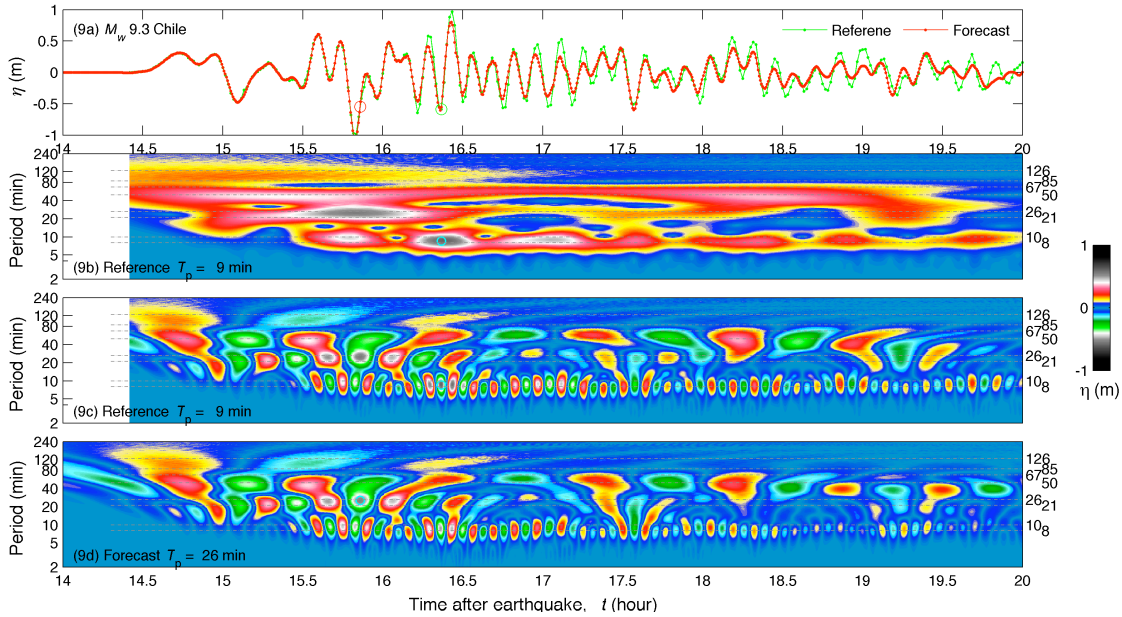
(9a) M_w 9.3 Chile
Referene
Forecast
η (m)
Period (min)
(9b) Reference T_p = 9 min
(9c) Reference T_p = 9 min
(9d) Forecast T_p = 26 min
η (m)
Time after earthquake, t (hour)

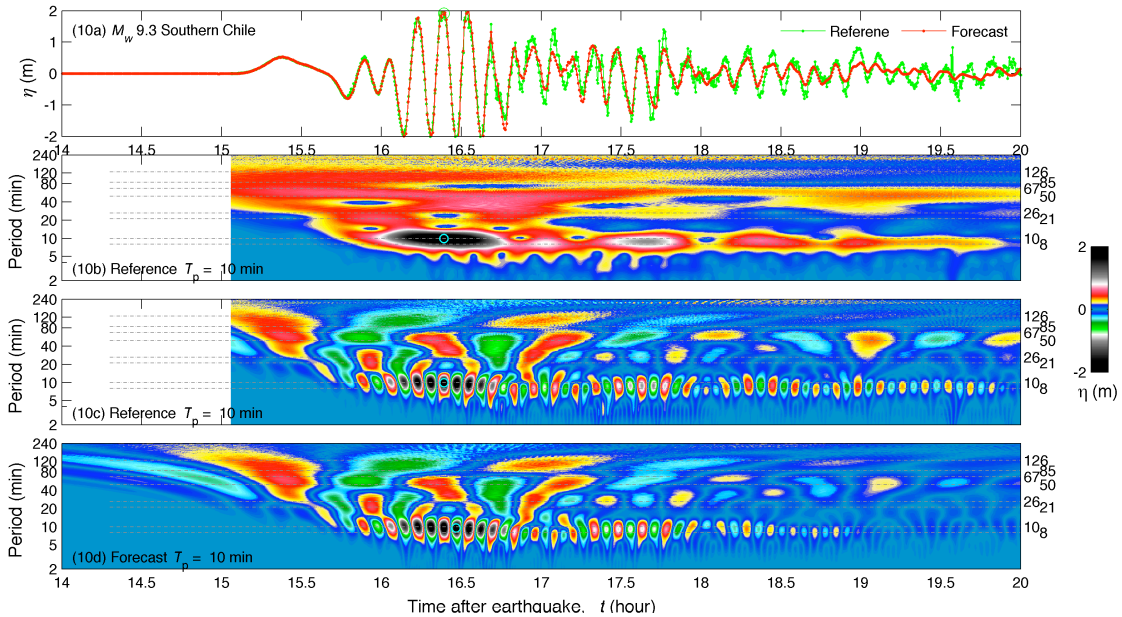
(10a) M_w 9.3 Southern Chile
Referene
Forecast
η (m)
Period (min)
(10b) Reference T_p = 10 min
(10c) Reference T_p = 10 min
(10d) Forecast T_p = 10 min
η (m)
Time after earthquake, t (hour)

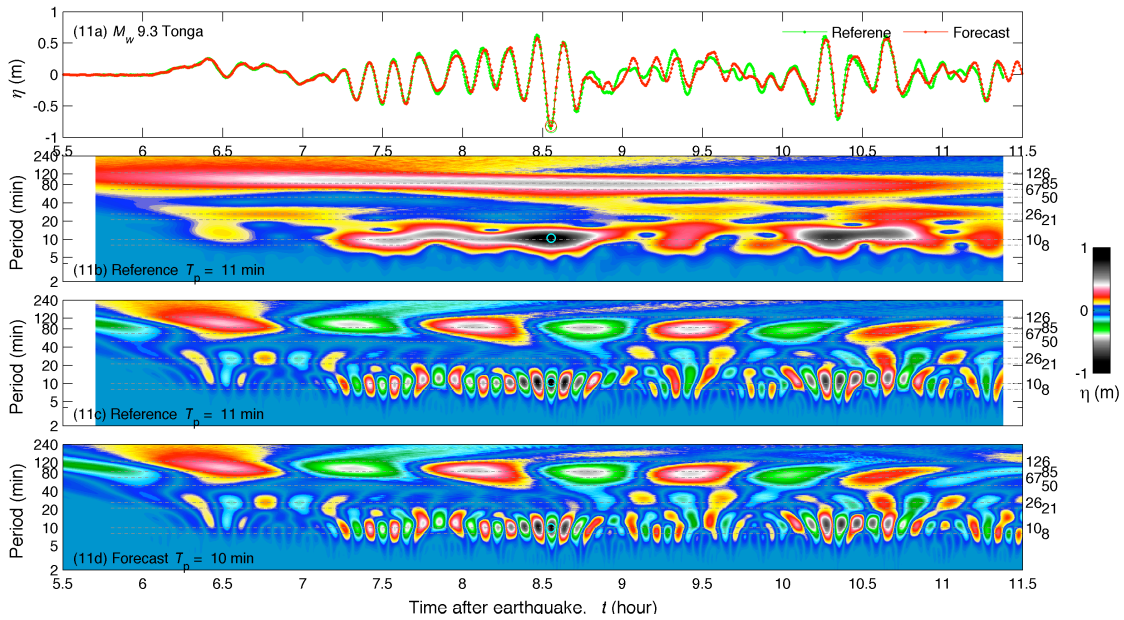
(11a) M_w 9.3 Tonga
Referene
Forecast
η (m)
Period (min)
(11b) Reference T_p = 11 min
(11c) Reference T_p = 11 min
(11d) Forecast T_p = 10 min
η (m)
Time after earthquake, t (hour)

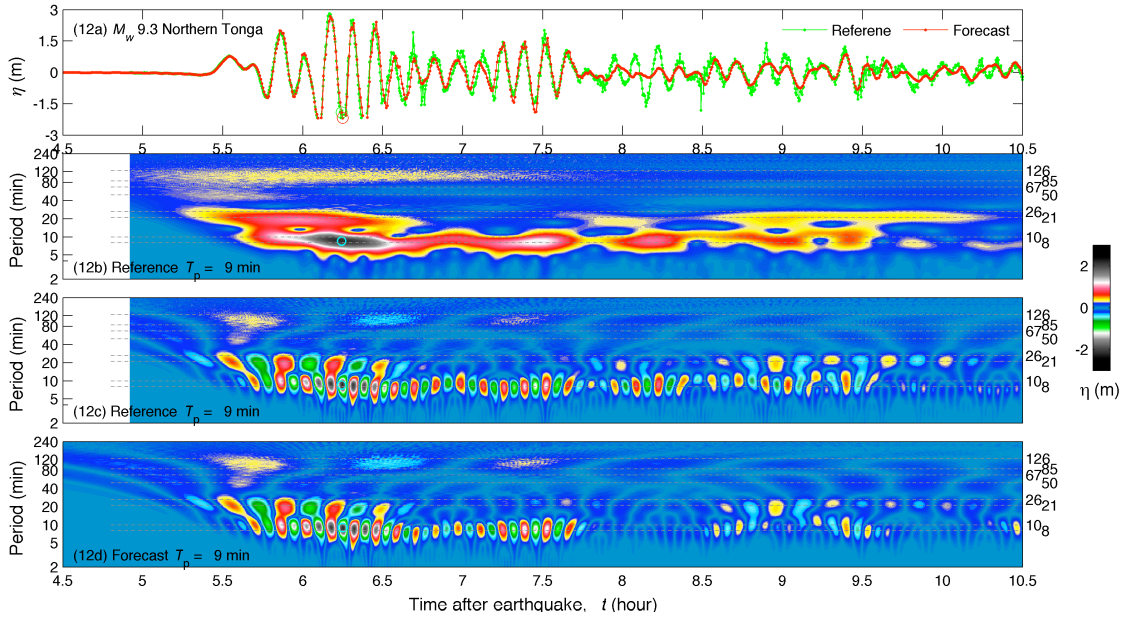
(12a) M_w 9.3 Northern Tonga
Referene
Forecast
η (m)
Period (min)
(12b) Reference T_p = 9 min
(12c) Reference T_p = 9 min
(12d) Forecast T_p = 9 min
η (m)
Time after earthquake, t (hour)

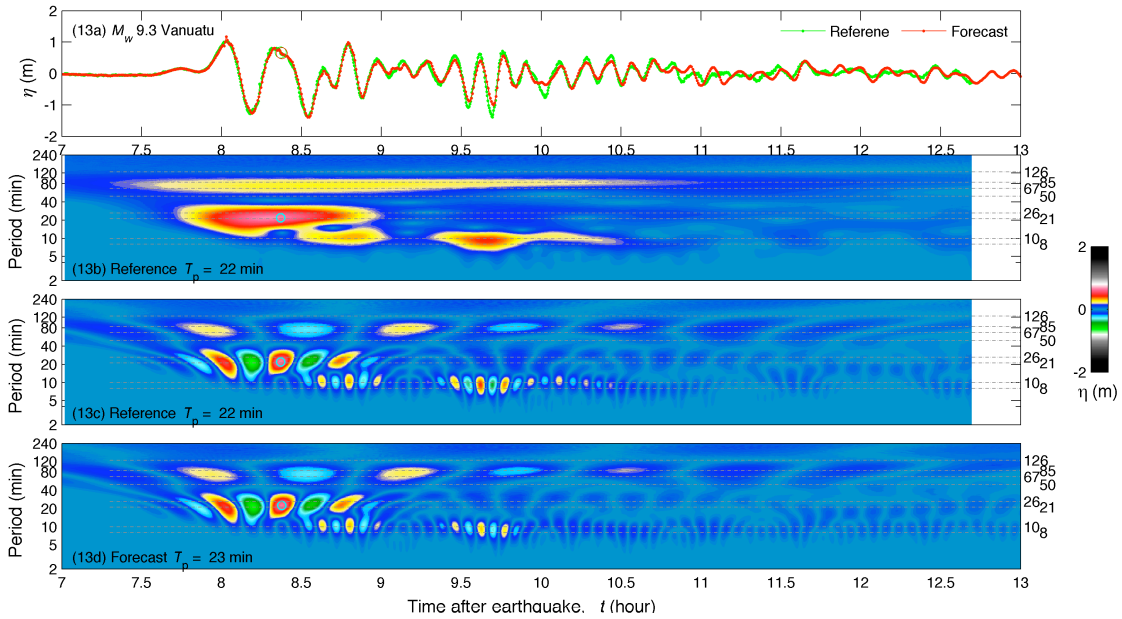
(13a) M_w 9.3 Vanuatu
Referene
Forecast
η (m)
Period (min)
(13b) Reference T_p = 22 min
(13c) Reference T_p = 22 min
(13d) Forecast T_p = 23 min
η (m)
Time after earthquake, t (hour)

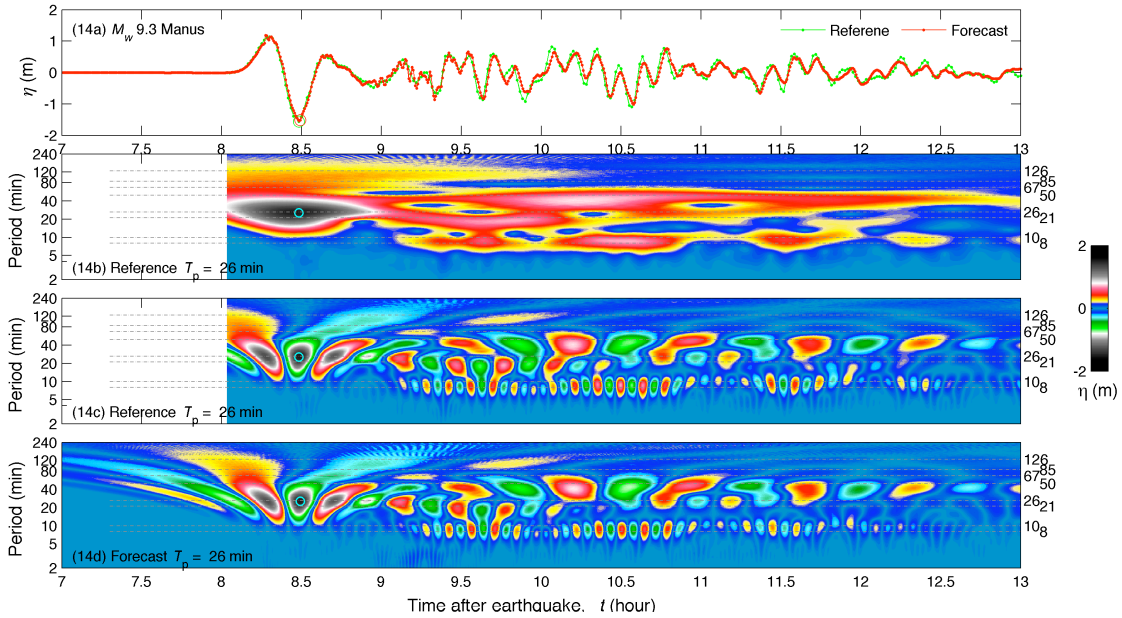
(14a) M_w 9.3 Manus
Referene
Forecast
η (m)
Period (min)
(14b) Reference T_p = 26 min
(14c) Reference T_p = 26 min
(14d) Forecast T_p = 26 min
η (m)
Time after earthquake, t (hour)

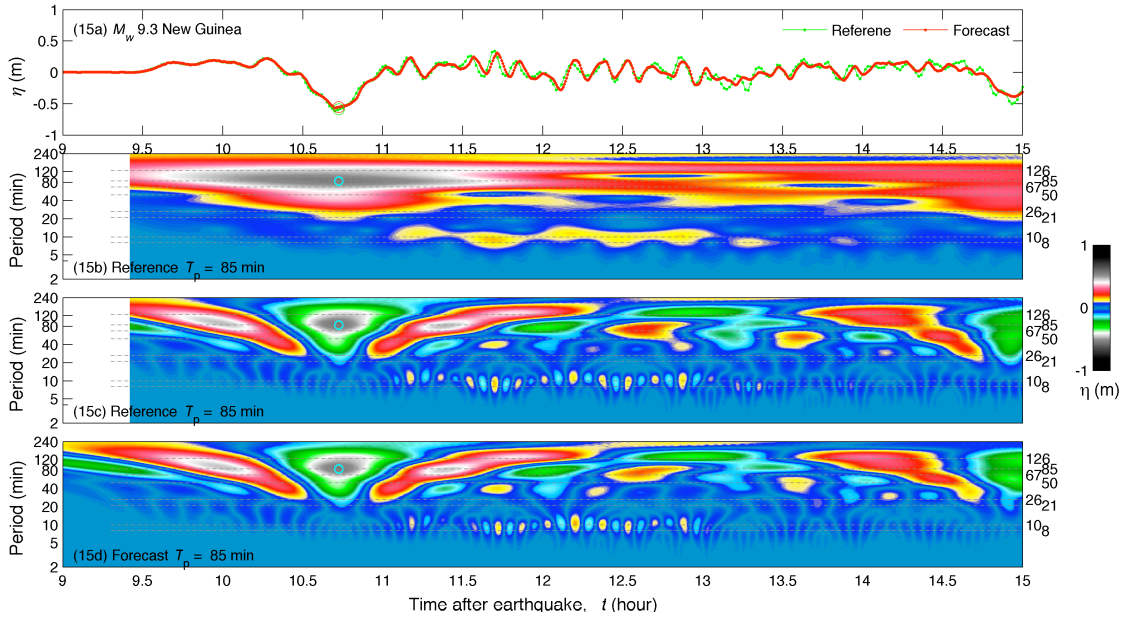
(15a) M_w 9.3 New Guinea
Referene
Forecast
η (m)
Period (min)
(15b) Reference T_p = 85 min
(15c) Reference T_p = 85 min
(15d) Forecast T_p = 85 min
η (m)
Time after earthquake, t (hour)

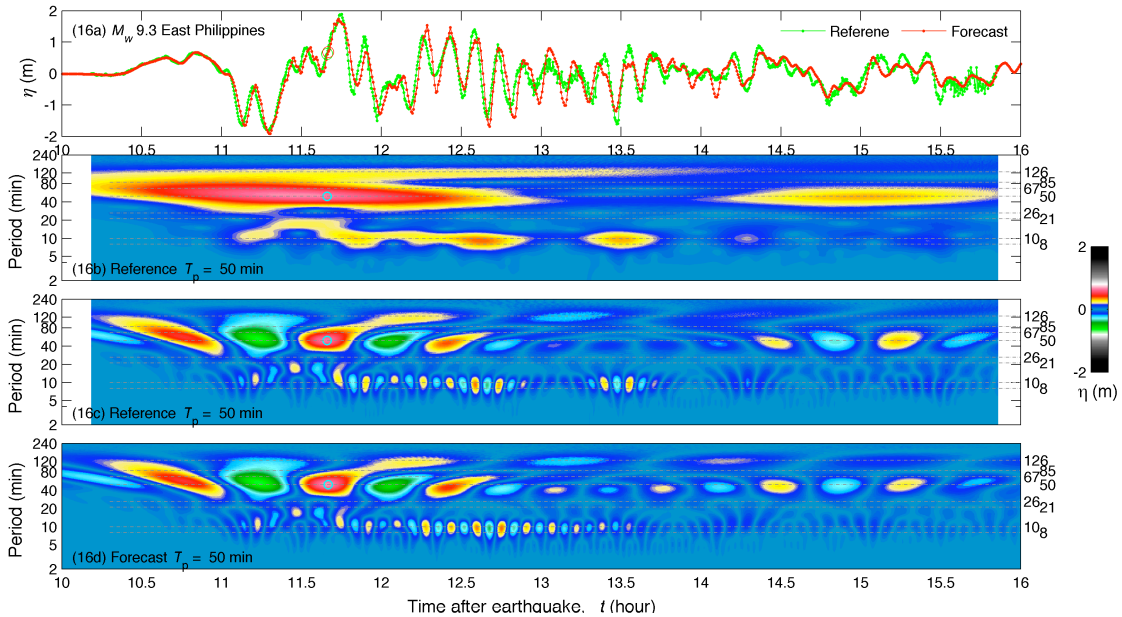
(16a) M_w 9.3 East Philippines
Referene
Forecast
η (m)
Period (min)
(16b) Reference T_p = 50 min
(16c) Reference T_p = 50 min
(16d) Forecast T_p = 50 min
η (m)
Time after earthquake, t (hour)

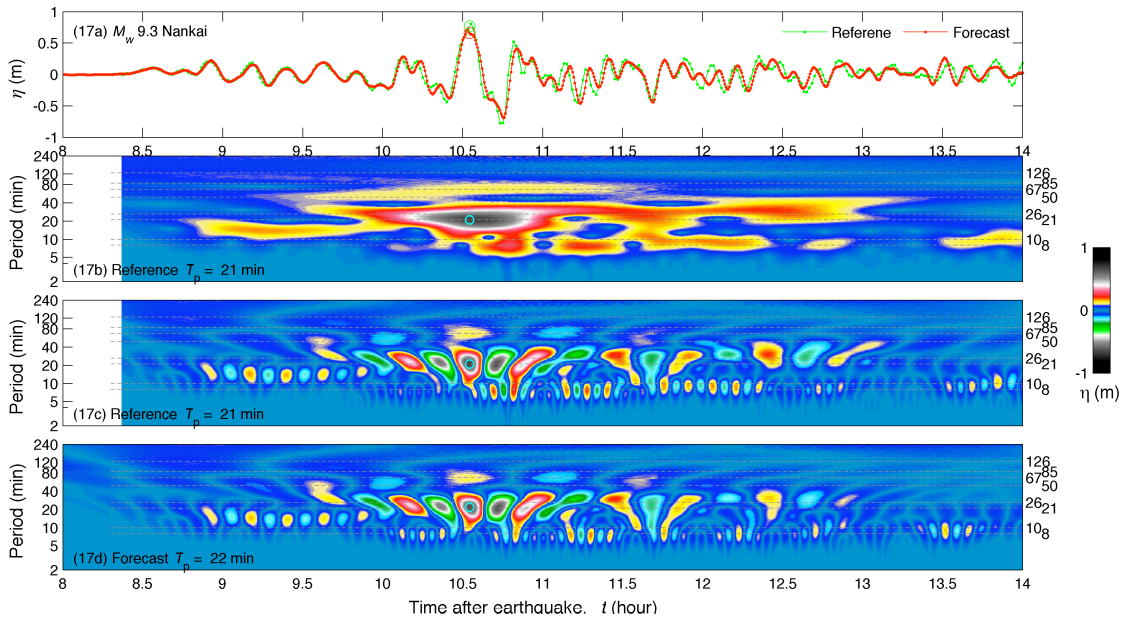
(17a) M_w 9.3 Nankai
Referene
Forecast
η (m)
Period (min)
(17b) Reference T_p = 21 min
(17c) Reference T_p = 21 min
(17d) Forecast T_p = 22 min
η (m)
Time after earthquake, t (hour)

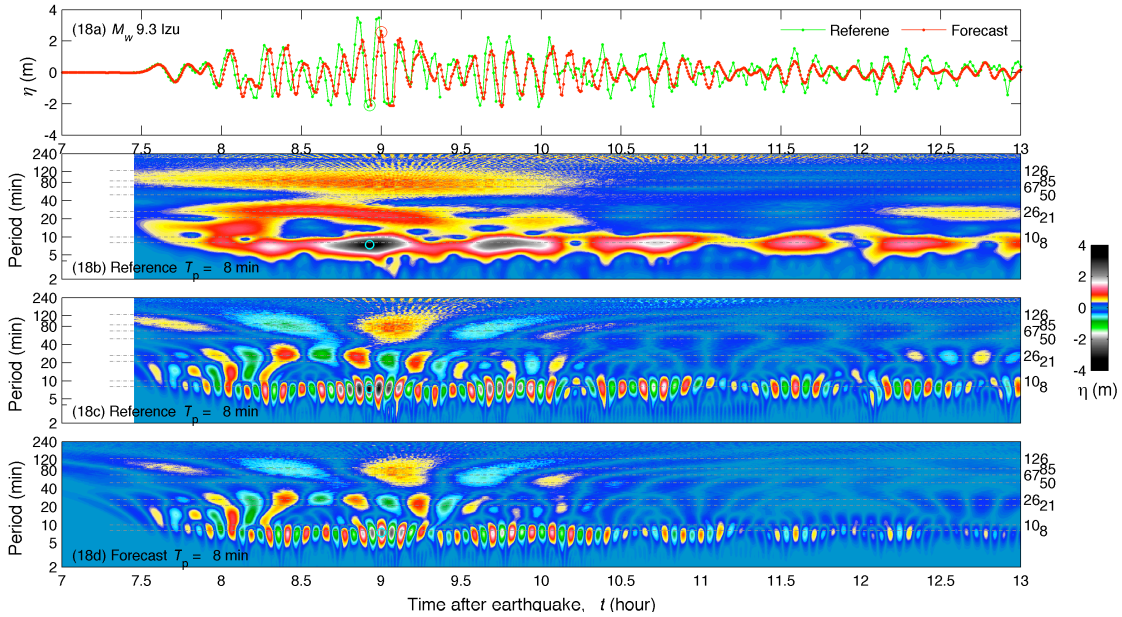
(18a) M_w 9.3 Izu
Referene
Forecast
η (m)
Period (min)
(18b) Reference T_p = 8 min
(18c) Reference T_p = 8 min
(18d) Forecast T_p = 8 min
η (m)
Time after earthquake, t (hour)

Figure 17 (a) Modeled η time series at Kailua-Kona warning point for the 18 simulated M_w=9.3 tsunamis. (b) Wavelet–derived amplitude spectrogram for the reference model. (c and d) Real part of the spectrograms computed by the reference and forecast models.

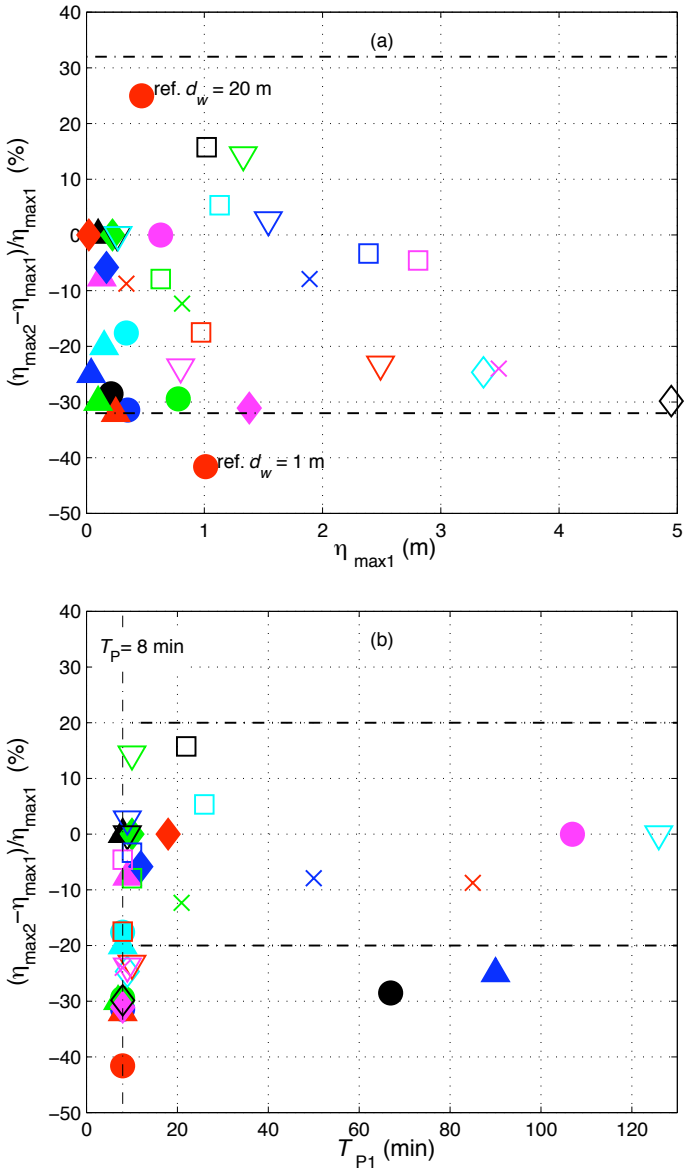

	η_{max1}	η_{max2}	$\Delta\eta$ (m)	(%)	T_{P1}	T_{P2}
19460401	1.01	0.59	−0.42	−42	8	8
19521104	0.35	0.24	−0.11	−31	8	8
19570309	0.78	0.55	−0.23	−29	8	8
19600522	0.63	0.63	0	0	107	107
19640328	0.21	0.15	−0.06	−29	67	67
19941004	0.34	0.28	−0.06	−18	8	8
19960610	0.25	0.17	−0.08	−32	8	8
20030925	0.04	0.03	−0.01	−25	90	90
20031117	0.1	0.07	−0.03	−30	7	8
20060503	0.13	0.12	−0.01	−8	9	9
20061115	0.1	0.1	0	0	8	8
20070113	0.15	0.12	−0.03	−20	8	8
20070815	0.02	0.02	0	0	18	18
20090929	0.17	0.16	−0.01	−6	12	12
20100227	0.22	0.22	0	0	10	10
20110311	1.38	0.95	−0.43	−31	8	8
Japan	4.95	3.47	−1.48	−30	8	8
Kamchatka	3.36	2.53	−0.83	−25	9	10
Central Aleutian	2.49	1.91	−0.58	−23	10	10
Unimak	1.54	1.58	0.04	3	9	9
Canada	1.33	1.52	0.19	14	10	9
Cascadia	0.8	0.61	−0.19	−24	9	8
Central American	0.26	0.26	0	0	9	38
Columbia–Ecuador	0.27	0.27	0	0	126	126
Chile	0.97	0.8	−0.17	−18	8	26
Southern Chile	2.39	2.31	−0.08	−3	10	10
Tonga	0.63	0.58	−0.05	−8	10	10
Northern Tonga	2.81	2.68	−0.13	−5	8	9
Vanuatu	1.02	1.18	0.16	16	22	22
Manus	1.13	1.19	0.06	5	26	26
New Guinea	0.34	0.31	−0.03	−9	85	85
East Philippines	1.89	1.74	−0.15	−8	50	50
Nankai	0.81	0.71	−0.1	−12	21	22
Izu	3.49	2.65	−0.84	−24	8	8

Figure 18 (a) Uncertainty in the η_{max} at Kailua-Kona warning point computed by the reference and forecast models for the 34 scenarios. (b) Large Uncertainty is associated with short peak wave period near 8 min. Filled markers, 16 past tsunamis; open markers, 18 simulated M_w = 9.3 tsunamis.